Marlene Hiesinger BSc

Characterization of tilimycin immunity genes in *Klebsiella oxytoca* AHC-6

MASTERARBEIT

zur Erlangung des akademischen Grades

Master of Science

Masterstudium

Molekulare Mikrobiolgie

eingereicht an der

Technischen Universität Graz

Betreuerin

Ao. Univ.-Prof. Dr. rer. nat. Ellen Zechner

Institute of Molecular Biosciences

Graz, März 2021

EIDESSTATTLICHE ERKLÄRUNG

Ich erkläre an Eides statt, dass ich die vorliegende Arbeit selbstständig verfasst, andere als die angegebenen Quellen/Hilfsmittel nicht benutzt und die den benutzten Quellen wörtlich und inhaltlich entnommenen Stellen als solche kenntlich gemacht habe. Das in TUGRAZonline hochgeladene Text-dokument ist mit der vorliegenden Masterarbeit identisch.

5.03.2021 M. Hiesinger

Datum, Unterschrift

Acknowledgements

I am deeply grateful for having a supervisor like

Prof. Dr. Ellen Zechner

and for the opportunity to perform my master's thesis on such a fascinating project.
Thank you for all the patience and constructive criticism. Your perfectionism and enthusiasm for science encouraged me to think rationally and led my love for science.

My appreciation also goes to

Dr. Sabine Kienesberger-Feist

for her constant intellectual and mental support. She always provided me scientific as well as personal advice.

I would like to thank

Sandra Raffl

for sharing her great technical knowledge. Her organizational skills, routine and kindness are what one wishes for as a lab colleague.

Thanks to my colleagues

Maksym, Amar and **Bianca** for making the work in the lab a really good and interesting time. Special thanks for the amusing after-work discussions.
I especially thank **Lisa** for always having had an open ear, the coffee's we had together, and for having shared her expertise on qRT-PCR and organoids.

My deepest gratitude goes to my parents

Mag. BEd Dipl.-Ing. Martina Hiesinger und **Dr. Manfred Tetz**

for their endless support. Thanks for giving me such opportunities in my life and for always believing in me.

Special thanks to my sister **Angela** for her emotional support and the funny late-night calls during my master.

Finally, I am grateful for **Stevo** and his love, understanding, support. You always supported and believed in me during stressful times.

Abstract

Typical antibiotic-producing bacteria possess a biosynthetic gene cluster including antibiotic synthesis genes and at least one antibiotic resistance gene that protects them from the antimicrobial molecules that they produce. Antibiotic resistance is mediated by multiple mechanisms and various regulatory mechanisms control resistance gene expression. *Klebsiella oxytoca* is a commensal of the human gut that can cause antibiotic-associated hemorrhagic colitis. However, the outbreak of the disease requires strains with a *til* gene cluster, which encodes enzymes for synthesis of the enterotoxin tilimycin (TM). TM was recently identified as a DNA binding and damaging agent with antimicrobial activities toward other gut residents.

In this study, the putative immunity genes *mfsX* and *uvrX* were investigated to gain more details about the self-resistance mechanisms of *K. oxytoca* against its own genotoxin TM. U*vrX* is homologous to *uvrA*, which encodes a conserved DNA repair enzyme. Here we show that heterologous *uvrX* expression in *E. coli* WT and *ΔuvrA* confers TM resistance to these sensitive strains. Further, targeted gene mutation indicated that *mfsX* and *uvrX* enable *K. oxytoca* AHC-6 to survive the self-produced TM.

Analysis of the protein sequence and the predicted structure identified that UvrX belongs to the class II UvrA proteins within the ABC protein family, suggesting that UvrX mediates TM resistance by DNA repair independent of the NER pathway. Further studies are needed to gain more insight into the activity of UvrX concerning TM resistance.

Furthermore, we established and validated a qRT-PCR method to monitor toxin-related gene expression profiles in *K. oxytoca*. Immunity gene expression prior to or concomitantly with TM production would permit *K. oxytoca* to endure the damaging effects of TM. Indeed, we observed a simultaneous increase of expression of *mfsX, uvrX* and the toxin synthetase gene *npsA*. Further studies will fully characterize the expression profiles of WT and toxin deficient *K. oxytoca.*

Zusammenfassung

Antibiotika-produzierende Bakterien besitzen einen biosynthetischen Gencluster. Dieser beinhaltet Antibiotika-Synthesegene und mindestens ein Resistenzgen, welches vor den produzierten antimikrobiellen Substanzen schützt. Die kreativen Mechanismen der Antibiotikaresistenz werden durch diverse Regulationsmechanismen der Resistenzgenexpression gesteuert. *Klebsiella oxytoca*, ein Bewohner des menschlichen Darms, kann zu Antibiotika-assoziierte hämorrhagische Kolitis führen. Jedoch benötigt der Ausbruch dieser Krankheit, Stämme mit einem *til*-Gencluster. Dieser enthält Gene, welche Enzyme für die Synthese des Enterotoxin Tilimycin (TM) codieren, welches kürzlich als DNA-bindendes und -schädigendes Toxin mit antimikrobieller Aktivität identifiziert wurde.

In dieser Studie wurden die potentiellen Resistenzgene *mfsX* und *uvrX* analysiert, um Information über die *K. oxytoca* TM-Resistenzmechanismen zu erhalten. *UvrX* zeigt eine Homologie zu *uvrA*, welches ein konserviertes DNA-Reparaturenzym kodiert. Die heterologe Expression von *uvrX* konnte den TM-empfindlichen Stämmen *E. coli* WT und *ΔuvrA* Resistenz verleihen. Zusätzlich zeigten gezielte Genmutationen, dass *mfsX* und *uvrX K. oxytoca* ermöglichen, das selbstproduzierte TM zu überleben.

Die Analyse der Proteinsequenz und vorhergesagten Proteinstruktur identifizierte UvrX als UvrA-Protein der Klasse II innerhalb der ABC-Proteinfamilie. Dies legt nahe, dass UvrX mittels DNA-Reparatur unabhängig vom NER-Weg, TM-Resistenz vermittelt. Weitere Studien sind nötig, um die Aktivität von UvrX bezüglich TM-Resistenz zu beschreiben.

Zusätzlich wurde eine qRT-PCR Methode etabliert, um Toxin-abhängige Genexpressionsprofile in *K. oxytoca* zu analysieren. Es konnte ein gleichzeitiger Anstieg der Expression von *mfsX*, *uvrX* und dem Toxin-Synthase-Gen *npsA* beobachtet werden, welches *K. oxytoca* ermöglicht die schädliche Wirkung von TM zu überleben. Studien werden die Expressionsprofile von WT und Toxin-defizienten *K. oxytoca* vollständig charakterisieren.

Contents

1 Introduction

1.1 Antibiotic resistance and self-resistance mechanisms

The problem of antibiotic resistance has received great attention during the last century due to the problem of the development and rapid expansion of antibiotic-resistant pathogenic bacteria. Antibiotic resistance has been described by the World Health Organization as one of the greatest global threats of the 21st century concerning individuals, health care and veterinary systems, as well as agricultural industries [1–3].

Even before penicillin treatment became common, observations indicated that bacteria could enzymatically degrade this substance, and the identification of resistance followed soon after. However, antimicrobial resistance is ancient and not a modern phenomenon. Microorganisms evolved resistance as a result of the interaction of many organisms within their environment. Most antimicrobial molecules are naturally produced and co-resident bacteria developed different mechanisms to survive [4,5]. These microorganisms are "intrinsically" resistant to one or even more antimicrobials. Besides intrinsic resistance, microorganisms can develop resistance after exposure to an antibiotic (acquired resistance) as a result of mutation or direct transfer of genes encoding a resistance mechanism [4,6]. These resistance genes were gained by horizontal gene transfer (HGT) from other environmental and non-pathogenic bacteria. To understand the development of antibiotic resistance in pathogens, we need to consider determinants that confer self-resistance in antibiotic-producing bacteria, particularly actinomycetes and common intrinsic resistance mechanisms present in non-producing environmental bacteria [7,8].

1.1.1 General mechanisms of antibiotic resistance and self-resistance

Over millions of years, bacteria have evolved various mechanisms to overcome the activities of antimicrobial molecules and particularly, self-resistance mechanisms of antibiotic-producing organisms against their own antibiotics are common [9]. Further, the co-existence of producing and non-producing bacteria leads to co-evolution of resistance mechanisms in non-producers. Common antibiotic resistance mechanisms can be classified into four main categories: i) modification of the antibiotic ii) blocked access to reach the target (permeability barriers and biofilms) iii) alterations of the target sites and iv) antibiotic efflux [10] (Figure 1). Examples of these different mechanisms are discussed in the following chapters.

Resistance to one class of antibiotics can typically be mediated by multiple biochemical pathways. Consequently, a bacterium is able to make use of a repertoire of resistance mechanisms to survive the effect of an antibiotic. However, it seems that bacterial species evolved towards one or another mechanism of resistance possibly due to major variations in the cell envelope of Gram-negatives and Gram-positives [4].

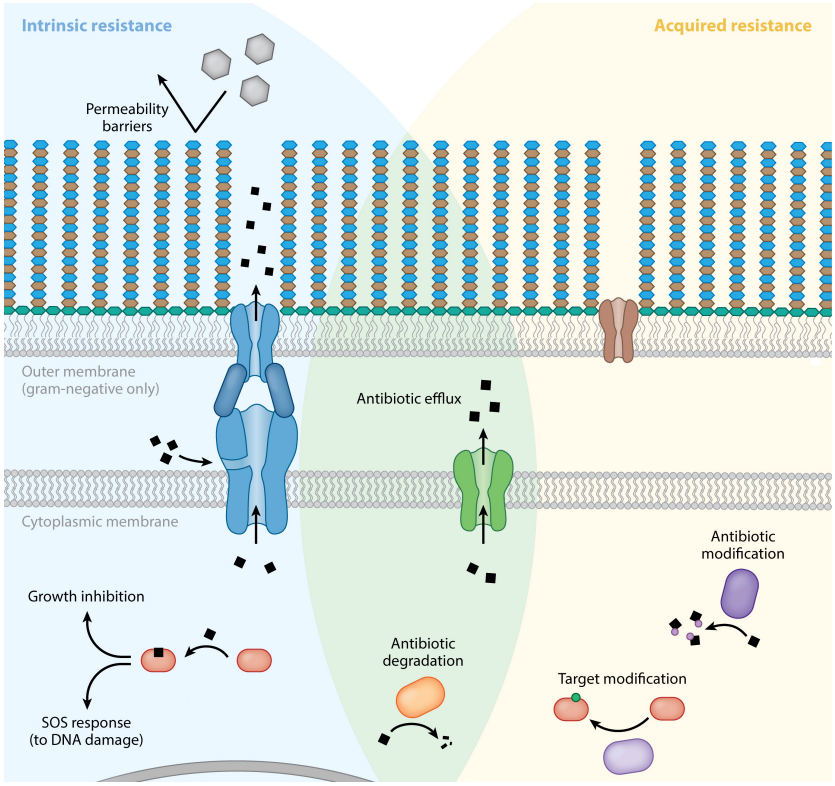

Figure 1. The intrinsic and acquired antibiotic resistance mechanism. (adapted from [10])

1.1.2 Modification or degradation of the antibiotic

One of the most successful bacterial strategies is the production of enzymes that inactivate the drug by actual degradation, or by transfer of a chemical group to the compound to avoid the interaction of the antibiotic with its target.

Bacteria encode several enzymes that modify antibiotics by adding chemical groups to vulnerable sites causing resistance as a result of steric effects. The modification mechanisms include acetylation (aminoglycosides, chloramphenicols and fluoroquinolones), phosphorylation (chloramphenicols and aminoglycosides), adenylation (aminoglycosides and lincosamides) and hydroxylation (tetracycline and tigecycline) [11,12]. Enzymes catalyzing these reactions were first identified in the producer *Streptomyces* species, but perform their biochemical reactions in

pathogenic strains too [8]. One example of drug modification is the alteration of chloramphenicol, an antibiotic that inhibits protein synthesis by interaction with the 50S ribosomal subunit. The modification of chloramphenicol is mainly triggered by the expression of an acetyltransferase called chloramphenicol acetyltransferase (CAT) in both Gram-positive and Gram-negative bacteria. CATs are not only prevalent in clinical strains but also likely to be common in *Streptomyces* [13,14].

Besides modification, inactivation of the antibiotic molecule by hydrolysis is a common mechanism to develop resistance. Resistance to β-lactam antibiotics relies on the destruction by the antibiotic-hydrolyzing enzymes called β-lactamases [15]. To date, thousands of β-lactamases have been described that are able to degrade various antibiotics within the same class, for example penicillins, cephalosporins, clavams, carbapenems and monobactams [16,17]. CTX-M genes encode extended-spectrum β-lactamases (ESBLs), that are significant for their greater activity against cefotaxime than oxyimino-β-lactams. ESBLs are commonly expressed in *K. pneumoniae*, *E. coli*, and other *Enterobacteriaceae*. Current studies indicate that CTX-M genes of clinical strains were likely acquired from *Kluyvera* species (environmental non-pathogenic soil bacteria) through HGT [18,19]. Further, diverse β-lactamases are widespread among *Streptomyces,* although oddly, a relationship between the concentration of enzymes and the level of resistance has not yet been established. *Streptomyces* express the β-lactamases constitutively and their production seems independent of resistance and β-lactam synthesis [20–22].

1.1.3 Impair access to the target

Many antibiotics have intracellular target sites. Therefore, they have to pass the outer and/or inner cytoplasmatic membrane to exhibit their antimicrobial activity. Bacteria exploit this circumstance by developing mechanisms to decrease the influx of antimicrobial molecules. In particular, Gram-negative bacteria are intrinsically less permeable than the Gram-positive organisms as their outer membrane acts as a permeability barrier. Hydrophilic antibiotics such as β-lactams, tetracyclines, and some fluoroquinolones diffuse through outer-membrane porin proteins and are therefore affected by changes in permeability [23,24]. In Gram-negative organisms (such as *Citrobacter*, *Enterobacter*, *Escherichia*, and *Klebsiella*), antibiotic sensitivity is closely related to the presence of non-specific porins [25,26]. Two of the best-characterized porins, the outer-membrane proteins OmpC and OmpF of *E. coli* function as non-specific

channels. Therefore, reducing permeability is achieved by the downregulation of these porins, a shift to more-selective porins and/or the presence of a mutated porin [23,26,27]. For example, clinical studies showed that *Klebsiella pneumoniae*, isolated during antibiotic therapy, exhibits a shift in porin expression from OmpK35 to OmpK36. Expression of OmpK35 in K. pneumoniae results in a 4-8 times decrease of the minimal inhibitory concentration (MICs) of a wide range of β-lactam antibiotics compared to expression of OmpK36. Therefore, this porin modification confers higher levels of susceptibility to β-lactams [28,29].

Another common phenomenon, the formation of biofilms by a bacterial community, prevents antimicrobial agents from reaching their target. The biofilm matrix provides structure and protection to the cells in the biofilm by serving as a barrier [30,31]. Further, the formation of a biofilm creates more mechanisms for resistance in the stationary bacteria: i) physiological changes (oxygen limitation and low metabolic activity) correlate with antibiotic tolerance [32] ii) quorum-sensing/growing conditions (regulation of extracellular polysaccharide synthesis or drug efflux pumps) [33–35] iii) efflux pumps [34], and iv) persister cells: a small number of cells that have not acquired mutations but instead survive as dormant, non-dividing cells [36].

1.1.4 Target modification/bypass/protection mechanisms

Most antibiotics bind to their targets with high affinity leading to a reduction or loss of target function. Therefore, bacteria have evolved several approaches to avoid antimicrobial-target interaction including modification of the target site to decrease the affinity for the antibiotic, protection of the target (i.e., block binding) as well as bypass of the target, as explained below.

During infection, a large and diverse population of pathogens can be involved. A single point mutation in the gene encoding an antibiotic target can lead to resistance to the antibiotic and strains with this mutation survive and proliferate. The classic example of mutational resistance is the rifampicin (Rif) resistance of pathogens like *E. coli* and *Mycobacterium tuberculosis*. The bactericidal activity of Rif can be attributed to its inhibition of bacterial transcription by high-affinity binding to the bacterial DNA-dependent RNA polymerase (RNAP). The catalytic core of RNAP (subunit composition $\alpha_2\beta\beta'\omega$) contains a ß subunit, which is encoded by *rpoB* and highly conserved among all cellular organisms. Rif binds in the β subunit of the RNAP and interrupts the path of the elongating RNA [37]. The predominant mechanism of Rif resistance is the modification of the target *rpoB* by mutation. Most of these mutations are single-point mutations

resulting in amino acid substitution in the *rpoB* gene and a decreased affinity of the antibiotic to the RNAP [38,39].

Modification of the target is an effective way to acquire antibiotic resistance without mutational changes in the target genes. This mechanism plays an important role in resistance to erythromycin of the clinically relevant *Staphylococci*. Studies revealed that erythromycin resistance is caused by methylation of the ribosomal target which is catalyzed by enzymes encoded by a variety of erythromycin ribosomal methylation *(erm)* genes. These enzymes are capable of mono- or dimethylation of the adenine in position A2058 (in *E. coli*) in the 23S rRNA moiety (50S ribosomal subunit) [40]. As a consequence of methylation, binding of the antimicrobial molecule to its target is impaired. Importantly, the binding site of erythromycin overlaps with those of macrolides, lincosamides, and streptogramin B antibiotics (MLS_B) leading to cross-resistance in producers and pathogens [41,42].

Another resistance mechanism bacteria have evolved is the bypass, or a complete replacement of the target site. For example, β-lactam producing *Streptomyces* species are highly resistant to penicillins due to overproduction of penicillin binding proteins (PBPs) or synthesis of low affinity PBPs. β-lactams have structures similar to the peptidoglycan substrates of PBP transpeptidases allowing them to bind and block enzyme activity and thus inhibit cell wall synthesis. Clinically relevant methicillin-resistant *Staphylococcus aureus* possesses the *mecA* gene, which encodes the low-affinity PBP2a. Expression of an altered PBP decreases or inhibits the ability of all β-lactam antibiotics to bind the protein, thus reducing bacterial sensitivity [43–45].

Tetracycline (Tc) is a broad-spectrum antibiotic active against Gram-positive and Gram-negative bacteria. The antibiotic binds primarily to the 16S rRNA of the 30S ribosomal subunit where it inhibits protein synthesis. Tc-resistance of bacteria is mediated through target protection via so-called ribosomal protection proteins (RPPs) [46]. Tet(O) from *Campylobacter jejuni* and Tet(M) from *Streptococcus spp.* are the best-studied tetracycline resistance determinants. These RPPs belong to the translation factor superfamily of GTPases and have similar sequences to the ribosomal elongation factors EF-G and EF-Tu. Tet(O) and Tet(M) actively remove Tc from the ribosome in a GTP-hydrolysis-dependent manner [47]. Additionally, studies showed that Tet(O) competes with Tc for the same ribosomal space and that binding of Tet(O) induces conformational changes in the 30S subunit to prevent rebinding of the antibiotic [48].

Streptomyces peucetius has a similar mechanism to protect the target of its own antibiotic daunorubicin. The bacteria express the protein DrrC, which removes the intercalated antibiotic from DNA resulting in normal transcription and replication [49]. This will be discussed in more detail later.

1.1.5 Antibiotic efflux mechanisms

Efflux of an antibiotic can be the fastest and most effective resistance mechanism bacteria possess. Especially for Gram-negative bacteria, the intrinsic activity of efflux pumps to rapidly export drugs is an essential mechanism to acquire multidrug resistance (MDR). The bacterial genome includes several genes coding for transporters that are expressed constitutively or induced/overexpressed under certain environmental stimuli [50]. Additionally, transporters are responsible for several antibiotic efflux pathways with overlapping substrate specificities that interplay in order to ensure resistance [51,52]. Currently, six families of efflux pumps encoded on the bacterial genomes have been identified: i) the ATP-binding cassette family (ABC), ii) the resistance-nodulation-cell-division family (RND), iii) the major facilitator superfamily (MFS), iv) the multidrug and toxic compound extrusion family (MATE), v) the small multidrug resistance family (SMR), and vi) the proteobacterial antimicrobial compound extrusion family (PACE) (Figure 2) [53].

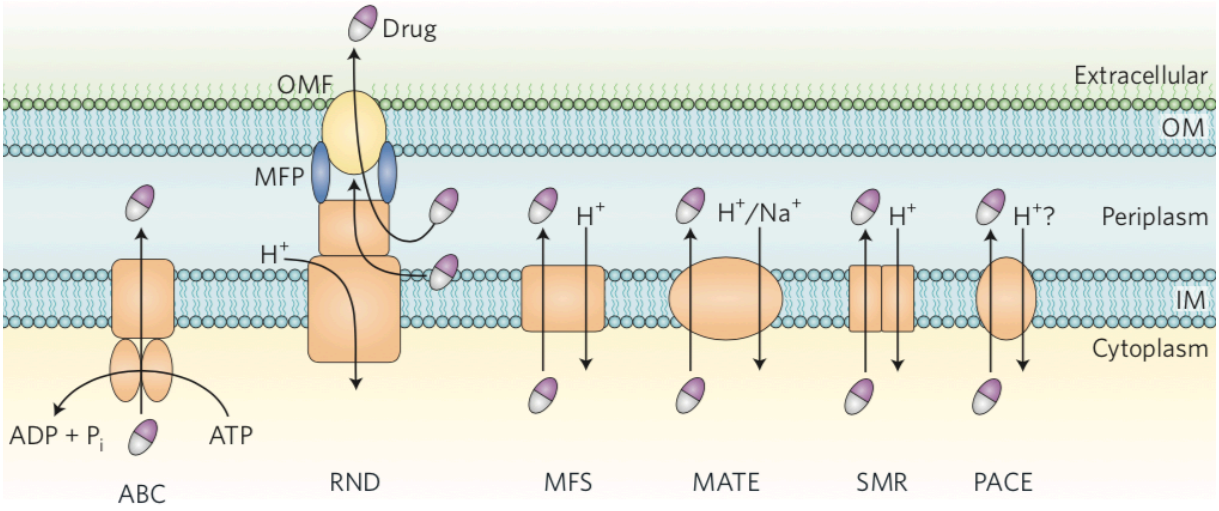

With the exception of ATP transporters, which utilize ATP hydrolysis as an energy source to

Figure 2. General structure and function of different types of efflux pumps in bacteria. Representation of the 6 major families of transporter. ATP-binding cassette family (ABC); resistance-nodulation-cell-division family (RND); major facilitator superfamily (MFS); multidrug and toxic compound extrusion family (MATE); small multidrug resistance family (SMR) and the proteobacterial antimicrobial compound extrusion family (PACE); outer membrane (OM); inner membrane (IM); membrane fusion protein (MFP); outer membrane factor (OMF) (adapted from [54])

transport drugs, the other types of efflux pumps are H^+ or Na^+ drug antiporters [54]. Further, the transporters differ in terms of structural conformation. Most of the efflux pump families are single-component pumps, located in the inner membrane (IM), that transport drugs from the cytoplasm into the periplasm, which are able to spontaneously diffuse back into the cytoplasm (particularly lipophilic antibiotics). To prevent reentry of the drug, Gram-negative bacteria developed a modular tripartite system (multiple-component pumps) consisting of an IM transporter (ABC, MFS, and RND), a periplasmic adaptor protein (or membrane fusion protein MFP) and an outer membrane channel (OMC) to excrete drugs from the periplasm. These tripartite systems can collaborate with single-component pumps and increase their efficiency [51,52,55]. Furthermore, multiple-component pumps allow the direct transport of antibiotics into the environment, bypassing the periplasm and the outer membrane [56]. This work will only focus on the ABC transporter superfamily.

1.1.5.1 ABC transporter

The ABC superfamily transporters are involved in ATP-dependent import and secretion of a wide range of substrates including ions, amino acids, drugs, polysaccharides, proteins and sugars.

ABC transporters are multiple-protein complexes that share a similar overall structure consisting of at least two nucleotide binding domains (NBDs), that bind and hydrolyze ATP, and two transmembrane permease domains (TMDs), that are embedded in the plasma membrane and contain substrate-binding pockets. A single TMD is fused to a NBD, named "half-size transporter", and a homo- or heterodimer of two half-transporters form the functional complex (Figure 3) [57,58].

The superfamily of ABC transporters shares a sequence identity and can be identified by highly conserved motifs in the NBDs. The ATP-binding site formed by two conserved amino acid sequence motifs, the Walker A (P-loop) and Walker B motifs for ATP binding, which are present in many ATP-binding proteins [58]. In addition, ABC transporters contain a number of unique motifs, such as the A-loop, the D-, H-(or "switch histidine") and Q-loops (support ATP hydrolysis and coupling hydrolysis to transport), and the important ABC signature motif (LSGGQ), that distinguish ABC proteins from other nucleotide-binding proteins [58–60].

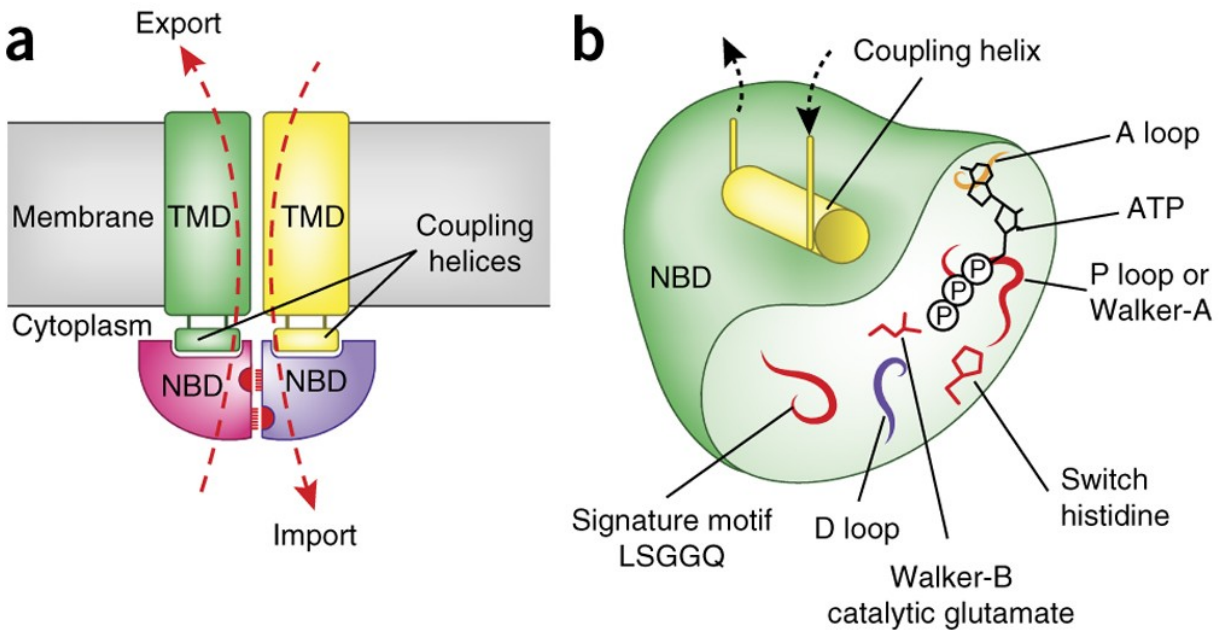

Figure 3. Molecular architecture of ABC transporters. (A) Domain arrangement of ABC transporter. Two half-size transporters consisting of each one NBD and TMD build the functional translocator. The coupling helices connect the two domains and enable conformational changes between the NBDs and the TMDs. The red arrows indicate the direction of the transport and the red marks in the NBDs indicate the P loops and ABC signature motifs. (B) Schematic representation of a single NBD with the relative positions of the conserved and

In contrast, the sequences and structure of TMDs are quite diverse, reflecting the diversity of the transported substrates. Depending on the type and function (import or export), each TMD consists of 6 to 10 putative transmembrane α-helices. The typical ABC exporter of bacteria usually consists of six α-helices per TMD, which was confirmed via crystal structures of the MDR transporter Sav1866 from *Staphylococcus aureus* [57].

The best-studied example of antibiotic efflux in producers is the ABC family transporter DrrAB of *S. peucetius* [58], that is why this transporter will be explained in detail in the next chapter.

1.2 Self-resistance mechanisms of *Streptomyces peucetius*

Streptomyces produce a variety of biologically active substances, like antibiotics, and possess resistance mechanisms to avoid suicide [61]. *Streptomycin peucetius* produces two antitumor antibiotics, daunorubicin (Dnr) and its hydroxyl derivate doxorubicin (Dox) [62]. Both anthracyclines intercalate between the base pairs of native DNA causing DNA damage such as fragmentations and single-strand breaks [63]. Dnr is a minor-groove binder drug that inhibits DNA and RNA synthesis due to its non-covalent intercalation in DNA. Additionally, Dnr unwinds the double-stranded DNA leading to an altered DNA topology [64]. *S. peucetius* possesses

resistance mechanisms to overcome the toxicity of these metabolites that are co-regulated together within the antibiotic biosynthetic gene cluster. Genes that activate antibiotic syntheses, as well as those that confer resistance were found within the Dnr/Dox biosynthetic gene cluster [65]. Dnr/Dox biosynthesis of *S. peucetius* is regulated by the genes *dnrO*, *dnrN* and *dnrI*, and self-resistance is mediated by the genes *drrA*, *drrB*, *drrC* and *drrD* [66–68]. These resistance genes encode proteins that facilitate the export of the antibiotics and the protection of the antibiotic target site.

1.2.1 Efflux of Daunorubicin occurs by an ABC transporter DrrAB

Initial work started with the sequence analysis of the *drrAB* operon from *S. peucetius*, which supplied a hypothesis to explain the significance of the genes *drrA* and *drrB* for Dnr and Dox resistance. These two genes were shown to encode an ABC family transporter that exports the antibiotics in an ATP-dependent manner [66,69]. DrrA binds to ATP or GTP in the presence of Mg^{2+} and the energy is passed to the carrier protein DrrB resulting in an ATP-driven export of drugs [69]. The DrrAB efflux pump represents the simplest form of an ABC transporter, which is assembled from two subunits each of DrrA (NBD) and DrrB (TMD) forming a tetrameric complex ($DrrA_2B_2$). The architecture of the DrrAB transporter is different from typical ABC family transporters because the NBD and TMD are present on separate subunits, that are biochemically coupled. Importantly, the interaction between the two domains is essential for their stability and function. DrrA is a peripheral membrane protein that functions as a catalytic nucleotide binding domain (NBD). The NBD of DrrA contains all previously known highly conserved motifs from other NBDs of ABC family transporters, including mammalian P-glycoprotein [70,71]. DrrB, a hydrophobic carrier protein, consists of eight membrane-spanning helices with N- and C-termini in the cytoplasm and forms the transmembrane domain [71,72].

Due to the location of the *drrAB* genes in the Dox biosynthetic gene cluster of *S. peucetius*, the DrrAB system was believed to be a dedicated transporter of Dnr and Dox. However, studies showed that the DrrAB efflux system belongs to the multi-drug transporter with a broad and overlapping substrate specificity with the mammalian P-glycoprotein. The system can transport the two most commonly studied MDR pump substrates Hoechst 33342 and ethidium bromide. Further, other well studied substrates of MD transporters including cerapamil, vinblastine, and rifampicin, inhibit DrrAB-mediated Dox transport. This finding indicated that they are also substrates of the DrrAB pump [73]. Additionally, recent analysis showed that DrrB has multiple

drug binding sites where it binds drugs (and already mentioned substrates) with variable affinities [74].

1.2.2 DrrC removes daunorubicin from intercalated DNA

The gene *drrC* is located in the same cluster as *drrAB* and encodes the DrrC protein that provides resistance to *S. peucetius* against Dnr. DrrC shows strong sequence similarity to the *E. coli* UvrA protein, which is involved in excision repair of damaged DNA caused by DNA-intercalating Dox or Dnr [67,75]. However, the expression of *drrC* in the E. coli *uvrA* mutant did not complement the *uvrA* mutation, suggesting a novel type of drug self-resistance (Figure 4). Further studies revealed that DrrC is a DNA-binding protein that removes Dnr from intercalated DNA. Similar to UvrA, DrrC may scan the DNA for lesions and when it encounters Dnr at intercalated sites, it binds to it and removes the drug. It is probable, that DrrC and Dnr are both released together from the DNA as a DrrC-daunorubicin complex. DrrC seems to play a crucial role in keeping the DNA of *S. peucetius* free from Dnr so that replication and transcription proceed unaffected [49].

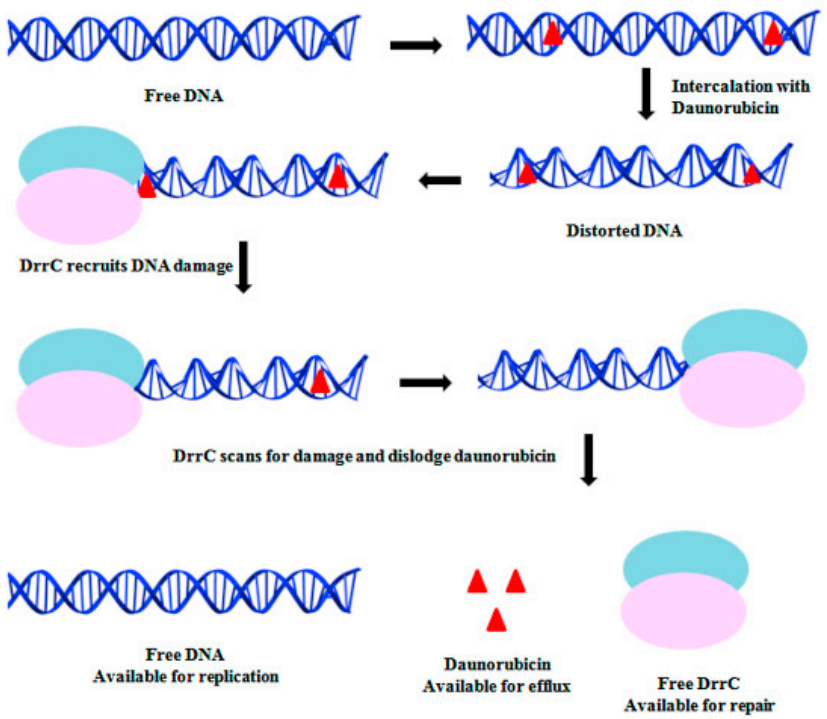

Figure 4. Possible mechanism of DrrC to ensure self-resistance to daunorubicin by binding to DNA and removing the drug. (Figure from [49])

1.3 *Klebsiella oxytoca* enterotoxin tilimycin has DNA-damaging activities

1.3.1 Antibiotic-associated hemorrhagic colitis (AAHC)

Antibiotic-associated diarrhea (AAD) and antibiotic-associated colitis (AAC) are common adverse side effects of antibiotic intake, which occur in up to 30% of patients. The underlying mechanisms are the toxic effects of the antibiotic on the intestinal mucosa and the intestinal motility, as well as the disruption of the protective intestinal flora [76]. Pathobionts such as *Clostridium difficile* take advantage of such conditions and overgrow causing 10 - 20% of AAD cases [77]. *C. difficile* is a harmless resident of the human gut in about 10% of healthy individuals. However, after the disruption of the microbiota by antibiotic treatment, *C. difficile* can cause various symptoms, ranging from mild, self-limiting diarrhea to fulminant colitis as well as pseudomembranous colitis [78,79]. Besides *C. difficile*, the pathogens *Clostridium perfringens, Staphylococcus aureus*, and *Klebsiella oxytoca* have been identified as a source of AAD [80]. *K. oxytoca* causes antibiotic-associated hemorrhagic colitis (AAHC), a subtype of AAC. *K. oxytoca* is a Gram-negative bacterium colonizing the intestine of healthy individuals with a rate of about 2-10% [81,82]. *K. oxytoca* expresses β-lactamases, which confer resistance to amino- and carboxy-penicillins [83]. Disruption of the intestinal microbiota and dysbiosis triggered by antibiotic therapy facilitates competitive overgrowth of *K. oxytoca*. Stool samples of AAHC patients revealed a high abundance of *K. oxytoca* (10^7 cfu/g feces during AAHC compared to 10^2 cfu/g feces in healthy individuals) [84].

1.3.2 The pathogenicity island of *K. oxytoca*

Previous members of our group investigated the underlying mechanism of *K. oxytoca* pathogenicity in AAHC and revealed a specific cytotoxic effect of *K. oxytoca* strains isolated from AAHC patients [81,85]. Further, they identified the cytotoxin as tilivalline, which already had been isolated and described [86–88]. As a next step, the group aimed to identify the essential genes for toxin synthesis. A mutant library of *K. oxytoca* AHC-6 mutants were generated via random Tn5 transposon mutagenesis and screened for loss of toxicity against human epithelial cells in vitro. Four mutants showed complete loss of cytotoxicity. The disrupted genes were named *aroX,* encoding a 2-keto-3-deoxy-D-arabinose-heptulosonate-7-phosphate (DAHP) synthase, *aroB*, encoding a 3-dehydroquinate-synthase, and *npsA* and *npsB*. The enzymes AroB and AroX were involved in the shikimate and chorismate pathway. The genes *npsA* and *npsB*

were identified as nonribosomal peptide synthetases (*NRPS*) [86]. NRPS produce so-called nonribosomal peptides (NRPs) independent of mRNA and ribosomes. They are large, multi-modular enzymes, wherein each module is responsible for the incorporation of a monomer, for example a single amino acid, into the final NRP [89]. Notably, NRPs often contain non-proteinogenic amino acids, fatty acids as well as α-hydroxy acids [90].

Sequencing of the *K. oxytoca* AHC-6 genome revealed that three of the four essential genes (*aroX, npsA,* and *npsB*) are located within a 7-kb region (NCBI accession number: HG425356.1), which is flanked by two asparagine tRNA genes. Comparison of the region with other enterobacterial genomes revealed different mobile DNA elements, which are located in this high-plasticity locus, and share characteristics of a pathogenicity island (PAI). PAIs characteristically contain genes encoding virulence factors, like toxins, that promote pathogenesis. Further, they show a different G+C content compared to the surrounding DNA sequences and are adjacently located to tRNAs, which are hotspots for the integration of foreign DNA [91]. This result suggests that the identified tilivalline biosynthesis genes are part of a PAI. The PAI of *K. oxytoca* AHC-6 consists of ten genes, of which the putative essential genes for tilivalline biosynthesis are clustered in two operons: AroX- and NRPS-operon (Figure 5). All genes located on the *K. oxytoca* AHC-6 PAI and their annotated function are listed in Table 1. The genes *npsA, thdA* and *npsB* are part of a nonribosomal peptide synthetase complex and are located next to each other within the NRPS operon (blue). Five genes (*aroX, dhbX, icmX, adsX, hmoX*) are located in the other operon (AroX operon) and were annotated to encode enzymes involved in the biosynthesis of aromatic amino acid via the shikimate and chorismate pathway (pink). The two genes *mfsX* and *uvrX* of the PAI (green) are not part of these operons and are annotated as transport elements and could play a role in self-resistance of *K. oxytoca* against its toxin. The gene *aroB* is not located on the PAI, but it is related to tilivalline biosynthesis.

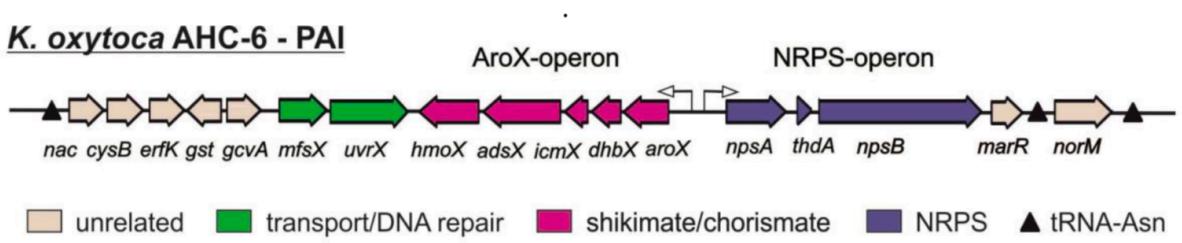

Figure 5. Pathogenicity island of the toxin-producing *K. oxytoca* AHC-6. Putative functions: NRPS (blue), production of aromatic amino acid derivatives (red), transport (green), and unrelated genes (white). tRNA genes (▲) flank the PAI. (Figure from [87]).

Table 1. Genes of the *K. oxytoca* AHC-6 PAI and their annotated function (87).

Gene	Putative function	Functional class
marR	Transcriptional regulator, MarR family	regulatory
npsB	Non-ribosomal peptide synthetase	NRPS
thdA	Peptidyl-carrier-protein, thiolation domain	NRPS
npsA	Non-ribosomal peptide synthetase	NRPS
aroX	2-Keto-3-deoxy-D-arabino-heptulosonate-7-phosphate synthase II (EC 2.5.1.54)	shikimate
dhbX	2,3-Dihydro-2,3-dihydroxybenzoate dehydrogenase (EC 1.3.1.28)	shikimate
icmX	Isochorismatase (EC 3.3.2.1)	shikimate
adsX	2-Amino-2-deoxy-isochorismate synthase (EC 4.1.3.-)	shikimate
hmoX	4-Hydroxyphenylacetate 3-monooxygenase (EC 1.14.13.3)	shikimate
uvrX	Excinuclease ABC subunit A paralog of unknown function	transport
mfsX	Permease of the major facilitator superfamily protein	transport

PCR analysis of the clinical isolates of K. oxytoca showed that 100% of the toxin-producing and 13% of the toxin-negative strains carry the PAI genes *npsB* and *npsA*. In other Klebsiella ssp. the PAI could not be detected [92].

1.3.3 *K. oxytoca* produces a second enterotoxin - tilimycin

To test the particular function of the genes essential for toxin synthesis the group analyzed the tilivalline biosynthesis. Elucidation of the TV biosynthesis revealed that the nonribosomal peptide pathway initially generates the cytotoxic secondary metabolite tilimycin (TM). TM shares the pyrrolo[2,1-c][1,4] benzodiazepine backbone with tilivalline but has a hydroxyl group instead of the indole ring at the C11 position. The *aroX*- and NRPS-operon, and additional enzymes of *K. oxytoca* are required to produce TM, which reacts spontaneously with indole to generate TV (Figure 6). Evaluation of the cytotoxic effects showed that TM (IC_{50} of 2.6 µM ± 0.4) is more cytotoxic to HeLa cells than TV (IC_{50} of 14.5 µM ± 0.5). The loss of cytotoxicity at later culture time points indicates that TV and/or TM are degraded in the bacteria. The group identified a second so far unknown metabolite named culdesacin, which was identified as the direct degradation product of TM after spontaneous ring-opening (Figure 6). Unlike TM and TV, culdesacin shows no cytotoxic activity [93]. Further studies revealed a toxic effect of TM on different human cancer cell lines and non-transformed vascular endothelial cells [94].

In summary, TM was identified as the initial product of the nonribosomal peptide assembly pathway. TM reacts spontaneously with indole to TV. Further, culdesacin is the nontoxic degeneration product of TM.

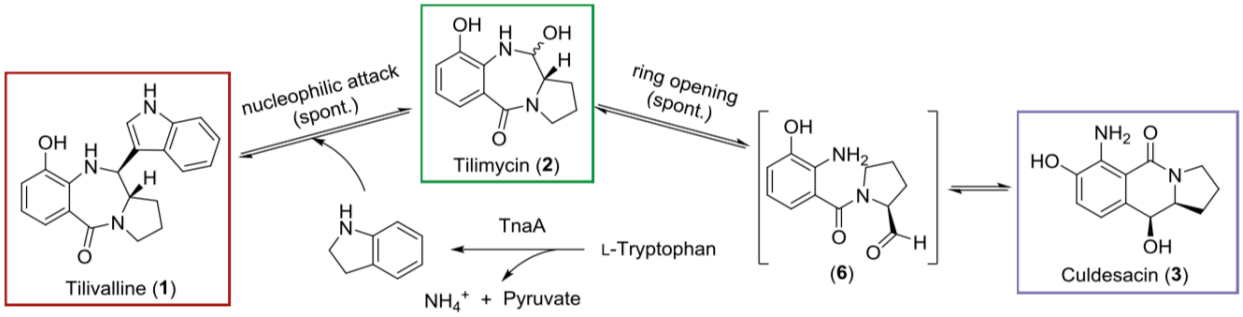

Figure 6. Chemical reactions of tilimycin (2). TM reacts to culdesacin (3) by spontaneous ring opening and to tilivalline (1) by nucleophilic attack of free indole. The free indole is released by the cleavage of L-tryptophan to indole, catalyzed by TnaA. (Figure from [94])

1.3.4 Tilimycin is a member of the pyrrolobenzodiazepine family

TM belongs to the chemical family of pyrrolo[2,1-c][1,4]benzodiazepines (PBDs) [95]. PBDs are well-known for their sequence-selective DNA interactions by forming a covalent bond to guanine bases within the minor groove of DNA. Members of PBDs like anthramycin, tomaymycin, neothramycin share a tricyclic ring system including anthranilate (A), diazepine (B), and hydropyrrole (C) moieties (Figure 7). Different substitutions at the A- and C-rings provide chemical diversity to the group of PBDs [96,97]. TM has a hydroxyl group at the C11 position [93].

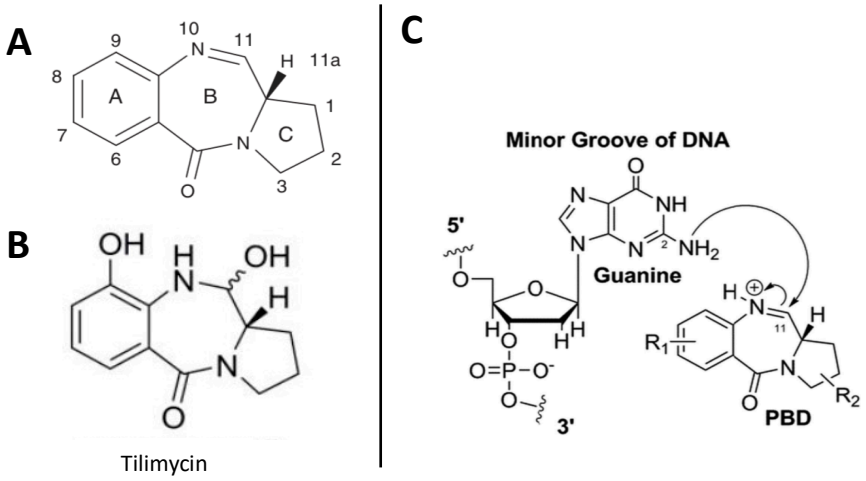

Figure 7. Basic structure of PBDs and the mechanism of binding to the DNA. (A) The basic structure of PBDs with the anthranilate (A), a diazepine (B) and a hydropyrrole (C) moieties. (B) The structure of the naturally produced tilimycin. (C) Mechanism of the nucleophilic attack of the C2–NH_2 group of a guanine residue to the N10-C11 imine moiety of PBD within the DNA minor groove. (Figure adapted from [95, 96, 97]).

Naturally occurring PBDs like anthramycin and tomaymycin span three base pairs of DNA. NMR, X-ray crystallography, molecular modeling, DNA melting experiments, and gel-based experiments, e.g. DNA footprinting, determined the binding of PBDs to DNA and disclosed a preference for binding to 5'-purine-G-purine-3' sequences [98,99]. PBDs exhibit numerous biological effects in cells including DNA strand breakage, inhibition of DNA processing enzymes (e.g., endonuclease BamH1, RNA polymerase and Ligase 1) and specific transcription factors (e.g., Sp1, NF-Y and NF-kB), and modulation of various signaling pathways (e.g., p53-dependent and -independent apoptogenic, JNK/AP-1, VEGF and SDF1a signaling) [100]. Due to their antimicrobial properties and selective cytotoxicity toward tumor cells, PBDs are regularly described as antitumor antibiotics [96,101].

The different PBD structures of TM and TV produced by *K. oxytoca* suggest different targets and cellular mechanisms during AAHC. PBDs are able to bind DNA. Therefore, it was hypothesized that TM binds and damages DNA. Compared to TM, the indole ring at the C11 atom of TV should block a possible TV-DNA interaction. In fact, Evan et al. recently confirmed an alkylation of putative N-2 guanine after TM exposure and detected a pyrrolobenzodiazepine-like N-2 deoxyguanine adduct [102].

1.3.5 Tilimycin disrupts cell cycle progression

Since TM and TV showed growth-inhibitory activities to various cell lines the group wanted to gain insights into the cellular processes and tested the effects of TM and TV on cell cycle progression. Using flow cytometry, they revealed an arrest of HeLa cells in G2/M-phase after TV treatment. In contrast, TM-treated cells were arrested in G_1 or S phase. The relative proportion of cells in different phases after TM and TV treatment compared to the solvent is shown (Figure 8) [95].

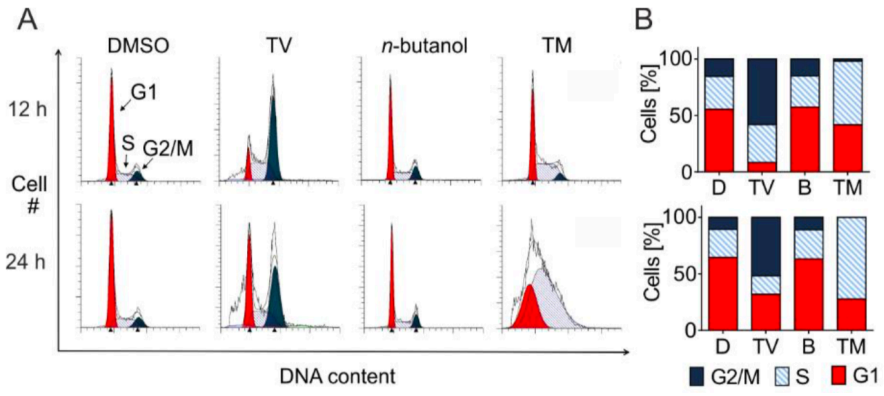

Figure 8. TV arrests cells at G2/M-phase and TM extends S-phase. HeLa cells were treated with TV (10 µM), TM (2.5 µM), DMSO (D) or *n*-butanol (B) for 12 and 24 h. DNA was quantified by flow cytometry of PI stained cells. (A) One representative cell cycle profile per treatment is shown. (B) Relative proportion of cells in phases are indicated as means (n=3). (Figure from [96])

1.3.6 Tilimycin acts as genotoxin

The accumulation of cells arrested in the G1/S-phase is consistent with a DNA damaging activity of TM. To determine the possible DNA damaging activity of TM, the group used biochemical and cellular DNA damage assays.

First, the formation of comets, which appear after DNA fragmentation, was observed. HeLa cells treated with TM and DNA-alkylating control GWL-78 formed comets but not when treated with TV or solvents. Calculation of tail DNA, tail length and tail moment revealed a significant difference in DNA from cells treated with either TM or etoposide compared to BuOH. Further, similar results were obtained with the colon cancer cell lines HT-29 and SW48 (Figure 9A) [95].To assess whether DNA fragmentation occurs in the intestinal epithelium when exposed to TM, mice were colonized (24h) with *K. oxytoca* AHC-6 (WT) or the toxin-deficient *ΔnpsB*-mutant. Comet analysis revealed a significant DNA fragmentation in enterocytes isolated from ceca of mice colonized by the WT strain, but not in the toxin-deficient mutant (Figure 9B) [95]

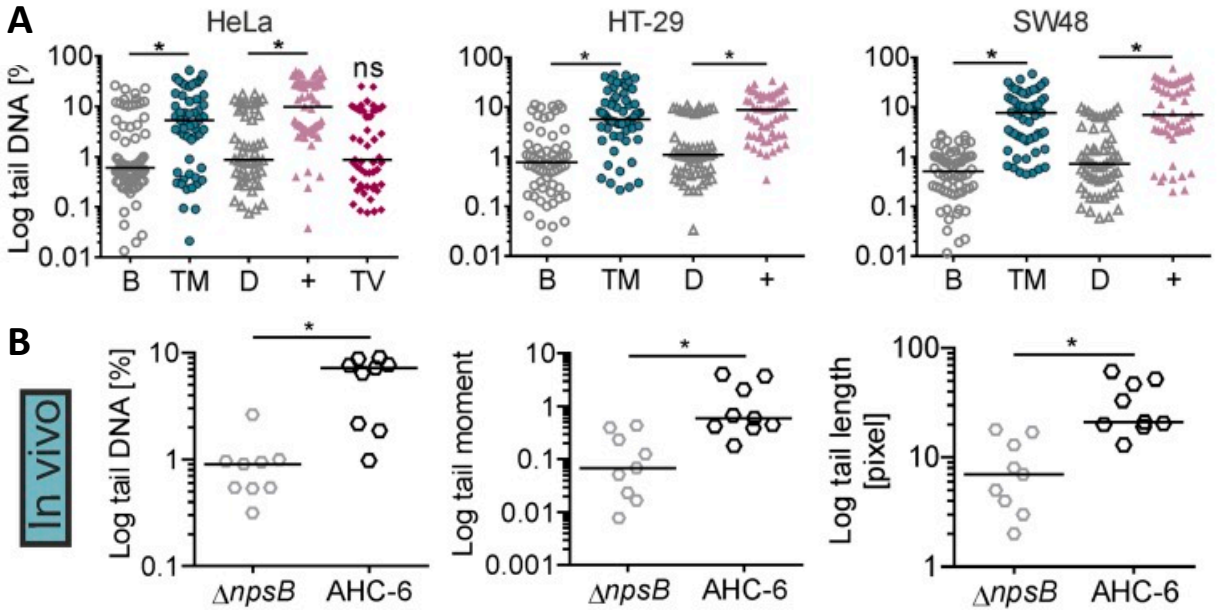

Figure 9. TM induce DNA fragmentation in vitro and in vivo. (A) Tail DNA (in percentage) for comet of HeLa treated 4 h with 10 µM TM, 10 µM GWL-78 (+), 20 µM TV, or solvents. HT-29 and SW48 cells were treated with 1 mM TM or controls. Bars represent medians of each dataset (n ≥ 50 cells). Kruskal–Wallis test followed by Dunn's multiple comparison (**P* ≤ 0.05). (B) Comet of cecal enterocytes of infected mice (24 h) showed tail DNA, tail length, and tail moment were significantly different when mice were colonized with *K. oxytoca* AHC-6 (WT) compared with the ΔnpsB-mutant. Bars represent medians of each dataset (n = 9 mice, with ≥50 cells per mouse), and significance was determined with Mann–Whitney test (**P* ≤ 0.05). (Figure from [96])

The diazepine ring of PBDs interacts with the minor groove and stabilizes double-stranded DNA (dsDNA) to thermal denaturation in vitro [100]. Incubation of DNA, containing a PBD binding site, with an equimolar amount of TM, leads to a 0.5 °C higher melting temperature (T_m), compared to BuOH. This result corresponds with the 0.7 °C T_m increase caused by DC81 (the closest structurally PBD related to TM) using calf thymus DNA [95].

Further, it was determined whether the sequence selectivity predicted for TM inhibits site-specific endonuclease activity. Cleavage of a BamHI recognition site was inhibited in a concentration-dependent manner by TM and the control GWL-78, compared to TV or buffer. In addition, TM did not inhibit endonuclease activity with an A-T-rich binding site, like SspI [95].

Since TM has been revealed to interact with DNA and induce DNA damage the group investigated the cellular DNA damage response to TM treatment. Therefore, the group analyzed the cycle checkpoint kinases CHK1 and CHK2 that are phosphorylated during DNA damage response and are control points of the complex DNA-damage response (DDR) pathway [103]. TM and GWL-78 treated HT-29 cells exhibited increased phosphorylation of both CHK1 and CHK2 (Figure 10). In addition, TM showed dose-dependent phosphorylation of CHK1 [95].

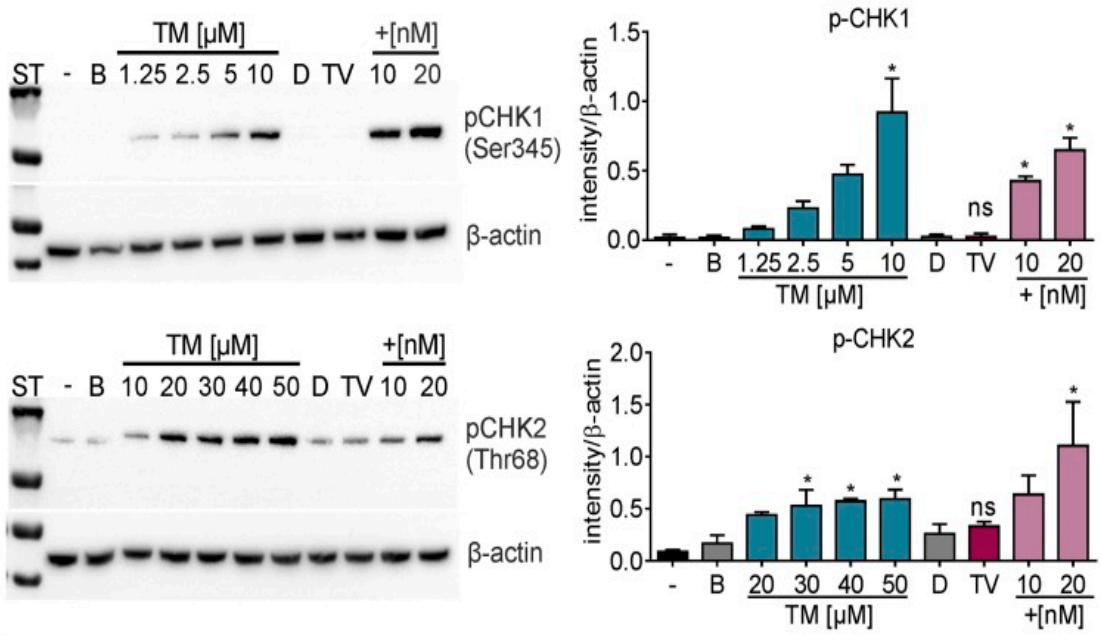

Figure 10. TM activates DNA damage response. Phosphorylated (p)-CHK1 in lysates of HT- 29 cells treated 4 h with increasing concentrations of TM, GWL-78 (+), 20 µM TV, or solvents. p- CHK2 detected in HT-29 lysates after 8-h treatment (Left). Means ± SEM of p-CHK1/2 signals obtained from three independent cell lysates normalized to β-actin are shown (Right). One-way ANOVA followed by Sidak's multiple comparison (*$P \leq 0.05$) (ns = not significant). (Figure from [96]

The next step was to characterize the recognition and repair of TM-induced DNA damage in host cells. Therefore, inactivating mutations of different genes encoding key repair factors were generated in the human haploid cell line HAP1. An equal number of cells with different mutations were cultured with increased concentrations of TM, TV, or control, and the cell viability was measured. Illudin S was used as DNA-alkylating control. Mutant cells lacking the Cockayne syndrome group A or B (CSA or CSB) showed hypersensitivity to TM compared to the wild-type survival [95]. CSA and CSB are genes involved in transcription-coupled repair (TCR), a sub-pathway of nucleotide excision repair (NER) that removes lesions from the template DNA strand of actively transcribed genes [104]. Mutant cells lacking the NER factor xeroderma pigmentosum protein A (XPA), which mediates TCR downstream of CSA/B, revealed a significantly enhanced sensitivity to TM. Mutant cell lines tested with TV exhibited no lower viability compared with the wild type, however mutant cells treated with the control illudin S showed sensitivity similar to TM (Figure 11A and B). Illudin S induced DNA lesions are poorly recognized by the global genome repair (GGR) of NER but can be efficiently repaired by TCR [105]. In addition, a long-term colony formation assay was performed to confirm the results of the short-term assay (Figure 11C and D). HAP1 cells lacking CSA, CSB, and XPA were significantly more sensitive to TM.

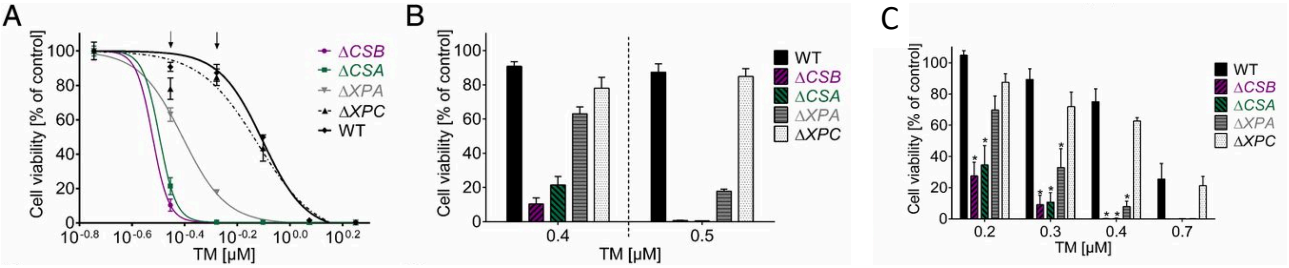

Figure 11. TM induces hypersensitivity in human DNA repair-deficient cells and causes DNA lesions in vivo. (A) Dose–response survival curves of TM-treated mutants deficient in CSA, CSB, and XPA, but not XPC, show TM hypersensitivity compared with wild type (WT). Values are normalized to solvent controls and represent means ± SEM of three technical replicates. Data from one of three biological replicates are shown. (B) Cell viability shown as means ± SEM at two assay concentrations (indicated with arrows in A). (C) Colony formation by cells treated with different concentrations of TM before recovery in drug-free medium. Values were normalized to solvent. Means ± SEM are shown (n = 3). Significance of results for mutants compared with WT was determined with one-way ANOVA followed by Sidak's multiple comparison (*P ≤ 0.05).

These results indicate that TCR proteins are able to recognize DNA lesions caused by TM. In addition, the group identified the TCR as a mechanism of DNA damage recognition in vivo [95].

1.3.7 Tilimycin show antibacterial activities toward other gut residents

Since TM was identified as a DNA-damaging agent it can be hypothesized that it also damages the DNA of bacteria. The group next asked whether TM affects other bacteria. An antimicrobial assay was performed according to a protocol of the Clinical and Laboratory Standards Institute (CLSI) using Curam® as positive antibiotic control and methanol as negative solvent control [106]. Interestingly, initial results showed that TM inhibited growth of various anaerobic bacteria, which are inhabitants of the human gastrointestinal tract, but exhibited no antimicrobial effects on aerobic strains (Table 2). Additionally, TM not only inhibited growth of human gut commensals, *like Bifidobacterium longum* or *Lactobacillus acidophilus* but also exerted an antimicrobial effect against pathogens such as *Bacteroides fragilis*, *Propionibacterium acnes*, *Fusobacterium nucleatum*, and *Yersinia enterocolitica*. Besides TM, TV was used for the antimicrobial assay. However, TV showed no antimicrobial effect (Table 2). The antimicrobial activity of TM toward other gut residents gives rise to the notion that TM provides an advantage to *K. oxytoca* during homeostasis [95].

Table 2. Bacterial susceptibility to TM and TV. Bacterial strains for antimicrobial assay and inhibition zones caused by TM or TV. Means ±SD are shown (values in upper box TM n=3, TV n=2; lower box n=1); n.d. not determined. (Table adapted from [95])

		Inhibition zone [mm]		
Strain	**Gram**	**TM (40 µg)**	**TV (50 µg)**	**Phylum**
Bifidobacterium longum	-	18 ± 2	0	*Actinobacteria*
Bifidobacterium bifidum	+	18 ± 3	0	*Actinobacteria*
Bacteroides fragilis	-	24 ± 3	0	*Bacteriodetes*
Pediococcus acidilactici	-	12 ± 1	0	*Firmicutes*
Lactobacillus acidophilus	+	24 ± 4	0	*Firmicutes*
Fusobacterium nucleatum	-	27 ± 1	0	*Fusobacteriia*
Proteus mirabilis	-	15 ± 1	0	*Proteobacteria*
Yersinia enterocolitica	-	17 ± 2	0	*Proteobacteria*
Enterobacter cloacae	-	0	0	*Firmicutes*
Staphylococcus aureus	+	0	0	*Firmicutes*
Enterococcus faecalis	+	0	0	*Firmicutes*
Escherichia coli	-	0	n.d.	*Proteobacteria*

2 Aim and objectives of this study

The genotoxin tilimycin of *K. oxytoca* is generating considerable interest due to distinct host DNA damaging and antimicrobial activities. Traditionally, antibiotic-producing bacteria possess self-resistance mechanisms leading to the suggestion that *K. oxytoca* itself is equipped with resistance mechanisms against its own TM product. This study aims to characterize the underlying self-resistance mechanisms of *K. oxytoca* against the genotoxin TM. Tilimycin-producing *K. oxytoca* strains share a PAI where essential genes for TM production and the two putative immunity genes *mfsX* and *uvrX* are localized. Our knowledge of these immunity genes is largely based on gene homology comparison. In this work, we planned to examine the action and expression of *mfsX* and *uvrX* regarding TM-resistance. For this analysis, we chose an in vitro genetic approach by complementation.

Previous gene homology comparison of *uvrX* revealed strong similarity to *Streptomyces peucetius drrC*, which encodes an UvrA-like protein. Therefore, we hypothesized that *K. oxytoca* UvrX functions similarly to the related proteins *S. peucetius* DrrC and *E. coli* UvrA. To investigate the molecular mechanism of UvrX regarding resistance we predicted its protein structure and analyzed the structural similarity between UvrX, DrrC, and UvrA.

It is well-known that antibiotic-producing organisms possess a biosynthetic gene cluster including the antibiotic synthesis genes and co-regulated immunity genes. The *til* gene cluster of *K. oxytoca* shares this organization. Therefore, we hypothesized that expression of the putative immunity genes is coordinately regulated with the TM biosynthesis gene expression. Here we aimed to establish the qRT-PCR method to monitor the in vitro gene expression profile of one toxin synthetase gene and the immunity genes in *K. oxytoca*.

3 Material and Methods

3.1 Strains, plasmids and oligonucleotides

Table 3. Bacterial strains used in this study, with number (#) in the AGZechner strain collection.

#	Strain	Plasmid	Relevant genotype	Reference
18	*E. coli* DH5α	-	ΔlacZ,	[107]
2197	*E. coli* DH5α	pBlue_UHF_TetRA_to_DHF	Amp_R, Tet_R, Cm_R	this study
2207	*E. coli* DH5α	pBAD33_*uvrX*_long	Amp_R, Cm_R	this study
2034	*E. coli* DH5α	pBAD33_*mfsX*	Amp_R, Cm_R	this study
2214	*E. coli* DH5α	pBAD33_*mfsX_uvrX*_l	Amp_R, Cm_R	this study
2078	*K. oxytoca* AHC-6 *aphA*	-	intergenic *aphA* (Kan_R); 5188::Tn5 (intergenic region between *gcvA* and *mfsX*)	[86]
2043	*K. oxytoca* AHC-6 Mut89	-	Kan_R; *npsB*::Tn5	[86]
2217	*K. oxytoca* AHC-6 Mut89	pBAD33	Kan_R; *npsB*::Tn5, Cm_R, Amp_R	[86]
1987	Keio *E. coli* JW0001_1 (parental strain)	-	Cm_R	[108]
2199	Keio *E. coli* JW0001_1	pBAD33	Cm_R, Amp_R	this study
2200	Keio *E. coli* JW0001_1	pBAD33_*uvrX*	Cm_R, Amp_R	this study
2210	Keio *E. coli* JW0001_1	pBAD33_*uvrX*_long	Cm_R, Amp_R	this study
1989	Keio *E. coli* JW4019_2	-	Δ*uvrA*, Kan_R	[108]
2201	Keio *E. coli* JW4019_2	pBAD33	Δ*uvrA*, Kan_R, Cm_R, Amp_R	this study
2202	Keio *E. coli* JW4019_2	pBAD33_*uvrX*	Δ*uvrA*, Kan_R, Cm_R, Amp_R	this study
2211	Keio *E. coli* JW4019_2	pBAD33_*uvrX*_long	Δ*uvrA*, Kan_R, Cm_R, Amp_R	this study
2212	Keio *E. coli* JW4019_2	pBAD33_*uvrA*	Δ*uvrA*, Kan_R, Cm_R, Amp_R	this study
2010	*K. oxytoca* AHC-6 Mut89 Δ*uvrX*	-	Kan_R; *npsB*::Tn5, Δ*uvrX*, Tet_R	from Sandra
2038	*K. oxytoca* AHC-6 *aphA* Δ*uvrX*	-	intergenic *aphA* (Kan_R), Δ*uvrX*, Tet_R	this study

2206	*K. oxytoca* AHC-6 Mut89 Δ*mfsX*, Δ*uvrX*	-	Kan_R; *npsB*::Tn5, Δ*mfsX* (78-1223), Δ*uvrX* (1-50), Tet_R	this study
2219	*K. oxytoca* AHC-6 Mut89 Δ*mfsX*, Δ*uvrX*	[pBAD33]	Kan_R; *npsB*::Tn5, Tet_R, Cm_R, Amp_R	this study
2221	*K. oxytoca* AHC-6 Mut89 Δ*mfsX*, Δ*uvrX*	[pBAD33_*uvrX*_long]	Δ*mfsX* (78-1223), Δ*uvrX* (1-50), Tet_R, Cm_R, Amp_R	this study
2220	*K. oxytoca* AHC-6 Mut89 Δ*mfsX*, Δ*uvrX*	[pBAD33_*mfsX*]	Kan_R; *npsB*::Tn5, Tet_R, Cm_R, Amp_R	this study
2222	*K. oxytoca* AHC-6 Mut89 Δ*mfsX*, Δ*uvrX*	[pBAD33_*mfsX_uvrX*_l]	Δ*mfsX* (78-1223), Δ*uvrX* (1-50), Tet_R, Cm_R, Amp_R	this study
2213	*K. oxytoca* AHC-6 *aphA* Δ*mfsX*, Δ*uvrX*	-	intergenic *aphA* (Kan_R), Δ*mfsX* (78-1223), Δ*uvrX* (1-50), Tet_R	this study

Amp_R, Cm_R, Kan_R, Tet_R: antibiotic resistance markers

Table 4. Plasmids used in this study, with number (#) in the AGZechner strain collection.

#	Plasmid	Description	Reference
454	pBluescript II Ks(-)	Amp_R, *lacZ*, T7 Promotor	Stratagene
1185	pBlue_UHF_TetRA_t0_DHF	Amp_R, Tet_R, *lacZ*::recombination cassette for *mfsX* and *uvrX;* upstream homologous fragment "UHF" (derived from *K. oxytoca* AHC-6 *aphA*; 412 nts noncoding region upstream of *mfsX* and 1-77 nts of *mfsX*); downstream homologous fragment "DHF" (derived from *K. oxytoca* AHC-6 *aphA*; 51-555 nts of *uvrX*), t0 terminator; TetRA	this study [109]
1106	pBlue_PMF_mono (pBlue_PMF_DHF)	Amp_R, Tet_R, *lacZ*::homologous fragments of *mfsX* and *hmoX* (*uvrX* recombination cassette)	from Nina Rupar [110]
1107	pBlue_PMF_TetRA_mono (pBlue_PMF_TetRA_DHF)	Amp_R, Tet_R, *lacZ*::recombination cassette for *uvrX*	[110]
1109	pBlue_UHF_DHF (pBlue_A_mono)	Amp_R, Tet_R, *lacZ*::homologous fragments of *mfsX* and *hmoX* (*mfsX*, *uvrX* recombination cassette)	[110]
1082	pBAD33	Cm_R, *araC*, P_{BAD}	[1]
1111	pBAD33_*uvrA*	Cm_R, *araC*, P_{BAD}, *uvrA* in MCS	from Zana Lousin

	pBAD33_*uvrX*	Cm_R, *araC*, P_{BAD}. *uvrX* in MCS; *uvrX* consisting of nt 6850 -9069 according to [109] (here also called *uvrX7G*)	from Alexandra Moik
1186	pBAD33_*uvrX*_long	Cm_R, *araC*, P_{BAD}. *uvrX* in MCS; *uvrX* consisting of nt 6850 - 9146 with an additional G at position 9020 according to [109] (includes a 36 nt non-coding region downstream of *uvrX*) (here also called *uvrX8G*)	this study
1114	pBAD33_*mfsX*	Cm_R, *araC*, P_{BAD}, *mfsX* in MCS consisting of nt 5613 - 6842 according to [109]	this study
1187	pBAD33_*mfsX_uvrX*_l	Cm_R, *araC*, P_{BAD}, *mfsX, uvrX* in MCS (nt 5613 - 9146 with an additional G at position 9020 according to [109]; includes a 36 nt non-coding region downstream of *uvrX*)	this study
217	pAR183	Km_R, Tet_R	[111] [1]
94	pKOBEG	*cat, araC, gam, bet, exo,* Cm_R, P_{BAD}	[2]
	pAR123	t_0 terminator, Amp_R, Tet_R	[3]

[1] Plasmid from Sandra, [2]already in strains; [3] isolated from strain *E. coli* K12 JM101 [pAR123], Amp_R, Cm_R, Tet_R: antibiotic resistance marker

Table 5. Oligonucleotides used in this study, with the number (#) in the oligonucleotide collection. Sequences complementary to the target are underlined and restriction sites are written in bold.

#	Oligonucleotide	Sequence (5' → 3')	Target
909	T7 terminator	GCTAGTTATTGCTCAGCGG	T7 terminator fragment
910	T7 promotor	TAATACGACTCACTATAGGG	T7 promotor
1169	rrnB_rev	GTATCAGGCTGAAAATCTTCTC	rrnB terminator fragment
1175	pBAD_araC_fw	CTGGCTCTTCTCGCTAAC	araC [pBAD33]
1686	M13_rev	CAGGAAACAGCTATGAC	M13 region
1726	GcvA_do_fw	GGTAAACAGTGAAGGTGAGTG	*mfsX, uvrX* upstream homologous fragment
2259	TetSeq2	TACAGGGAGTGATGTCTATCC	TetRA
2393	PMF_BamHI_r	TAT**GGATC**CCACACTATCCTTTTTTACCTG	*mfsX*
2395	Mono_PstI_r	TTA**CTGCAG**GTTTAGCCTACCGTTGGTTTATG	*hmoX*

2396	BamHI_Ucas	ATA**GGATCC**CAAGAATTGCCGGCGGAT	TetRA resistance cassette
2397	BamHI_Dcas	tta**GGATCC**GGTATTTCACACCGCATAGC	TetRA resistance cassette
2411	TetSeq1	CAATTCAAGGCCGAATAAG	TetRA
2412	mfsX_fw	CCACTCTGCTCAGTAGTC	mfsX
2413	hmoX_fw	AACCTCTTCTGGGCCATAAG	*hmoX*
2414	uvrX_rev	ATGGTATTGCCTTTGTCGC	*uvrX*
2415	uvrX_fwd	TTGGATGCCATGTGTGCAG	uvrX
2416	SacI_RBS_uvrX_fw	ATTC**GAGCTC**GCAGGAGGAATTCACCATGAAAA CCCATGACGCTATAAAAATC	*uvrX*
2470	SacI_RBS_mfsX_fw	ATTC**GAGCTC**GCSGGSGGSSTTCACCATGCGACC GAAAGAAGTTCAGG	*mfsX*
2470	SacI_RBS_mfsX_fw	ATTC**GAGCTC**GCAGGAGGAATTCACCATGCGAC CGAAAGAAGTTCAGG	*mfsX*
2471	SphI_mfsX_rev	AGCTT**GCATGC**CTATCCTTTTTTACCTGTCAATAA CAATGC	*mfsX*
2472	SphI_HIS_mfsX_rev	AGCTT**GCATGC**CTAATGATGATGATGATGATGTC CTTTTTTACCTGTCATAACAATGC	*mfsX*
2475	GcvA_do_fwd_NotI	TTA**GCGGCCGC**GGTAAACAGTGAAGGTGAGTG	*mfsX, uvrX* upstream homologous fragment
2476	GcvA_do_rev_BamHI	TTT**GGATCC**TTACTGGAAAGCAAACCTCTACT	*mfsX*
2477	SacI_RBS_HIS_mfsX_ fwd	ATTC**GAGCTC**GCAGGAGGAATTCACCATGCATC ATCATCATCATCTCGACCGAAAGAAGTTCAGG	*mfsX*
2516	BamHI_t0_fw	CGACT**GGATCC**CGAAAAGAGAGACCACATGG	t0 terminator fragment
2517	SalI_t0_rev	GCTTA**GTCGAC**GGTATTTCACACCGCATAGC	t0 terminator fragment
2518	NheI_uvrX_fw	ATA**GCTAGC**GCAAGATATTGATGTAGAGGTCC	*mfsX, uvrX* downstream homologous fragment (*uvrX*)
2519	SalI_uvrX_rev	TTA**GTCGAC**TGAATAAACATAACGTTTCCAGCG	*mfsX, uvrX* downstream homologous fragment (*uvrX*)
2520	HindIII_TetRA_rev	TTA**AAGCTT**GGAATAACATCATTTGGTGACGAA	TetRA resistance cassette

2521	DHF_uvrX_rev	TGAATAAACATAACGTTTCCAGCG	*mfsX, uvrX* downstream homologous fragment (*uvrX*)
2530	SphI_uvrX_long_rev	AGCTT**GCATGC**CTATTGCCAGTCTCTACTGGCTG	*uvrX*
2584	qRT_npsA_1_f	GTGGTGTCGGGAGACTTTGT	*npsA*
2585	qRT_npsA_1_r	ACCACCATCTCAACCAGAGG	*npsA*
2572	qRT_gapA_1_f	AGTGGGTGTTGACGTTGTTG	*gapA*
2573	qRT_gapA_1_r	GAAACGATGTCCTGGCCTTC	*gapA*
2554	qRT_uvrX_1_f	AACCGTACGACCCCTAGCTT	*uvrX*
2555	qRT_uvrX_1_r	GCCTTTGTCGCGTAGTTTTC	*uvrX*
2550	qRT_mfsX_1_f	ATTGGGCAGCTGTTTATTGG	*mfsX*
2551	qRT_mfsX_1_r	TCGGGAAAGAACGATACCAG	*mfsX*
2578	qRT_marR_1_f	GTTCCAGCCGATGACTCCAA	*marR*
2579	qRT_marR_1_r	GCAATCTCTCCCTGCGACAT	*marR*
2590	qRT_mdh_1_f	GCGTCGGGATTATCACCAAC	*mdh*
2591	qRT_mdh_1_r	CCTTTCAGTTCCGCCACAAA	*mdh*
2596	qRT_rpoB_1_f	CAGATCAGCTCGCCAGTAGA	*rpoB*
2597	qRT_rpoB_1_r	GTACGTTGAGAAAGGACGCC	*rpoB*
2604	16SrRNA_eco_fw	GCCTAACACATGCAAGTCGAA C	16S rRNA
2605	16SrRNA_eco_rev	TGCGGTATTAGCTACCGTTTCC	16S rRNA
2602	qRT_proC_f	TGGCCAGGCGGAAATTATTG	*proC*
2603	qRT_proC_r	CACACCATATCCTTCAGCGC	*proC*
2600	qRT_rho_f	CTGTTGCGATGATGGTCAGG	*rho*
2601	qRT_rho_r	TCGACTCGATTACCCGTCTG	*rho*

3.2 Growth Conditions

E. coli strains were grown on LB-agar plates or in LB broth and *K. oxytoca* strains were grown on CASO-agar plates or in CASO bouillon. All liquid cultures were incubated at 37°C with shaking under aerobic conditions. Plasmid-containing strains or strains containing chromosomal selection markers were grown with antibiotic selection (Table 6). Additionally, *K. oxytoca* strains were

grown on M63 minimal media with all amino acids except tryptophan and proline (Concentrations: 200mg/100ml of leucine and 300 mg/100ml of the other amino acids).

Table 6. Antibiotics and concentrations used in this study

Antibiotics	Concentration [µg/ml]
Ampicillin (Amp)	100
Tetracycline (Tet)	16 and 12 for recombination experiment
Chloramphenicol (Cm)	10 - 40
Kanamycin (Kan)	40

3.3 DNA methods

3.3.1 DNA purification

Kits from QIAGEN were used for all DNA purifications. The DNeasy Blood&Tissue Kit were used for chromosomal DNA isolation of *K. oxytoca* AHC-6 *aphA*. Plasmid extraction from *E. coli* DH5α was achieved via QIA prep^R Spin Miniprep Kit. DNA extraction and purification were performed with QIA quick^R PCR Purification Kit and QIA quick^R Gel Extraction Kit. Concentration of the purified DNA were measured on the *NanoDrop* Spectrophotometer.

3.3.2 Polymerase chain reaction (PCR)

DNA fragments used for cloning were amplified with 'Phusion High-Fidelity Polymerase' from New England Biolabs Inc. (NEB) according to manufacturer's manuals. The NEB 'Taq DNA Polymerase' was used for colony and other control PCRs. Annealing Temperatures of primers were calculating via the inline tool 'NEB Tm Calculator'. For colony PCR a single colony was resuspended in 30 µl Fresenius water, heated at 95°C for 10 min, centrifuged (30 s, 13.000rpm) and 2 µl were used in the PCR reaction.

3.3.3 Other enzymatic reactions

Restriction digestions were performed using restriction enzymes from NEB and the 'T4-DNA Ligase' from LifeTech Austria was used for ligation reactions. All enzymes were used according to manufacturer's manuals.

3.3.4 Agarose gel electrophoresis

In this study agarose gels (0.8 % to 1.2 %) containing 1xTAE were used and supplemented with 0.05 µg/ml ethidium bromide. Running buffer was 1xTAE and electrophoresis was performed with 5-10 V/cm. GeneRuler 100bp DNA ladder or 1kb Ladder were used as DNA markers.

3.3.5 Preparation of plasmid DNA and purification

Qiagen QIAprep® SPin Miniprep Kit was used for all plasmid DNA preparations, Qiagen QIAquick® PCR purification Kit was used to purify PCR products and Qiagen QIAquick® Gel Extraction Kit was used for DNA extraction from the agarose gel slices. All Kits were used according to the manufacturer's manuals.

3.3.6 Sequencing

Chromosomal or plasmid DNA was isolated from an ONC and the concentration was determined via NanoDrop® Spectrophotometer. Sequencing was performed by Microsynth according to their protocol.

3.4 Electrotransformation

3.4.1 Generation of electrocompetent *E. coli* cells

Electrocompetent *E. coli* cells were generated by inoculation of 100 ml LB medium with 1ml of a *E. coli* overnight culture. The cells were incubated at 37°C to an OD_{600} of 0.5 - 0.7. The culture was put on ice for 10 min, split in 50 ml and centrifuged (5000 rpm, 10 min, 4°C). The pellets were resuspended in 50 ml ice-cold 10% glycerol and centrifuged again. The washing step was repeated twice with 25 ml and 1 ml ice-cold 10% glycerol. After the last washing step, the pellets were pooled and resuspended in 400 µl and split in aliquots of 80 µl.

3.4.2 Generation of electrocompetent *K. oxytoca* cells

For the transformation of *K. oxytoca* AHC-6 cells were made electrocompetent. 100 ml of CASO media containing 0.7 mM EDTA were inoculated with an overnight culture to an OD_{600} of 0.05. The cells were incubated at 37°C. After reaching an OD_{600} of 0.6-0.7 the culture was split into two 50 ml Greiner tubes and put in ice for 10 min. After centrifugation with 5000 rpm for 20 min at 4°C the pellets were resuspended in 50 ml ice-cold 10% glycerol. The resuspensions were centrifuged with the same conditions and the pellets were resuspended in 10 ml ice-cold 10%

glycerol. The resuspensions were centrifuged again with the same conditions and the pellets were resuspended in 2.5 ml ice-cold 10% glycerol. After the last washing step, the two pellets were resuspended together in 100 µl 10% glycerol. The cells were split in 80 µl aliquots and stored at -20° or used straight away for transformation.

3.4.3 Transformation of *E. coli* and *K. oxytoca* cells

For the transformation 40 µl of electrocompetent *E. coli* cells were thawed on ice for 10 min and mixed with 10-200 ng of the plasmid in a cold electroporation cuvette and electroporated at 1800 Volt. Immediately after the electroporation 1 ml of preheated LB media was added and the cells were incubated for 1h at 37°C. After regeneration, dilutions were prepared and plated on LB agar plates with the relevant antibiotics and incubated overnight at 37°C.

Electrocompetent *K. oxytoca* cells were transformed similarly. For transformation 80 µl of electrocompetent cells were transformed with 20-60 ng of plasmid and electroporated at 2000 Volt. The transformed cells were regenerated in 1 ml CASO media with 0.7 mM EDTA for 1 ½ h at 37°C.

3.5 Knock-out via the lambda red recombination system

3.5.1 Homologous recombination

K. oxytoca AHC-6 *aphA* [pKOBEG] and *K. oxytoca* AHC-6 Mut89 [pKOBEG] cells were grown at 30°C in 100ml of CASO media with 0.7 mM EDTA and 30 µg/ml Cm starting from OD_{600}=0.05. After reaching an OD_{600} of 0.2, 0.2% arabinose was added to induce the expression of the phage λ recombination genes. After 2 h of incubation the culture was split in two 50 ml Greiner tubes and put on ice for 10 min. After centrifugation with 5000 rpm for 20 min at 4°C the pellets were resuspended in 50 ml ice-cold 10% glycerol. The resuspensions were centrifuged under the same conditions and resuspended in 10 ml ice-cold 10% glycerol. The two suspensions were pooled, centrifuged and resuspended in 5 ml ice-cold 10% glycerol. Again, the suspensions were pooled and centrifuged. After the last wash step, the pellet was resuspended in 250 µl ice-cold 10% glycerol and used straight away for recombination.

For the transformation, 80 µl of fresh electrocompetent *K. oxytoca* AHC-6 *aphA* [pKOBEG] and *K. oxytoca* AHC-6 Mut89 [pKOBEG] cells were mixed with 100-600 ng of the recombination cassette on ice and transformed via electroporation at 2000 Volt. Immediately after the electroporation 1

ml CASO-media or M63-media with 0.7mM EDTA and 0.2% arabinose were added, and the cells were incubated for two h at 30°C. Then the cells were centrifuged and resuspended in 300 µl CASO-media or M63-media. 100 µl of cells were plated on CASO and M63 with 16 µg/ml Tet and incubated overnight at 30°C.

3.5.2 Knockout design for *K. oxytoca* AHC-6 Δ*mfsX, uvrX*

The plasmid pBluescript_UHF_DHF (pBlue_A_mono) was chosen as start vector for cloning the recombination cassette because this vector already had the upstream homologous fragment UHF (derived from *K. oxytoca* AHC-6 *aphA*; 412 nts noncoding region upstream of *mfsX* and nts 1 to 77 of *mfsX* [nts 5201-6845 [109]) for recombination. We amplified 500 nt of *uvrX* for the downstream homologous fragment (DHF*;* nt 50-555) with NheI_uvrX_fw and SalI_uvrX_rev and inserted it downstream of a tetracycline resistance cassette (TetRA) amplified from pAR183 (BamHI_Ucas and HindIII_Tet_rev) and a t0 terminator sequence amplified from pAR124 (BamHI_t0_fw and SalI_t0_rev).

We digested the PCR products with the respective restriction enzymes and ligated them into the digested pBlue_UHF_DHF. The t0 terminator sequence was ligated in the pBlue_UHF_DHF downstream of the already inserted UHF (exchange of DHF with t0 terminator sequence) to prevent the expression of the downstream part of *uvrX*. The downstream homologous fragment was ligated in the pBlue_UHF_t0 downstream of the t0 terminator sequence and the TetRA between the t0 terminator and the UHF. The *mfsX, uvrX* recombination cassette was amplified via PCR with GcvA_do_fwd and DHF_uvrX_rev using the pBlue_UHF_TetRA_t0_DHF as template. We digested the amplified recombination cassette with DpnI to remove residual template plasmid to earn only the linear DNA fragment for transformation.

3.6 Design of complementation vectors

As complementation vectors we used the pBAD33. We amplified the particular gene from the *K. oxytoca* AHC-6 *aphA* genomic DNA using the corresponding primer pairs listed in Table 3. Resulting gene products and pBAD33 were digested with SacI and SphI for ligation. The pBAD33 vector contains the P_{BAD} promotor of the *araBAD* (arabinose) operon and the regulator of this promotor, *araC*. The expression can be induced by addition of 0.2% arabinose.

3.7 Cell viability assay

To study the effect of TM on different *E. coli* and *K. oxytoca* AHC-6 Mut89 strains, we performed a cell viability assay. We inoculated 5 ml of LB media containing 0.4% arabinose and 40 µg/ml Cm with an *E. coli* overnight culture to an OD_{600} of 0.2. Afterwards, 0.5 ml culture were either treated with TM or ethanol as control and filled up with media to 1ml to a final concentration of 85 µM TM or 0.58% ethanol. After incubation for 2h at 37°C dilutions were plated on LB agar plates with the relevant antibiotics. The cell viability was scored as CFU/ml after incubation overnight at 37°C.

The cell viability of *K. oxytoca* AHC-6 Mut89 strains were determined similarly with the exception of a longer treatment time of 16h and the use of M63 media with 40 µg/ml Kan or 16 µg/ml Tet to avoid a conversion of TM to tilivalline and a possible recombination (of genes from plasmid back into the genome).

3.8 RNA methods and qRT-PCR

3.8.1 qRT-PCR

To monitor the gene expression profile of a representative biosynthesis gene (*npsA*), the immunity genes (*mfsX, uvrX*) and the gene *marR* we applied quantitative real-time PCR (qRT-PCR). We used the following in vitro culture conditions. 100 ml CASO media were inoculated with cells from overnight culture in M63 (to prevent toxin production) to an OD_{600} of 0.05. To harvest cells, we centrifuged an OD_{600} of 0.1 at 5000 g and resuspend the pellet in 500 µl M63 media. For cell lysis and RNA isolation the RNAprotect® Bacteria Reagent and RNeasy® Protect Bacteria Kits from QIAGEN were used. The extracted RNA concentration was measured via NanoDrop®. The RNA integrity was assessed via denaturing agarose electrophoresis of the isolated RNA. DNase I digestion was performed with the TURBO DNA-*free*™ Kit from Invitrogen using 2.2 µg of RNA. Immediately afterwards we transcribed 800 ng RNA to cDNA using the RevertAID First Strand cDNA Synthesis Kit from ThermoFisher Scientific and diluted the cDNA 1:3. All enzymes were used according to manufacturer's manuals. After reverse transcription we performed a control PCR to test the cDNA quality. Melting curve analysis was performed to confirm the specificity of each reaction. qRT-PCR of candidate genes was performed by using SYBR Green PCR Master Mix and 33.3 µg of cDNA. Real-time PCR conditions were as follows: 95°C for 10 min, 40 cycles of 95°C for 15 s and 60°C for 60, 50°C for 30 s and 65°C for 5 s performed on a CFX Connect Real-Time PCR Detection System (Biorad). Primers were designed by the Primer3 software and are

listed in Table 5. No template control (NTC) and no reverse transcription control (RT-) were also performed. After PCR amplifications, the threshold cycle (C_T) was calculated using CFX Manager software (Biorad). The target gene mRNA levels were normalized internally to the level of the reference gene 16S rRNA. To calculate the fold difference of target gene expression we used the Pfaffl-Method (normalized to timepoint 0.5 h). Therefore, qRT-PCR analysis was performed for serially diluted cDNA template of each gene to assess the efficiency of the amplification. qRT-PCR analysis was performed in technical triplicates for each cDNA sample.

3.9 Denaturing agarose gel electrophoresis

To study the integrity of isolated RNA, a denaturing agarose gel electrophoresis was performed.

3.9.1 Sample preparation

In total, 500 ng of RNA per sample was used and filled up with nuclease-free water to a total volume of 5 µl. 15 µl of sample buffer and 3 µl of loading buffer were added to the samples and denatured for 10 min at 65°C. The samples were immediately cooled on ice and the whole amount loaded on the gel. The gels were run for 1.5 h at 50 V.

3.9.2 Buffers

For the denaturing agarose gel electrophoresis agarose gels were prepared to a final concentration of 1.2% with 1xMOPS and 0.036 µl/ml formaldehyde (37%).

Table 7. Buffers used for RNA sample preparation

Buffer	Components
Sample Buffer	1 ml formamide 350 µl formaldehyde (37%) 200 µl 10xMOPS
Loading Buffer	for 1 ml: 500 mg glycerol (87%, water-free) 2 µl 0.5 M EDTA; pH 8 200 µl 1% bromophenol blue 70 µl 10 µg/µl ethidium bromide add nuclease-free water to 1g
10x MOPS; pH 7	2 M MOPS; pH 7

	3 M NaAc; pH 7 0.5 mM EDTA; pH 8

3.10 Computational methods

For 3D protein structure prediction, the amino acid sequence of *K. oxytoca* AHC-6 UvrX was analyzed via the Phyre2 web-based server [112]. The prediction was based on the best hit from Phyre2: the structure of UvrA2 from *Deinococcus radiodurans* (PBD ID: 2VF7). The output file was improved using the 3D refine server [113]. The quality of the final structure prediction was controlled using the Procheck web-based server [114]. The predicted protein structure of UvrX was visualized with PyMOL and then compared to the 3D structure of UvrA1 and UvrA2 from *Deinococcus radiodurans* and DrrC from *Streptomyces peucetius* [115].

The NCBI's Conserved Domain Database (CDD) was used to find conserved protein domains of UvrX. Therefore, we entered the protein sequence of UvrX and searched against the CDD database using the default settings [116].

The BLAST Web server was used to find similarities between sequences. The Standard Nucleotide BLAST (blastn) was utilized to compare nucleotide sequences to the standard database of nucleotide collection. Megablast was selected to optimize the comparison for highly similar sequences. Protein sequences were compared to the database containing Non-redundant protein sequences via the algorithm blastp. The algorithm parameters were set to the default settings [117]. Restriction to a subset of entries (taxonomic groups) were described in the next section.

DNA and protein alignments were generated via Clustal Omega or EMBOSS Needle (default settings) of the EMBL-EBI web server and colored via the web program Boxshade [118].

4 Results

4.1 *E. coli* Δ*uvrA* is hypersensitive to TM

Since *K. oxytoca* tilimycin had been identified as a DNA-damaging agent with antimicrobial activities toward other gut residents we aimed to examine the TM-resistance of the Keio *E. coli* parental stain and Keio *E. coli* with mutations in *uvrA* [119]. We expected that the *E. coli* Δ*uvrA* mutant should be more sensitive to TM compared to the WT because UvrA is involved in DNA repair by nucleotide excision repair. To test this hypothesis, we treated Keio *E. coli* strains with TM and the viable counts were determined.

To establish the best TM concentration for the cell viability assay we treated Keio *E. coli* WT [pBAD33] and Δ*uvrA* [pBAD33] for 2h with three concentrations of TM (42.5, 85, and 170 µM TM). These concentrations are lower, higher or correspond approximately to the in vivo enterotoxin concentration of patient samples during the acute phase of AAHC. Therefore, we attempted to imitate the natural environment of the human gut. Ethanol was used as solvent control. Next, the cells were plated on LB plates and the viable counts were determined the next day. Afterward, the viable counts were normalized to the solvent control. The cell viability assay revealed a dose-dependent effect of TM on the viability of *E. coli* WT and Δ*uvrA* (Figure 12). Both *E. coli* strains were highly sensitive to 170 µM TM and less than 13% survived compared to the control culture. Additionally, the viability assay indicated that *E. coli* Δ*uvrA* is more sensitive to

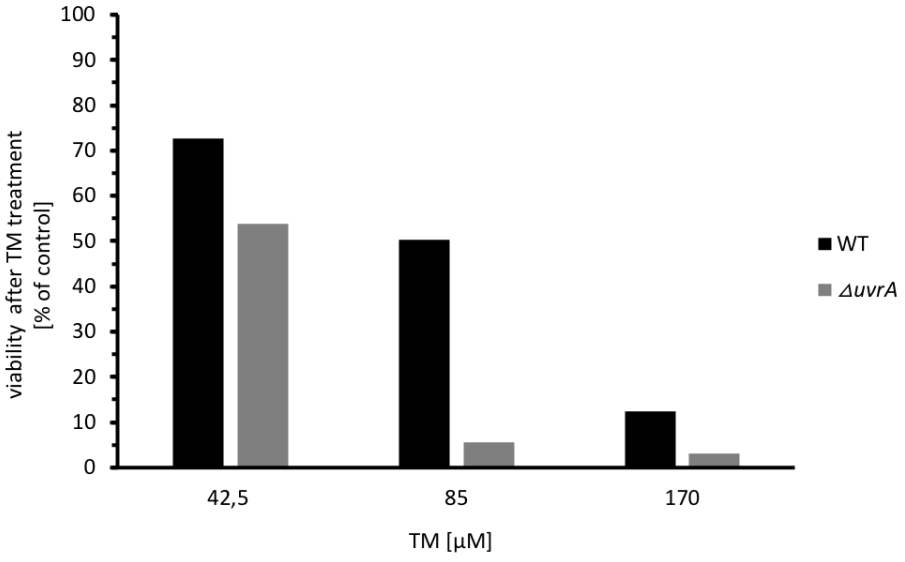

Figure 12. TM has a dose dependent effect on the viability of *E. coli* WT and Δ*uvrA*. Viable counts of Keio *E. coli* strains after 2h of treatment with 42.5, 85 and 170 µM TM. The viable counts were normalized to the solvent (EtOH) control.

TM compared to the WT strain.

For further investigations, we used 85 µM of TM because this concentration corresponds to approximately the half maximal inhibitory concentration (IC_{50}) of the *E. coli* WT strain.

Repetitions of the established viability assay revealed that the *E. coli uvrA* mutant is up to 6-fold more sensitive to TM compared to the WT strain after we treated the cells 2h with 85 µM TM. Further, *uvrA* complementation in trans increased significantly TM-resistance of *E. coli* Δ*uvrA* (21% viability compared to 5% without complementation) (Figure 13).

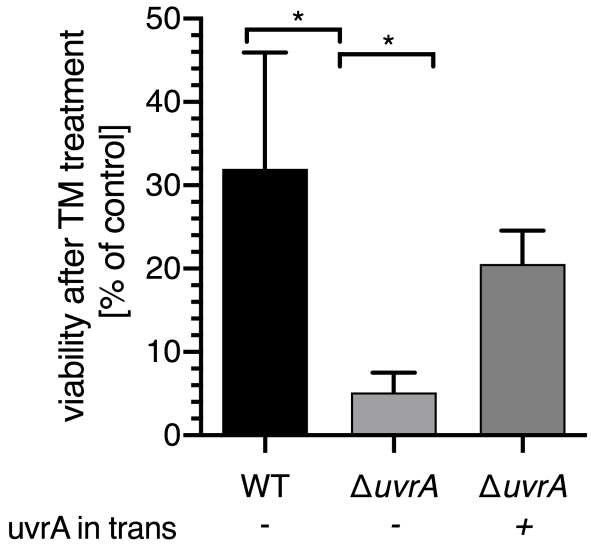

Figure 13. *E. coli* Δ*uvrA* is hypersensitive to TM. Viability of Keio E. coli strains after 2h of treatment with 85 µM TM. The viable counts were normalized to the solvent (EtOH) control and the means ± SD are shown (n = 5). Significance of results was determined with one-way ANOVA followed by Bonferroni multiple comparison (*$P \leq 0.05$).

4.2 Sequence analysis of the *K. oxytoca* AHC-6 *uvrX* gene

Toxin producing *K. oxytoca* strains share a toxin gene cluster which is part of a larger pathogenicity island (PAI). This gene cluster contains an operon with the putative immunity gene *uvrX* and *mfsX* [86]. *K. oxytoca* AHC-6 *uvrX* gene revealed 50% similarity via Clustal Omega to the related *E. coli* K-12 *uvrA* (NCBI Accession no. M13495.1) [118]. Therefore, we assumed that *uvrX* could be involved in repairing DNA that had been damaged by TM or in providing TM-resistance. Since *E. coli ΔuvrA* were highly sensitive to TM we asked whether *uvrX* could impart TM resistance to *E. coli*.

K. oxytoca AHC-6 *uvrX* (6850 - 9072 nt according to the annotated sequence NCBI accession no. HG425356.1) was cloned into pBAD33 vector and transformed into *E. coli ΔuvrA*. Sequencing of the constructed complementation vectors pBAD33_uvrX (Alexandra Moik) and three different

plasmids (with identically cloned *mfsX*, *uvrX* sequence) of the later relevant vectors pBAD33_mfsX_uvrX (Zana Lousin) revealed a guanine (G)-stretch consisting of 8 G's (here called *uvrX8G*) at position 2164 nt of *uvrX* from *K. oxytoca* AHC-6 compared to previously identified 7 G's (*uvrX7G*) by whole-genome Illumina sequencing (NCBI accession no. HG425356.1) (Figure 14). The difference in the sequences emerged during synthesis reaction of whole-genome Illumina sequencing as sequencing of four constructed complementation vectors revealed an 8 G-stretch.

```
uvrX                  gaaggg-ggggattattgtttagcggtacacccgaatcgatgctggcctgtcgccattca    2219
pBAD33_uvrX           GAAGGGGGGGGATTATTGTTTAGCGGTACACCCGAATCGATGCTGGCCTGTCGCCATTCA    409
pBAD33_mfsX_uvrX_2    GAAGGGGGGGGATTATTGTTTAGCGGTACACCCGAATCGATGCTGGCCTGTCGCCATTCA    406
pBAD33_mfsX_uvrX_1    GAAGGGGGGGGATTATTGTTTAGCGGTACACCCGAATCGATGCTGGCCTGTCGCCATTCA    406
pBAD33_mfsX_uvrX_3    GAAGGGGGGGGATTATTGTTTAGCGGTACACCCGAATCGATGCTGGCCTGTCGCCATTCA    404
                      ****** **************************************************
```

Figure 14. Sequencing of the vectors pBAD33_uvrX and pBAD33_mfsX_uvrX revealed 8 G's at position 2164 nt compared to *uvrX* which is lacking one G. To verify the sequence, the complementation vectors pBAD33_uvrX and pBAD33_mfsX_uvrX isolated from three different colonies were sequenced and aligned with *uvrX* (*uvrX7G*).

The differences of both alleles on the genome level are displayed in (Table 8). This inaccuracy during sequencing of the annotated *uvrX* leads to a truncated protein due to a frameshift. To examine the differences of the protein products encoded by the two *uvrX* alleles we pairwise aligned their amino acid sequences via EMBOSS Needle. The alignment revealed an identity between the two sequences of 96% and a similarity of 96.3% (Figure 15A). These differences appear after the G-stretch at the C-terminal end of the protein as the additional G of *uvrX8G* leads to a frameshift. These frameshift results in a different aa sequence and a 13 aa longer protein (753 aa in total) compared to the protein encoded by *uvrX7G* (740 aa in total) (Figure 15B).

Table 8. Gene length, nucleotide position in the annotated sequence of the PAI and protein length of the two *uvrX* alleles.

Allele	Gene length (nt)	Position in the annotated sequence (nt) (NCBI accession no. HG425356.1)	Protein length (amino acids)
uvrX7G	2223	6850 - 9072	740
uvrX8G	2262	6850 - 9110 (with an additional G at position 9020)	753

A

```
#=======================================
#
# Aligned_sequences: 2
# 1: uvrX7G
# 2: uvrX8G
# Matrix: EBLOSUM62
# Gap_penalty: 10.0
# Extend_penalty: 0.5
#
# Length: 755
# Identity:     725/755 (96.0%)
# Similarity:   727/755 (96.3%)
# Gaps:          17/755 ( 2.3%)
# Score: 3741.5
#
#
#=======================================
```

uvrX7G GGG GGG GAT

uvrX8G GGG GGG GGA

B

```
UvrX7G            701 NMELIAQADWIIDIGPYAGKEGGDYCLAVHPNRCWPVAIH----------    740
                      ||||||||||||||||||||||...:..|...  :|..
UvrX8G            701 NMELIAQADWIIDIGPYAGKEGGGLLFSGTPESM--LACRHSLTAEWLRK    748

UvrX7G            741 -----    740

UvrX8G            749 HCRME    753
```

Figure 15. Pairwise sequence alignment results of UvrX7G and UvrX8G. (A) The alignment revealed an identity of 96% and a similarity of 96.3%. (B) Alignment of the C-terminal end of the protein sequences where the differences occur. The aa encoded by the G-stretch is framed in blue. Further, the *uvrX7G* and *uvrX8G* nucleotide sequences of the G-stretch is displayed.

Examination of the expression of the His-tagged *uvrX7G* from pBAD33_uvrX_His and pBAD33_His_uvrX via Western Blot analysis from Sandra strengthen the hypothesis that *K. oxytoca* AHC-6 possess the *uvrX8G* allele. If the *uvrX7G* is the actual allele than the C-terminal His-Tag would be in frame and show a visible fragment after induction (Figure 16A). Only the N-terminally tagged UvrX showed a bright fragment (83 kDa) after 60 and 90 minutes of induction compared to the C-terminally tagged UvrX due to the additional G in the native sequence of *uvrX* (8G's in total) (Figure 16C). This leads to a frameshift and a nonfunctional His-Tag. Further, both tagged proteins were visible on the Coomassie gel after induction (Figure 16B). This results supports the conclusion that the cloned allele actually contains 8 G's.

A

uvrX7G: GGG GGG GAT TAT TGT TTA GCG GTA CAC CCG AAT CGA TGC TGG CCT GTC GCC ATT CAT CAT CAT CAT CAT CAT CAT TAG

uvrX8G: GGG GGG GGA TTA TGT TTA GCG GTC ACC CGA ATC GAT GCT GGC CTG TCG CAT TCA TCA TCA TCA TCA TCA TCA TTA G

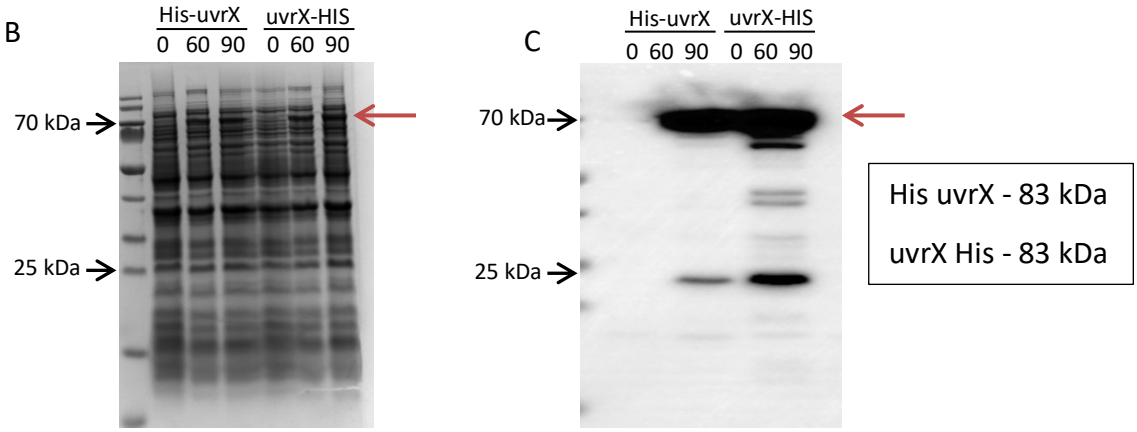

Figure 16. The His-Tag of C-terminal tagged UvrX is not expressed functionally. (A) Sequence of C-terminally tagged *uvrX7G* and *uvrX8G* (short version like *uvrX7G* but with 8G's) allele including the G-stretch (blue), the His-Tag (green) and the Stop-Codon (red). (B) Coomassie gel of His-tagged UvrX expression in *E. coli* BL-21 cells. (C) The Western blot of His-tagged UvrX expressed in *E. coli* BL-21 is shown. N-terminally tagged UvrX (83 kDa) showed a bright signal after 60 and 90 minutes after induction. In contrast, C-terminally tagged UvrX shown no signal. [Data provided by Sandra Raffl]

To identify whether *uvrX* from *K. oxytoca* is more likely to contain 7 or 8 G's in this region, the nucleotide sequence of *uvrX7G* was blasted on NCBI against sequences of *K. oxytoca* strains. The Blast search revealed 20 sequences including the PAI from *K. oxytoca* AHC-6 (NCBI accession no. HG425356.1), which was excluded for sequence analysis. A summary of the results is shown in Table 9. All identified *K. oxytoca* sequences contain either a 7 G-stretch with an additional adenine (A) afterward or five G's followed by three A's. Interestingly, the Blast search revealed the sequence of the Kleboxymycin (alternative name of TM) biosynthetic gene cluster of *K. oxytoca* MH43-1, which contains a 5 G-stretch followed by three A's. Further, the alignment of both *uvrX* alleles with six different *K. oxytoca* sequences shows that the allele *uvrX7G* is 39 nt shorter compared to the other sequences (includes the missing G) (Figure 17). These results suggest the 8 G-stretch at the C-terminal end of the *uvrX8G* allele most likely replaces the G-stretch with the additional adenines afterward carried by other *K. oxytoca* genomes. This allele would be 2262 bp long and encodes 754 amino acids (aa).

Table 9. The Blast result of *uvrX7G*. The *uvrX7G* nucleotide sequence was blasted against sequences of *K. oxytoca* strains. The table shows the number of revealed sequences (Hits), the minimal query cover, the minimum Percentage Identity and the number of different G-stretch versions.

Number of hits	Minimal query cover (%)	Minimum Percentage Identity of all hits (%)	Number of sequences containing 7 G's and 1 A'S	Number of sequences containing 5 G's and 3 A's
19 (HG425356.1 excluded)	100	93.12	13	6

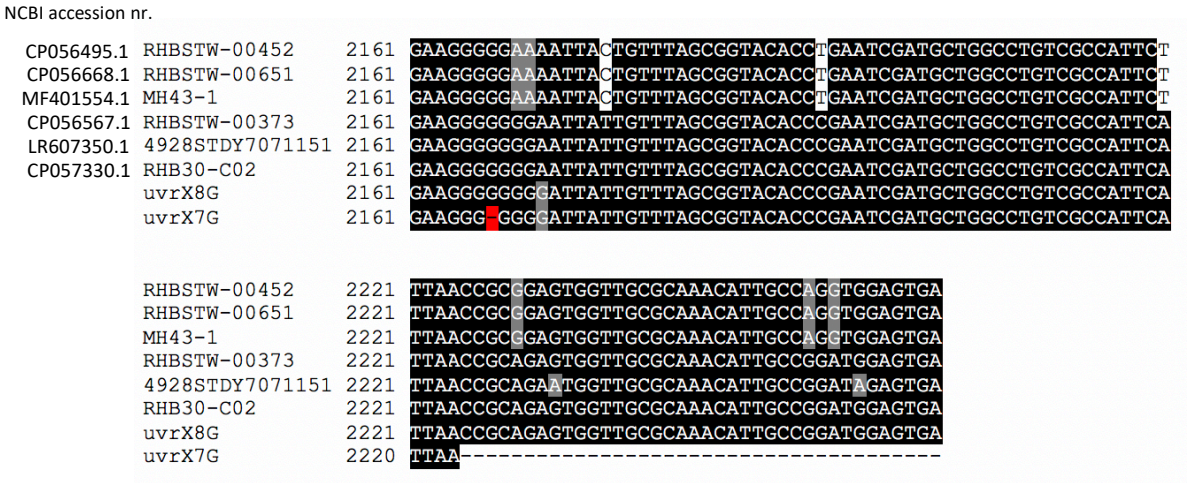

Figure 17. Alignment of *K. oxytoca* AHC-6 *uvrX* alleles and sequences of 6 *K. oxytoca* strains revealed via Blast search. The *uvrX7G* allele from *K. oxytoca* AHC-6 was blasted on NCBI against sequences of *K. oxytoca* strains. Both *uvrX* alleles and 6 of the revealed sequence were aligned and differences were highlighted in grey. The missing G of *uvrX7G* is highlighted in red.

The sequence of the predicted proteins encoded by the two *uvrX* alleles was blasted against other *K. oxytoca* sequences to identify the correct protein sequence. The Blast results revealed the same 45 *K. oxytoca* sequences for both alleles that consist of excinuclease ABC subunit UvrA and ATP-binding cassette domain-containing protein sequences. In addition, the UvrX8G sequence exhibits higher identity to the revealed *K. oxytoca* sequences compared to UvrX7G (Table 10).

Table 10. Blast result of the UvrX7G and UvrX8G protein sequence. The protein sequence of UvrX7G and UvrX8G was blasted against protein sequences of *K. oxytoca* strains. The number of revealed sequences (Hits) and the number of sequences with over 99% identity are shown.

Allele	Number of revealed hits	Number of hits with over 99% identity
UvrX7G	45	2
UvrX8G	45	27

The four *K. oxytoca* protein sequences with the highest identity were aligned to the UvrX7G and UvrX8G sequences via Clustal Omega. The alignment revealed a higher identity between UvrX8G, and the selected *K. oxytoca* protein sequences compared to UvrX7G (Figure 18A). Once again, the differences between UvrX7G and the other sequences occur after the G-stretch of the proteins. Comparison of the C-terminal UvrX8G protein sequence with those of the selected *K. oxytoca* sequences revealed 100% identity (Figure 18B). The whole alignment is shown in the appendix section (Figure A1).

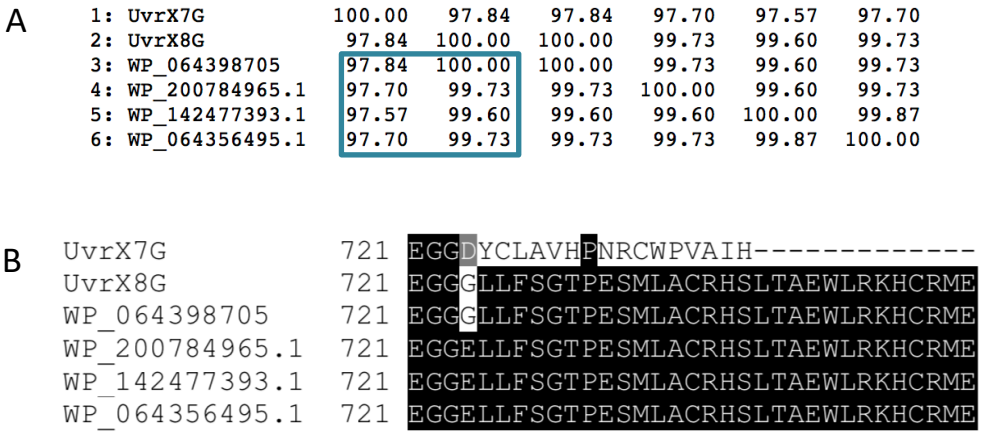

Figure 18. Alignment results of protein sequences from UvrX7G, UvrX8G and *K. oxytoca* sequences (NCBI accession number is shown) via Clustal Omega. (A) Percent Identity Matrix of the aligned sequences created by Clustal Omega. The relevant identities are boxed in blue. (B) Alignment of the C-terminal protein sequences.

The nucleotide and protein sequence analysis of both *uvrX* alleles supports the conclusion that *K. oxytoca* AHC-6 *uvrX* contains 8 G's.

In addition, we asked whether *uvrX7G* or *uvrX8G* is the biologically relevant sequence. Since sequence analysis led to the evidence that *K. oxytoca* AHC-6 possess the allele *uvrX8G*, we hypothesize that *uvrX7G* encodes a truncated and non-functional protein. Therefore, we assume that *uvrX7G* expression is incapable of imparting TM resistance in Keio *E. coli ΔuvrA*. To challenge this hypothesize we transformed Keio *E. coli ΔuvrA* with the vector pBAD33_*uvrX*, which contains the *uvrX7G* allele. The expression of *uvrX7G* was induced and the TM-resistance was quantified in the viability assay. Expression of *uvrX7G* in Keio *E. coli* Δ*uvrA* (n=1) revealed no increase in viability compared to Keio *E. coli ΔuvrA* [pBAD33] after 2h treatment with 85 µM TM (Figure 19). These results indicate that *uvrX7G* encodes a defective protein.

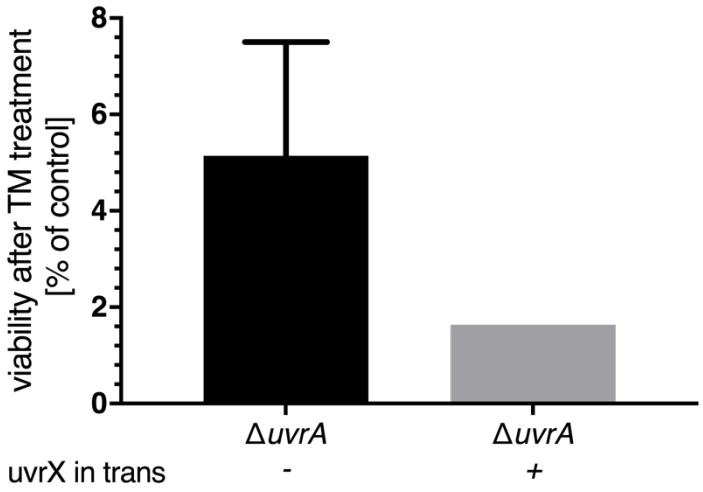

Figure 19. Complementation of Keio *E. coli* Δ*uvrA* with the allele *uvrX7G* revealed no increase in viability. Viability of Keio *E. coli* strains after 2h of treatment with 85 µM TM. The viable counts were normalized to the solvent (EtOH) control and the means ± SD are shown (Δ*uvrA*: n = 5, Δ*uvrA* + *uvrX*: n = 1).

In summary, these results indicate that *K. oxytoca* AHC-6 encodes the *uvrX8G* allele with the 8 G-stretch at the C-terminal end of *uvrX*. The *uvrX8G* contains 2262 nt, that encodes a 753 aa long protein. Since our findings support that the allele *uvrX8G* is the chromosomal *uvrX* of *K. oxytoca* AHC-6 we used the sequence of *uvrX8G* in the further course of this project. The nucleotide sequence of *uvrX8G* is displayed in the appendix section (Figure A2).

4.1 *uvrX* expression increases significantly TM-resistance of *E. coli* WT & Δ*uvrA*

As already mentioned, we hypothesized that *uvrX* could be involved in repairing DNA that had been damaged by TM or in providing TM-resistance. To examine whether the *uvrX8G* allele could impart TM resistance to Keio *E. coli ΔuvrA* we cloned this allele into the pBAD33 vector (pBAD33_*uvrX*_I) and transformed *E. coli ΔuvrA* with the construct. The expression of *uvrX* was induced and the TM-resistance was quantified in the viability assay. The expression of *uvrX* or *uvrA* in the hypersensitive *E. coli ΔuvrA* strain revealed an increase (13.8-fold and 4-fold respectively) in viable counts compared to the *ΔuvrA* mutant carrying the empty vector (Figure 20A). Moreover, *uvrX* expression conferred a 3.4-fold higher resistance to *E. coli ΔuvrA* compared to *uvrA* expression. Moreover, *uvrX* expression in *E. coli* WT supported a 3.6-fold higher viability after TM-treatment (Figure 20B). For all strains at least three biological replicates were

performed (n ≥ 3). These results identified that *K. oxytoca* AHC-6 *uvrX8G* encodes a functional protein that could perform as TM resistance gene.

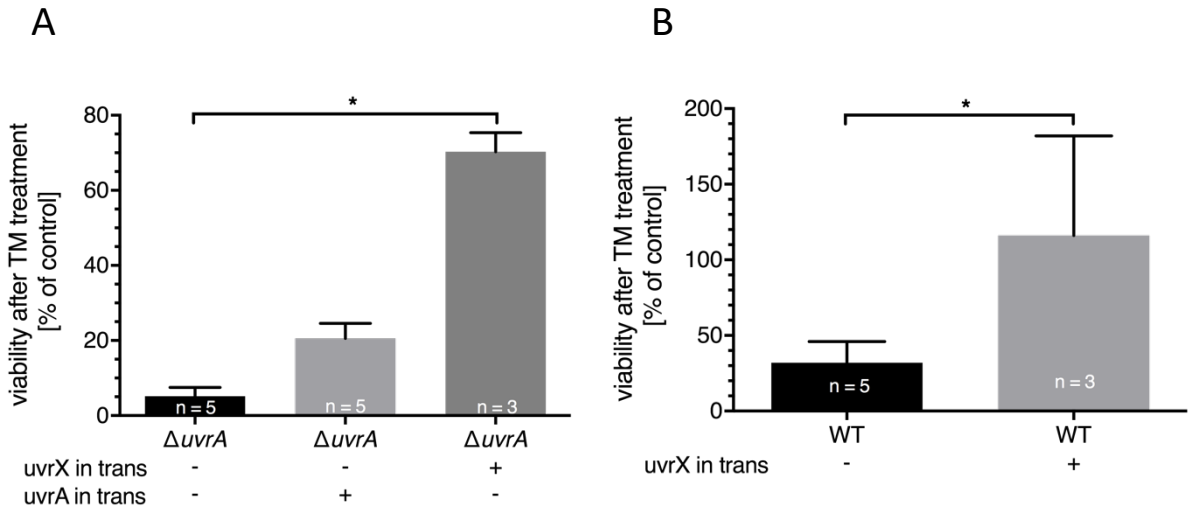

Figure 20. *uvrX* expression increases significantly TM resistance of *E. coli* WT & *ΔuvrA*. Viability counts of Keio *E. coli* strains after 2h of treatment with 85 µM TM. The viability counts were normalized to the solvent control (EtOH) and the means ± SD are shown (n = see graph). (A) Statistical significance was determined with Kruskal-Wallis followed by Dunn's multiple comparison (**P* ≤ 0.05). (B) Statistical significance was determined with Mann-Whitney (**P* ≤ 0.05).

4.2 *K. oxytoca* AHC-6 UvrX belongs to the class of UvrA2 proteins

The viability assay results (section 4.1) indicated that UvrX is involved in providing TM-resistance. We hypothesized that this activity results from a direct role in DNA repair. To investigate the biochemical activity of UvrX we predicted its protein structure and analyzed the protein sequence, structure and function.

4.2.1 Homology modelling - UvrX is a member of the ATP-binding cassette protein family (ABC)

To gain insights into the molecular function of *K. oxytoca* AHC-6 UvrX (UvrX8G), a protein structure prediction was performed using the Phyre2 web portal. The protein prediction was accomplished based on the 3D structure of UvrA2 from *Deinococcus radiodurans* (drUvrA2), which revealed the highest confidence, which represents the probability that the match between the used sequence and the template is a true homology, and percentage identity (Confidence: 100; %id: 40; PDB ID: 2VF7) (Figure 21A). The structures of UvrX and the template drUvrA2 were compared and aligned using PyMOL. In general, UvrX and drUvrA2 showed a high similarity of

40%. Comparison of the two structures identified different domains: two nucleotide binding domains (NBD) including an NBD ATP-binding domain (red and blue) and an NBD signature domain (pink and turquoise), and an insertion domain (green) presented by the example of drUvrA2 (Figure 21B and C).

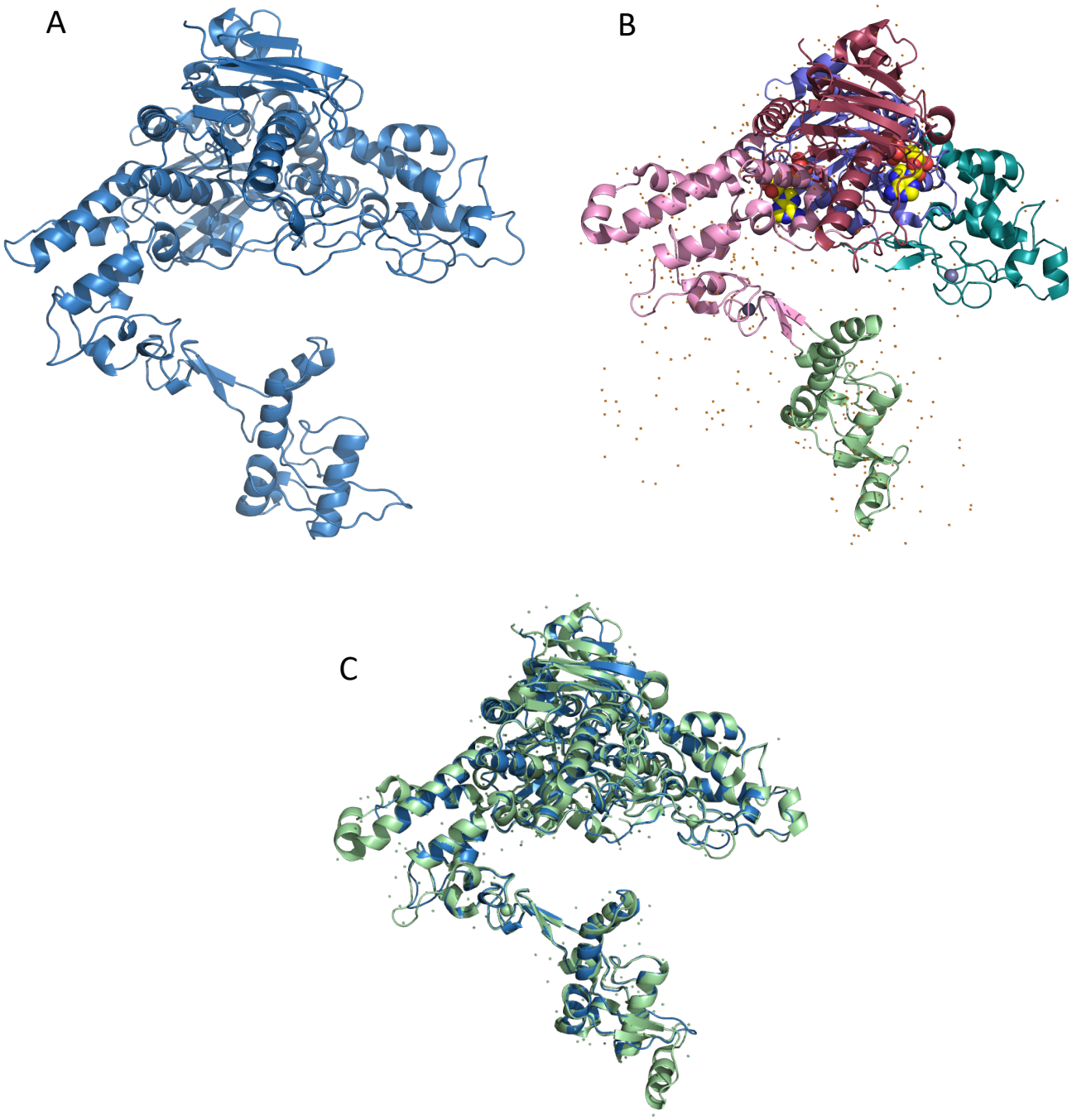

Figure 21. 3D model of *K. oxytoca* UvrX and *D. radiodurans* UvrA2. (A) Predicted protein structure of UvrX (B) Structure of monomeric drUvrA2. The domains are colored as followed: NBD-I signature domain (pink), NBD-I ATP-binding domain (red), NBD-II signature domain (turquoise), NBD-II ATP binding domain (blue) and an insertion domain (green). Zink ions and ADP molecules are illustrated as spheres. (C) Alignment of *K. oxytoca* UvrX (blue) and drUvrA2 (green).

Further, we used the NCBI Conserved Domain Database (CDD) to identify conserved domains. The analysis determined a homology to the UvrA superfamily and a ABC transporter signature motif including the conserved ABC motifs: Walker A, Walker B, Q-loop, the ABC-signature motif as well as the D-loop and the H-loop [120–122]. To verify the outcome of the motif prediction we located the motifs within the UvrX protein sequence. The protein sequence of UvrX is depicted in Appendix Figure A3 and conserved ABC motifs are underlined: Walker A (red), Walker B (green), ABC-signature motif (orange), Q-loop (blue) and H-motif (purple). Zinc-coordinating residues are indicated with stars. In summary, motif prediction and localization identified UvrX as member of the ATP-binding cassette protein family.

4.2.1 Functional characterization of UvrX - UvrX lacks the UvrB-binding domain

Since motif prediction identified *K. oxytoca* UvrX as a member of the ABC transporter we aimed to further investigate the function of UvrX. UvrA proteins are members of the ABC protein family which are involved in transport, translation of RNA or DNA repair. Literature revealed that drUvrA2 belongs to the class II of UvrA proteins which lacks a 150-residue domain that that is required for the interaction of UvrA with UvrB during nucleotide excision repair [123]. Due to the structural similarity between *K. oxytoca* AHC-6 UvrX and drUvrA2 we asked whether UvrX lacks the UvrB recognition/interaction domain. We compared the structures of UvrX with the well characterized UvrA1 protein of *Bacillus stearothermophilus* (bstUvrA1) using PyMOL. The UvrB binding domain was visible in the 3D structure of bstUvrA1 (PDB ID: 2R6F) and absent in the predicted *K. oxytoca* AHC-6 UvrX structure (Figure 22). In addition, we compared the protein sequences of UvrX, *D. radiodurans* drUvrA1 and drUvrA2, as well as B. stearothermophilus bstUvrA1. T-coffee web server was used to create a multiple sequence alignment [124,125] (Appendix Figure A3). Similar to drUvrA2, *K. oxytoca* AHC-6 UvrX lacks a 150-residue domain which corresponds to the UvrB binding domain. In summary, the findings of the structure and sequence comparison revealed that UvrX belongs to the class II of UvrA proteins.

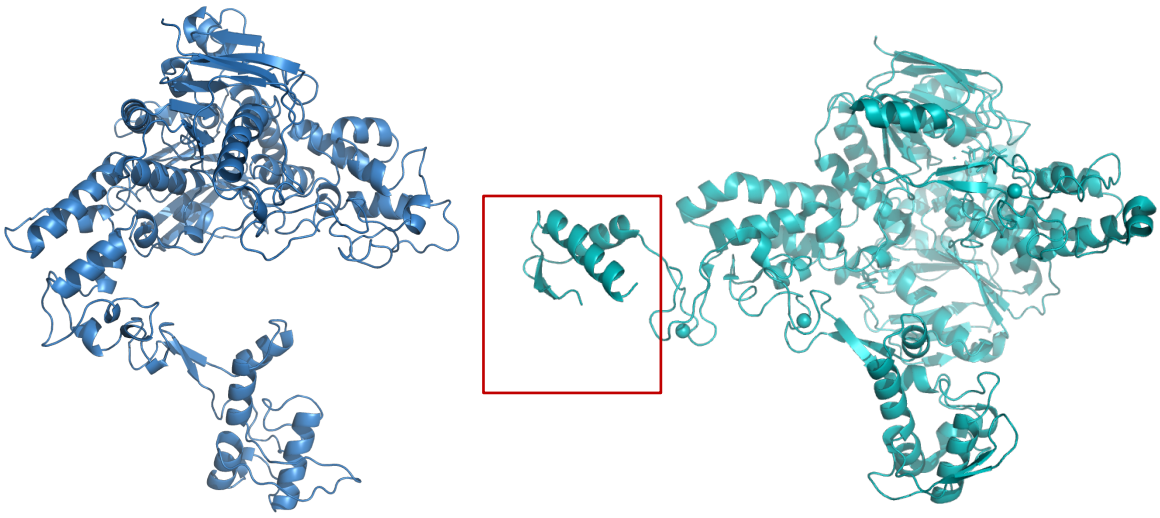

Figure 22. 3D model of *K. oxytoca* UvrX and *Bacillus stearothermophilus* bstUvrA1. *K. oxytoca* UvrX is depicted in dark blue and bstUvrA1 in light blue. The UvrB binding domain is visible in the protein structure of bstUvrA1 (red box) and absent in the predicted structure of UvrX.

4.3 *mfsX* and *uvrX* are TM immunity genes in *K. oxytoca* AHC-6

Gene homology comparison identified *K. oxytoca* AHC-6 *uvrX* and *mfsX* as putative immunity genes which provide resistance against the self-produced tilimycin. Further, previous results of this study revealed that *uvrX* mediates TM-resistance in *E. coli* WT and in *E. coli* Δ*uvrA*. To test whether *uvrX* and *mfsX* are required for TM immunity in *K. oxytoca* AHC-6 we took a genetic approach.

4.3.1 Knockout of *mfsX* and *uvrX*

The genes *mfsX* and *uvrX* were inactivated in the toxin producing *K. oxytoca* AHC-6 *aphA* (WT) and the non-producing *K. oxytoca* AHC-6 Mut89 (Δ*npsB*) via the lambda red recombination system. Both genes are part of one operon within the biosynthetic gene cluster.

The attempt to knock-out the whole operon in *K. oxytoca* AHC-6 failed. Because *mfsX* and *uvrX* are large genes we assumed that the homologous regions are too far away for the lambda red recombination system. Therefore, the recombination cassette was designed to partially delete *mfsX* (nt 77-1233) and the first 50 bp of *uvrX* including its ribosomal binding site and the start codon. This leads to a polar mutation of *uvrX* and the inhibition of *uvrX* expression. The location of *mfsX* and *uvrX* in the *K. oxytoca* AHC-6 gene cluster and the design of the recombination cassette is sown in Figure 23 and described in section 3.5.2.

K. oxytoca AHC-6 genome

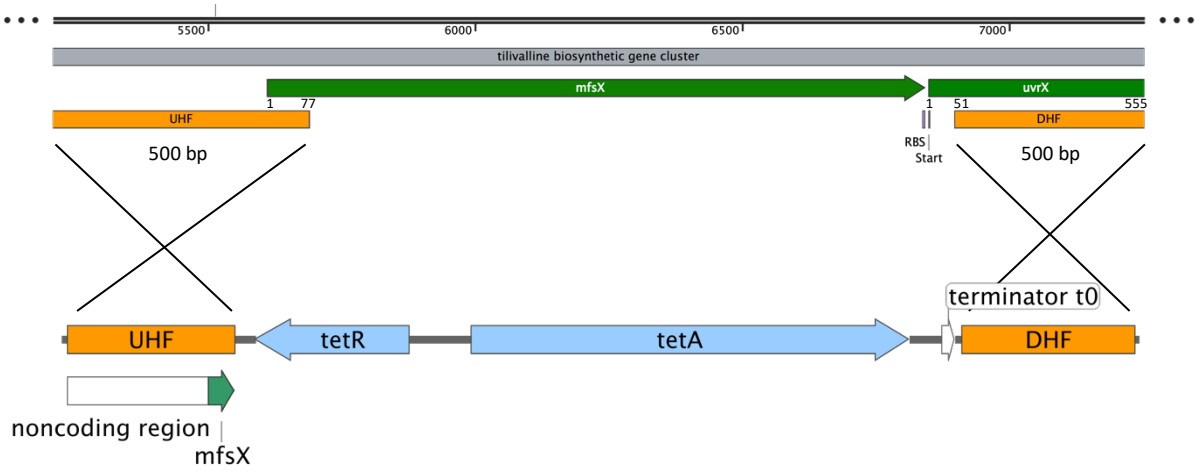

Recombination cassette

Figure 23. Fragment of the *K. oxytoca* AHC-6 pathogenicity island and the recombination cassette. Top: Part of the *K. oxytoca* AHC-6 gene cluster with *mfsX* and *uvrX*. Bottom: Map of the recombination cassette with upstream homologous fragment (UHF), tetracycline resistance marker (tetR and tetA), t0 terminator fragment (t0 terminator) and the downstream homologous fragment (DHF). The recombination sites are indicated with black lines and important features were shown.

For homologous recombination, competent *K. oxytoca* AHC-6 *aphA* and *K. oxytoca* AHC-6 Mut89 carrying pKOBEG were transformed with the linear recombination cassette and selected on tet plates. To avoid TM-production, we used M63 plates in addition to CASO for the selection of recombinants. The M63 media contained all amino acids, except proline and tryptophan. Since L-proline is the substrate of NpsB to produce N-acylproline, which then spontaneously forms TM (ring closure), the absence of proline inhibits TM-production by the WT strain. The correct integration of the recombination cassette was validated using PCR, colony PCR and sequencing.

Homologous recombination in the Mut89 strain resulted in 33 recombinants in total (Table 11) after they were streaked on CASO plates with Tet. All tested (PCR with isolated gDNA as template) recombinants integrated the recombination cassette correctly (Appendix Figure A4). Two *K. oxytoca* AHC-6 Mut89 Δ*mfsX, uvrX* recombinants were sequenced and validated (from nt 1 of UHF to the beginning of *tetR* and from nt 760 of *tetA* to the end of DHF). The validated *K. oxytoca* AHC-6 Mut89 Δ*mfsX, uvrX* K1 was used for the following cell viability assays.

Homologous recombination in the WT strain resulted in 12 recombinants in total using both selection strategies. 12 recombinants were tested via colony PCR to verify the correct integration

of the recombination cassette (Figure A5). Further, the gDNA of three positive recombinants was isolated and the integration of the recombination cassette and the absence of the deleted *mfsX* was tested via PCR (Figure A6). Out of 12 recombinants, two recombinants integrated the recombination cassette correctly. Specific recombinants, which were verified by PCR carry the disrupted *mfsX, uvrX* operon were obtained with both selection strategies. The *K. oxytoca* WT Δ*mfsX, uvrX* was verified via sequencing (same regions as Mut89 strain). This recombinant was obtained using 600 ng of the recombination cassette and CASO plates (Table 11). Since *K. oxytoca* AHC-6 *aphA* Δ*mfsX, uvrX* were able to grow on CASO plates, the disruption of *mfsX* and *uvrX* showed no lethal effects on the cells. This indicates that both genes are not essential to *K. oxytoca* AHC-6 *aphA* under these conditions.

Table 11. Summary of recombination results

Strain & media	Recomb. cassette (ng)	Colonies	Colonies after streak-out	Number of recombinants analyzed at insertion site	Positive recombinants (colony PCR)	Sequenced recombinants	Positive sequenced recombinants
Mut89 CASO	100	24	6/10*	2	2	2	2
	300	16	16	1	1	-	-
	600	11	11	0	-	-	-
WT CASO	100	0	-	-	-	-	-
	300	3	3	3	0	-	-
	600	4	4	4	2	1	1
WT M63	100	1	1	1	0	-	-
	300	1	1	1	0	-	-
	600	3	3	3	1	-	-

* 6 of the 10 streaked colonies grew

4.3.2 *K. oxytoca* Δ*mfsX, uvrX* is hypersensitive to TM compared to the Δ*npsB* parent strain

In order to investigate whether *mfsX* and *uvrX* are TM-resistance genes the specific operon deficient mutant created above, *K. oxytoca* AHC-6 Mut89 Δ*mfsX, uvrX* was tested for its resistance against TM. Although *mfsX* and *uvrX* genes didn't look as if they were essential to *K. oxytoca* AHC-6 *aphA*, we suspected *K. oxytoca* AHC-6 Mut89 Δ*mfsX, uvrX* to be more sensitive to TM added externally to the culture media compared to *K. oxytoca* AHC-6 Mut89.

Cells were treated with 85 µM TM for 16h and survival was measured using the previously described viability assay. Ethanol was used as solvent control. Because of the minor difference in survival (10%) between *K. oxytoca* AHC-6 Mut89 Δ*mfsX, uvrX* and the Mut89 parent strain after 85µM TM treatment for 2h we increased the time of treatment to 16h (Figure A7). The *K. oxytoca* AHC-6 Mut89 parental strain and the Δ*mfsX, uvrX* knockout strain carried the empty pBAD33 as control. To complete the viability assay we complemented the Δ*mfsX, uvrX* knockout strain with both genes in trans. OD_{600} values were measured after 16h of TM-treatment to monitor the effect of TM on the growth of the cells. Cells treated with TM revealed grew comparably to the EtOH treated cells, indicating TM has no effect on proliferation under these conditions (Figure 24A). However, when these cultures were plated on medium in the absence of TM, *K. oxytoca* Δ*mfsX, uvrX* showed very low viability compared to the Mut89 parent strain (9.8% and 122.5% survival, respectively). Simultaneous trans-expression of the *mfsX, uvrX* operon increased the survival up to 7-fold of *K. oxytoca* Mut89 Δ*mfsX, uvrX* (69% survival). In Figure 24B the viability of strains after TM treatment expressed as percentage of solvent control is shown (n=5). These results support the conclusion that *mfsX*, *uvrX* or both genes mediate resistance to TM.

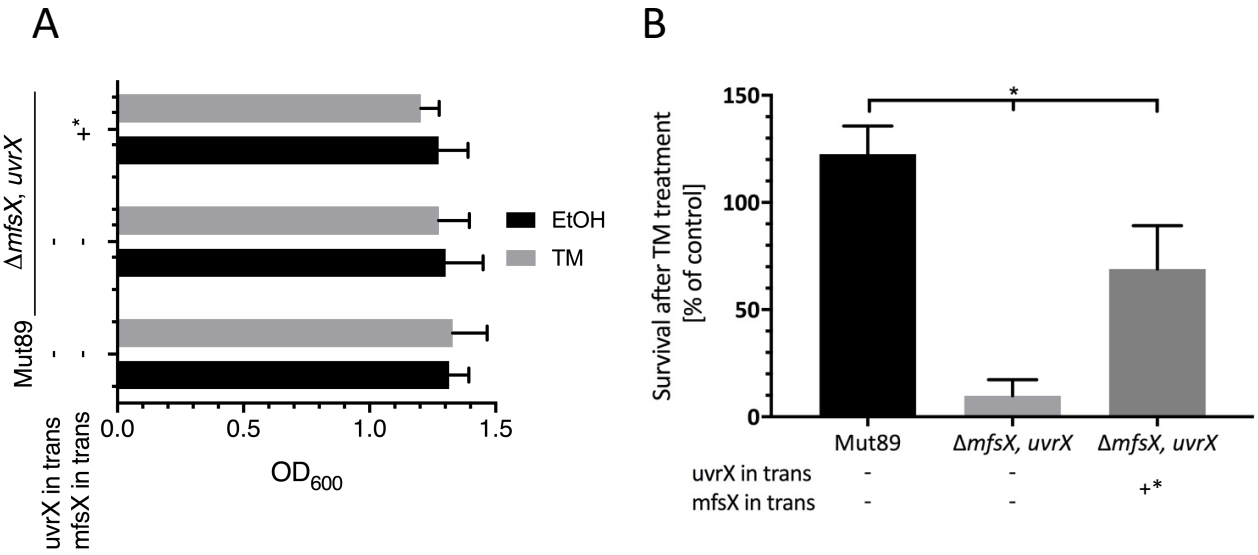

Figure 24. *K. oxytoca* Δ*mfsX, uvrX* is hypersensitive to TM compared to the Mut89 parent strain. (A) TM treatment has no inhibitory effect on growth of *K. oxytoca* AHC-6 strains. OD_{600} values of each culture were measured after treatment. Means ± SD are shown (n = 5). (B) Viability of *K. oxytoca* strains after 16h of treatment with 85 µM TM. The colony forming units were normalized to the solvent control (EtOH) and the means ± SD are shown (n = 5). Significance of results was determined with one-way ANOVA followed by Tukey's multiple comparison (*P ≤ 0.05). +*: trans expression of the *mfsX, uvrX* operon

4.3.3 *uvrX* confers higher TM-resistance in *K. oxytoca* Δ*mfsX, uvrX* compared to *mfsX*-complementation

The next step was to evaluate the importance of the individual *mfsX* and *uvrX* genes in TM-resistance in *K. oxytoca* AHC-6. Therefore, we constructed inducible *mfsX* and *uvrX* complementation vectors using the vector pBAD33. *K. oxytoca* AHC-6 Mut89 Δ*mfsX, uvrX* were transformed with the complementation vectors [pBAD33_mfsX, pBAD33_uvrX_l, pBAD33_mfsX_uvrX_l] to determine if expression of the *mfsX* or *uvrX* genes confers resistance to TM. We treated the cells of the different *K. oxytoca* complementation strains with 85 µM TM for 16h and analyzed the effect of TM on viability and proliferation. OD_{600} measurement revealed that TM and ethanol treated strains exhibited similar bacterial growth which indicates no growth inhibitory effect of TM (Figure 25A). We observed a significant increase in survival of *K. oxytoca* strains carrying a plasmid with *uvrX* or *mfsX* genes compared to *K. oxytoca* AHC-6 Mut89 Δ*mfsX, uvrX* (10-fold and 4.6-fold, respectively). Further, the 2.2-fold better survival conferred by *uvrX* compared to *mfsX* in trans was statistically significant. Simultaneous expression of the *mfsX, uvrX* operon increased the survival up to 7-fold of *K. oxytoca* AHC-6 Mut89 *ΔmfsX, uvrX* (Figure 25B).

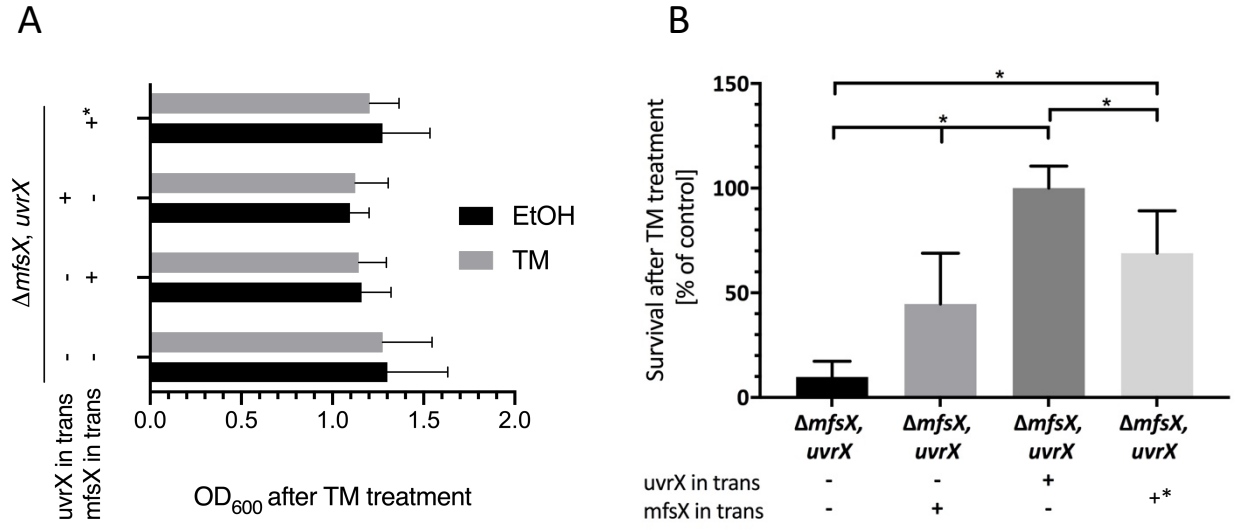

Figure 25. *uvrX* confers higher TM-resistance in *K. oxytoca* Δ*mfsX, uvrX* compared to *mfsX*-complementation. (A) TM treatment has no inhibitory effect on growth of *K. oxytoca* AHC-6 strains. OD_{600} values of each culture were measured after treatment. Means ± SD are shown (n = 5) (B) Viability of *K. oxytoca* strains after 16h of treatment with 85 µM TM. The colony forming units were normalized to the solvent control (EtOH) and the means ± SD are shown (n = 5). Significance of results was determined with one-way ANOVA followed by Tukey's multiple comparison (*$P \leq 0.05$).

In summary, the present study has shown that *mfsX* and *uvrX* mediate resistance against TM and are therefore identified as TM immunity genes in *K. oxytoca* AHC-6. Further, *uvrX* expression confers higher TM-resistance in *K. oxytoca* Δ*mfsX, uvrX* compared to *mfsX*.

4.4 Establishing a qRT-PCR method to monitor in vitro gene expression in *K. oxytoca* AHC-6

In general, expression of immunity genes in antibiotic producing bacteria is tightly linked to antibiotic biosynthesis gene expression. Typically expression of immunity occurs either in advance of or simultaneously with antibiotic biosynthesis [126]. Therefore, we predicted that the tilimycin immunity gene expression is coordinately regulated with synthetase gene expression. In order to analyze the correlation between these gene sets, a Reverse Transcription Quantitative real-time Polymerase Chain Reaction (qRT-PCR method) had to be developed. The reliability of RT-qPCR assays can be affected by several variables including the initial amount of the sample, integrity and quantity of extracted RNA, primer design, reaction efficiency and the selection of reference genes [127]. The aim of this study was to establish a reliable qRT-PCR method.

Dornisch et al showed that *K. oxytoca* AHC-6 TM production increased after around 4 h with a maximum of TM production at 16 h in conditioned media [119]. To establish the qRT-PCR method we focused on the first 6 h of culture under the same conditions and analyzed the expression of the representative synthetase gene *npsA*, the immunity genes *mfsX* and *uvrX* as well as the putative transcriptional activator *marR.*

4.4.1 Validation of RNA integrity

First, we inoculated CASO broth media with a *K. oxytoca* AHC-6 overnight culture (M63 media) to turn off toxin production (lack of L-proline, the substrate of NpsB, prevents synthesis of TM). Cells were harvested at different culture time points (before inoculation, immediately after, after 0.5 h, 1 h and then every 1 h up to 6 h) to isolate total RNA. During the course of experiment, cell growth was observed by measuring OD_{600} at each time point (Figure 26). The nucleotide concentrations and the ratios of the isolated RNA were measured via Nanodrop and were shown in Table 12.

Table 12. Concentration [ng/µl] and measured RNA purity of RNA isolated from *K. oxytoca* AHC-6. Cells were shifted from M63 to CASO media and RNA was isolated from the cells at times indicated.

Time [h]	RNA concentration (ng/µl)	260/280 RNA	260/230 RNA
Before inoculation (v.I.)	935.5	2.18	2.18
0	184.2	2.15	1.15
½	414.9	2.15	2.13
1	1244.5	2.21	1.8
2	2217	2.15	2.39
3	1244.9	2.16	2.21
4	858.4	2.18	2.09
5	797.1	2.14	2.17
6	874.7	2.15	2.01

To assess the RNA integrity after RNA isolation, the RNA samples were loaded on a denaturing agarose gel (Figure 27). RNA isolated from *K. oxytoca* AHC-6 ONC showed significant RNA degradation. In contrast, RNA isolated from the other time points revealed clear sharply migrating fragments on the gel. Therefore, we excluded the ONC sample in further experiments. Interestingly, total RNA isolated from *K. oxytoca* AHC-6 was separated in four species of molecules during denaturing agarose gel electrophoresis.

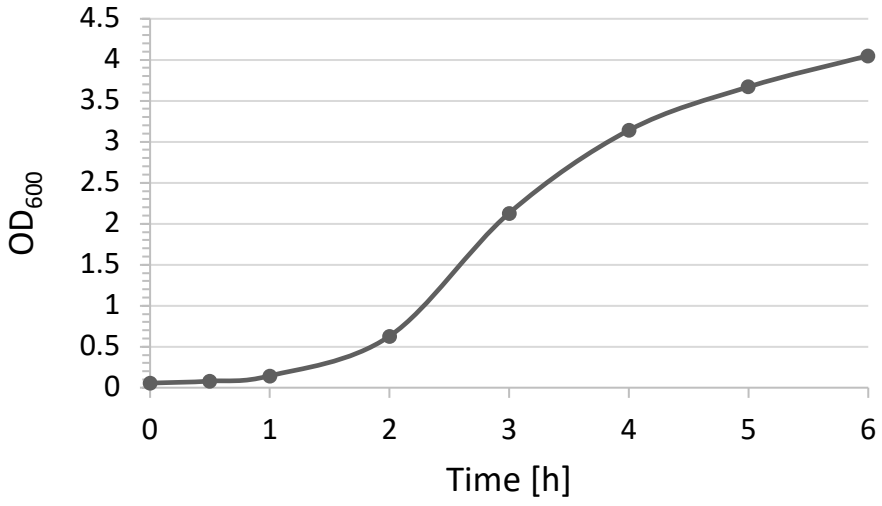

Figure 26. Growth curve of *K. oxytoca* AHC-6 cells during RNA isolation experiment. OD_{600} was measured at each time point to monitor the growth of the cell culture.

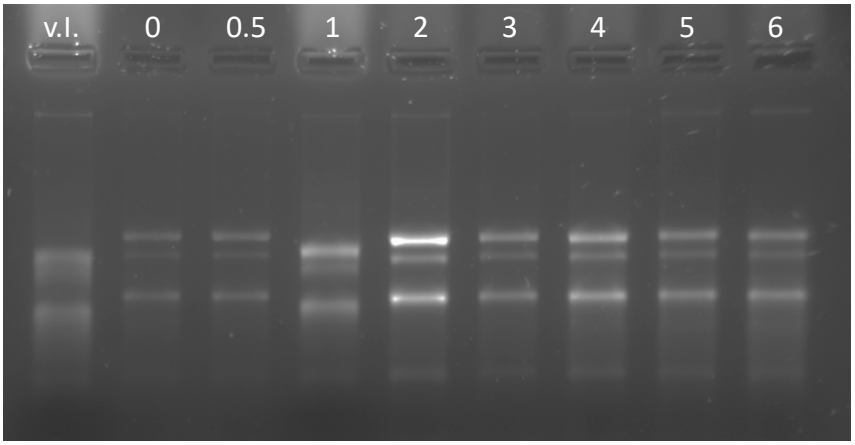

Figure 27. Only RNA isolated from *K. oxytoca* AHC-6 ONC showed degradation. RNA was isolated from a *K. oxytoca* AHC-6 culture at different time points and 500 ng RNA per sample was loaded on a denaturing agarose gel. RNA sample isolated from the ONC (v.I.) showed significant RNA degradation compared to the other samples.

Afterwards the RNA was treated with DNase to digest remaining DNA. To assess the effect of DNase digestion on the RNA quality we performed a denaturing agarose gel electrophoresis using DNase digested and undigested RNA harvested at time point 2 h. No effect of DNase treatment on the quality of RNA could be observed (Figure 28). Further, DNase treatment revealed no significant decrease of RNA concentration measured via Nanodrop: 2.2 µg of total RNA before DNase digestion compared to around 2 µg of total RNA afterwards.

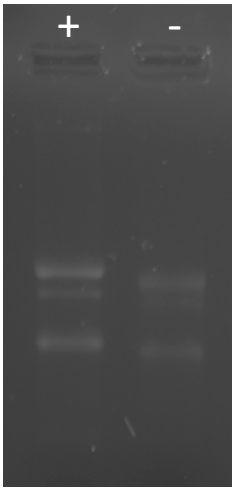

Figure 28. DNase treatment has no effect on RNA quality. *K. oxytoca* RNA isolated at time point 2 h was digested with DNase (+) and loaded on a denaturing agarose gel together with undigested RNA (-).

4.4.2 Examination of first strand cDNA synthesis

The same amount of digested RNA from each sample was used for reverse transcription. To exclude genomic DNA contamination and reagent contamination a reverse transcriptase minus

negative (RT-) control and a no template negative control (NTC) was used. To check the reverse transcription reaction ,we performed a control PCR using primers binding within the *rpoB* gene. The PCR products were loaded on an agarose gel. As expected, all samples revealed a 1120 bp fragment. The absent fragment of the RT- and NTC, as well as the negative control for the control PCR confirmed no contaminations (Figure 29). Further, the signal intensity of the 0.5 h - 3 h samples is higher compared to other timepoints.

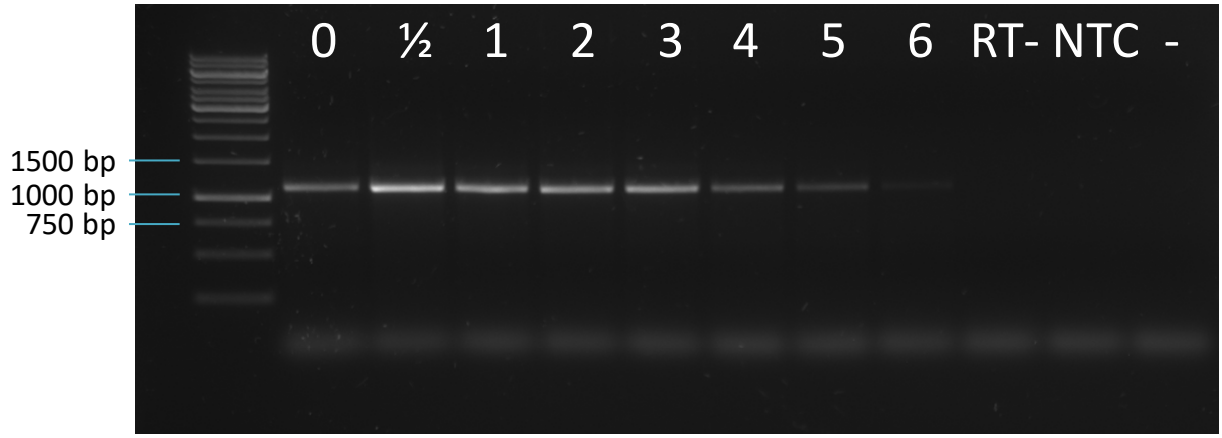

Figure 29. Reverse transcription control PCR. A reverse transcription was performed with the same amount of DNase digested RNA from each sample. Reverse transcriptase minus negative (RT-) control and no template negative control (NTC) were used to evaluate contaminations. To assess the reverse transcription reaction a control PCR was performed with primers targeting the *rpoB* gene and the PCR products were separated using agarose gel electrophoresis. For the PCR negative control (-) we used water instead of template to assess contaminations of the control PCR.

4.4.3 Validation of primer efficiencies for gene expression studies

For reliable and reproducible results, qRT-PCR analysis requires optimization and validation. Quantitative cycles (Cq) values are only representative of the template amount when the reaction efficiency is near 100% [127]. Since qPCR is dependent on reaction efficiency, we performed amplification efficiency experiments to validate primers, the reaction efficiencies and annealing temperatures. The validated reaction efficiencies and the sample dilutions of each gene were shown in Table 13. The reaction efficiencies for all target genes ranged between the desired 90% and 110%, except *pehX* (tested three different primer pairs targeting *pheX*). This gene was therefore excluded in further experiments. In addition, the amplification specificity was confirmed by revealing a single PCR product of expected size on agarose gel electrophoresis and melting curve analysis revealed only single peaks (Figure 30 and Figure 31). The RT- control and NTC of *16S* revealed Cq values during the amplification efficiency experiments. These qRT-PCR

amplicons showed a fragment on agarose gel electrophoresis, which indicates possible dimer forming in the qRT-PCR. However, this should not disturb the qRT-PCR results due to the desired reaction efficiency and the large difference of the Cq values between the controls and the samples (difference of minimum 12 cycles).

Table 13. Selected candidate gene and reference genes and their amplicon size, respective PCR amplification efficiencies and RNA dilutions assessed in *K. oxytoca* AHC-6 cells at different time points. Candidate reference genes were underlined.

Target genes	Amplicon size	Reaction efficiency [%]	Validated RNA dilution
npsA	197 bp	107.9	1:20
uvrX	174 bp	103.6	1:20
mfsX	183 bp	106.4	1:20
marR	243 bp	99.6	1:20
16S rRNA (*16S*)	132 bp	108.3	1:20,000
proC	228 bp	106.6	1:20
gapA	177 bp	109.0	1:20
mdh	151 bp	108.9	1:20
pehX	183 bp	not calculated[1]	
rpoB	150 bp	105.0	1:20
rho	165 bp	103.3	1:20

[1]not possible due to very low and different Cq values

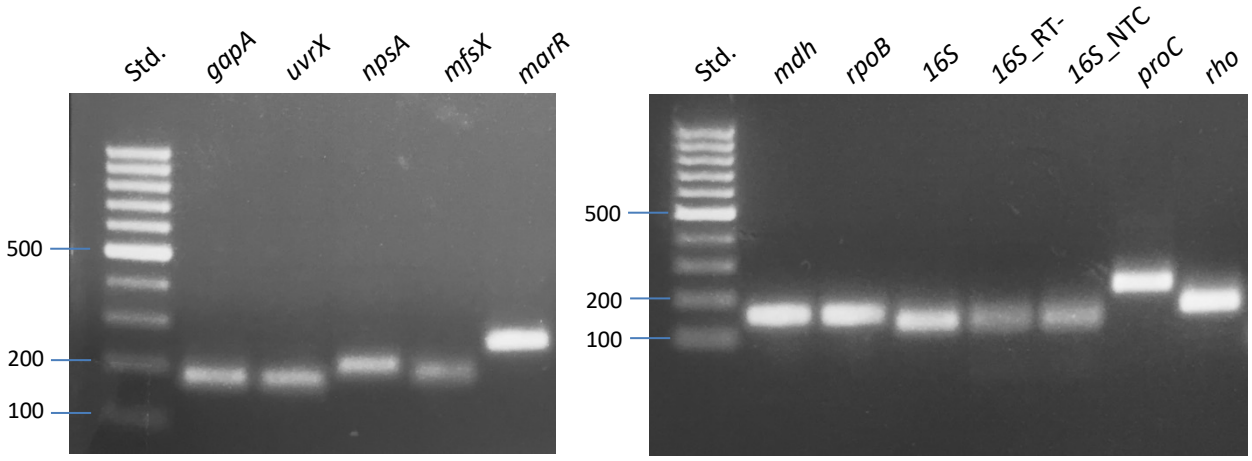

Figure 30. Agarose gel electrophoresis of qRT-PCR amplicons. The qRT-PCR amplicons from primer efficiency experiment were loaded on an agarose gel to assess the primer specificity, purity and identity.

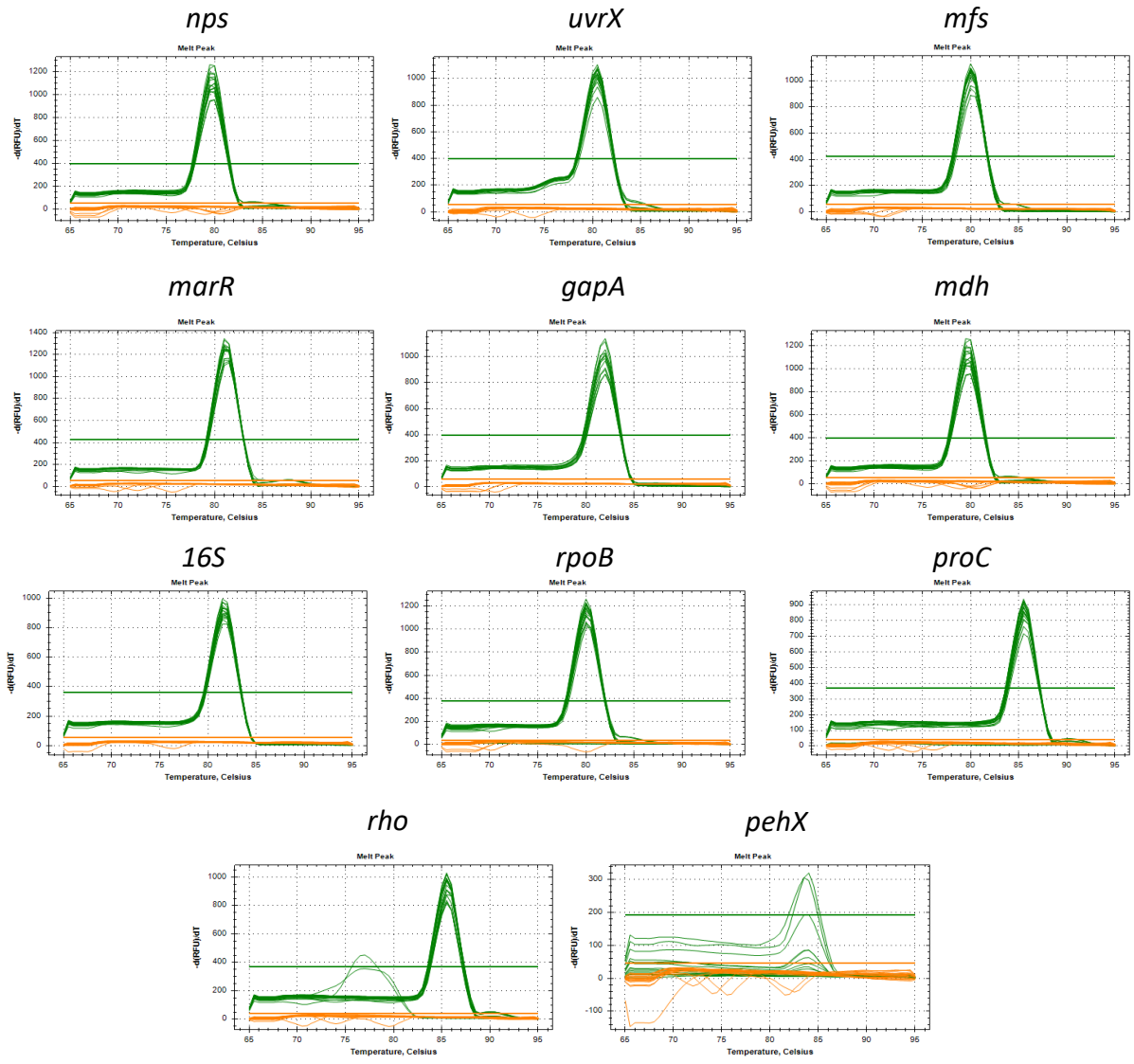

Figure 31. Melting curve analysis of all genes except *pehX* showed only single peaks and specific amplification.

4.4.4 Expression stability of candidate reference genes

In order to achieve reproducible data that truly reflects the experimental expression conditions being evaluated it is common to normalize the expression level of a target gene to the expression level of an endogenous stably expressed gene, also called the reference gene. Since accurate normalization is important and relies on the stable expression of the reference gene, choosing an appropriate reference gene is a crucial step for the establishment of gene expression analysis [128].

In this study, the expression profile of six candidate reference genes (gapA, *16S,* mdh, rpoB, proC and rho) was examined in *K. oxytoca* AHC-6 cells to identify the most suitable reference gene for our qRT-PCR approach. The genes were identified as housekeeping genes according to previous literature and therefore selected as candidates [128,129]. Expression of the candidate reference genes was observed at the time points 0 h, 0.5 h, 1 h and 2 h. Since the Cq values of time point 0 h were identified as outliers over all genes we excluded this time point (Appendix Table A1). The transcript levels of the candidate genes are given as Mean Cq (mean of 0.5 h, 1 h, 2 h ± SD) values in Table 14. Overall, the selected reference genes revealed cycle variation across all samples. *16S* followed by *mdh* and *proC* displayed the lowest cycle variation (0.17, 0.30 and 0.34, respectively). *rho* and *gapA* showed the largest variation in cycle number (2.01 and 1.24).

Table 14. Selected candidate reference genes, their corresponding product name, amplicon size in base pairs (bp), their reaction efficiency and the mean Cq values of all time points (± SD) assessed in *K. oxytoca*. The different transcript levels of the candidate reference genes at the time points 0.5, 1 and 2 h in *K. oxytoca* AHC-6 were measured via qRT-PCR. The differences in expression levels are given as Mean ± SD.

Genes	Product Name	Amplicon size	E (%)	Mean Cq ± SD
gapA	Glyceraldehyde-3-phosphate dehydrogenase	177 bp	109.0	17.75 ± 1.24
16S	16S ribosomal RNA	132 bp	108.3	17.99 ± 0.17
mdh	Malate dehydrogenase	151 bp	108.9	24.49 ± 0.30
rpoB	RNA polymerase subunit	150 bp	105.0	19.20 ± 0.97
proC	Pyrroline-5-carboxylate reductase	228 bp	106.6	23.93 ± 0.34
rho	Transcription termination factor rho	165 bp	103.3	21.75 ± 2.01

E: Reaction efficiency (%); SD: Standard deviation

The two most promising reference genes, *16S* and *mdh*, were selected for further validation. We extended the period for analysis of transcript levels of these candidates up to 3 h. The Cq values

of *16S* presented lower variation in Cq values compared to *mdh* (0.5 cycles and 1.16 cycles, respectively)(Table 15).

Table 15. *16S* revealed the lowest cycle variation. Candidate reference genes *16S* and *mdh*, their mean Cq values each time point, the cycle variation showed as the maximum difference between Cq values (range) and the mean and SD of Cq values of all time points assessed in *K. oxytoca*. The different transcript levels of the candidate reference genes at the time points 0.5, 1, 2 and 3 h in *K. oxytoca* AHC-6 culture were measured via qRT-PCR. The differences in expression levels are given as Mean ± SD and as Cq range.

Genes	Time point [h]	Mean Cq per Time point	Range Cq	Mean ± SD
16S	0.5	18.39	0.5	18.85 ± 0.22
	1	18.35		
	2	18.74		
	3	18.85		
mdh	0.5	25.4	1.16	24.92 ± 0.43
	1	25.19		
	2	24.87		
	3	24.24		

Reference genes should be expressed at relatively constant levels unaffected by differences in samples and treatments (Δ Cq < 0.5). For this reason, *mdh* was considered unsuitable for a reference gene and was excluded on further analysis.

Because in literature they propose to use at least two reference genes as internal standards we decided to subjected the candidate *proC* together with *16S* to a second optimization experiment testing the effect of extended growth on expression [127,130]. The expression stability of the two candidate reference genes was monitored over time from 0.5 h to 6 h (Table 16). Both genes *16S* and *proC* were expressed relatively stably during growth (Table 16 and Figure 32). *proC* revealed a variation in Cq values of 0.69 cycles and was ranked as most stably expressed gene closely followed by *16S* with a variation in Cq values of 0.71. The expression date showed that the use of *16S* and *proC* as reference genes is sufficient for reliable data normalization in this expression analysis in *K. oxytoca* AHC-6.

Table 16. *16S* and *proC* were expressed relatively stable. Candidate reference genes *16S* and *proC*, their mean Cq values of the technical replicates, the cycle variation showed as maximum difference between Cq values (Range) and the mean and SD of Cq values of all time points assessed in *K. oxytoca* AHC-6. The different transcript levels of the candidate reference genes at different time points (0.5, 1 to 6 h) in *K. oxytoca* AHC-6 culture were measured via qRT-PCR. The differences in expression levels are given as Mean ± SD and as Cq Range.

Genes	Time point [h]	Mean Cq per time point	Range Cq	Mean ± SD
16S	0.5	17.17	0.71	17.24 ± 0.20
	1	16.85		
	2	17.30		
	3	17.29		
	4	17.20		
	5	17.32		
	6	17.56		
proC	0.5	24.48	0.69	24.32 ± 0.21
	1	24.24		
	2	24.30		
	3	24.08		
	4	24.12		
	5	24.27		
	6	24.77		

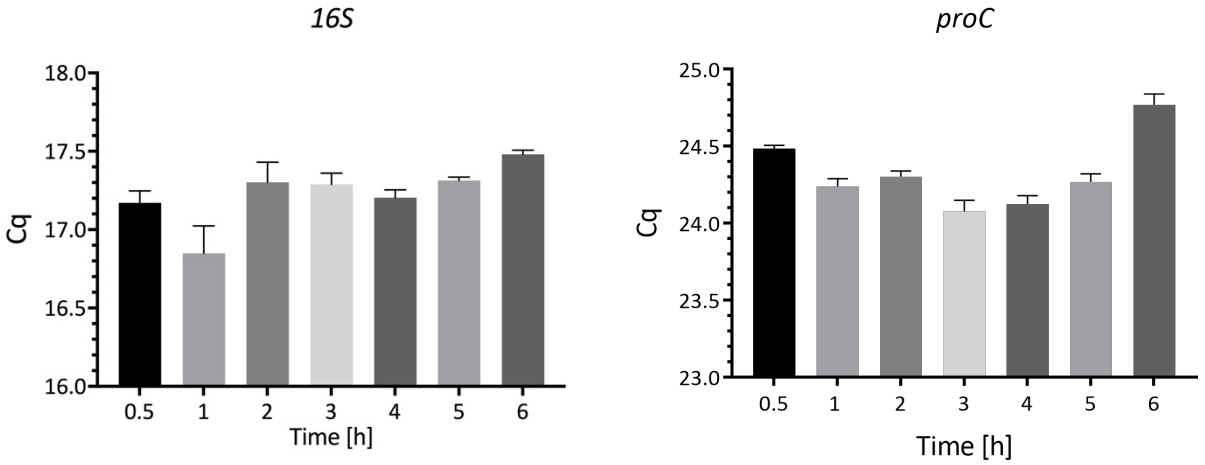

Figure 32. In vitro expression levels of reference genes *16S* and *proC* during growth of in *K. oxytoca* AHC.6. Gene expression levels shown as average Cq values of *16S* and *proC*. Each bar represents the mean of three technical samples of one culture. Error bars indicate standard deviations.

In contrast to the first expression experiment, *proC* showed no stable expression during the following gene expression analysis of the genes *npsA*, *uvrX*, *mfsX* and *marR*. These experiments revealed a mean variation of 1.17 between the cycles of the reference gene *proC* (n = 3, except time point 0.5: n = 6) (Table 17). In addition, *proC* transcript levels of the determined control time point 0.5 h differed the most from the other transcript levels. The determined relative quantity represents the fold change between the different time points relative to the selected normalization factor time point 0.5 h. For this reason, the expression variance of the normalization factor time point 0.5 h leads to an alteration of the whole data analysis and qRT-PCR data do not represent the true expression differences between samples.

Table 17. *proC* transcript levels showed high variations. The mean Cq value per time point, the range and the total mean (± SD) of Cq values from the reference gene *proC* assessed in *K. oxytoca* AHC-6. The different transcript levels of the candidate reference genes at different time points (0.5, 1 to 6 h) in *K. oxytoca* AHC-6 culture were measured via qRT-PCR (n = 3, except 0.5 h: n = 6). The differences in expression levels are given as Mean ± SD and as Cq range.

Genes	Time point [h]	Mean Cq per time point	Range Cq	Mean ± SD
proC	0.5	24.95	1.17	24.25 ± 0.37
	1	24.49		
	2	23.88		
	3	23.78		
	4	24.07		
	5	24.20		
	6	24.39		

One goal of this study was to examine the gene expression of the toxin gene *npsA*, the immunity genes *mfsX* and *uvrX*, as well as *marR*. Therefore, a qRT-PCR experiment was established including the analysis of the effect of RNA extraction procedure and DNase treatment on RNA integrity, primer validation and the reference gene validation. In summary, we developed a method to acquire appropriate RNA yield and quality, validated the required primer and reference genes. In this project, the expression stability of six candidate reference genes was validated. *16S* was the most stable expressed reference gene. Consequently, *16S* was identified as the most suitable reference gene for the following gene expression experiments.

4.4.5 *npsA, uvrX, mfsX* and *marR* expression increase with time

In order to investigate the correlation between TM immunity gene expression and TM gene expression we analyzed the transcript levels of gene *npsA*, the immunity genes *mfsX* and *uvrX* along with the putative transcriptional activator *marR*. Cell growth was monitored by measuring OD_{600} at each time point shown in Figure 33. qRT-PCR results revealed that the upregulation of expression of all genes starts after 4 h and increases with time (Figure 34A). The genes *npsA, mfsX, uvrX and marR* showed a 143-fold, 49-fold, 46- fold and 11.7-fold upregulation, respectively, compared to the 0.5 h time point (Appendix Table A2). Further, a significant increase of upregulation in *npsA*, *mfsX* and *uvrX* expression could be observed after 5 h and for all genes after 6 h, when compared with time point 0.5 h (Figure 34B).

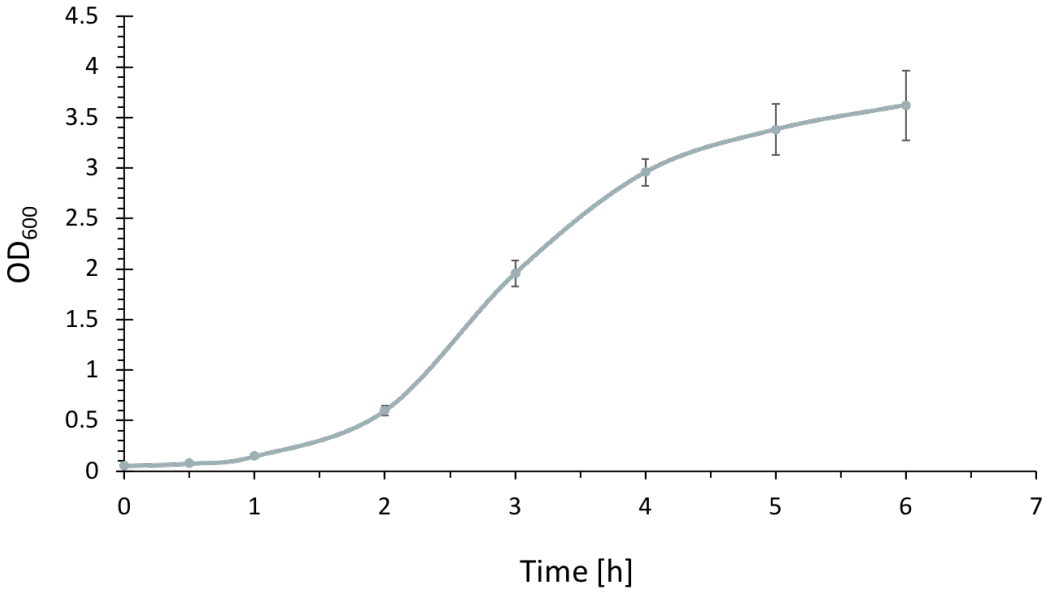

Figure 33. Continuous culture growth of *K. oxytoca* AHC-6 during the qRT-PCR experiment. OD_{600} was measured at each time point to monitor the growth of the cell culture. Bars represent the mean ± SD from three biological replicates.

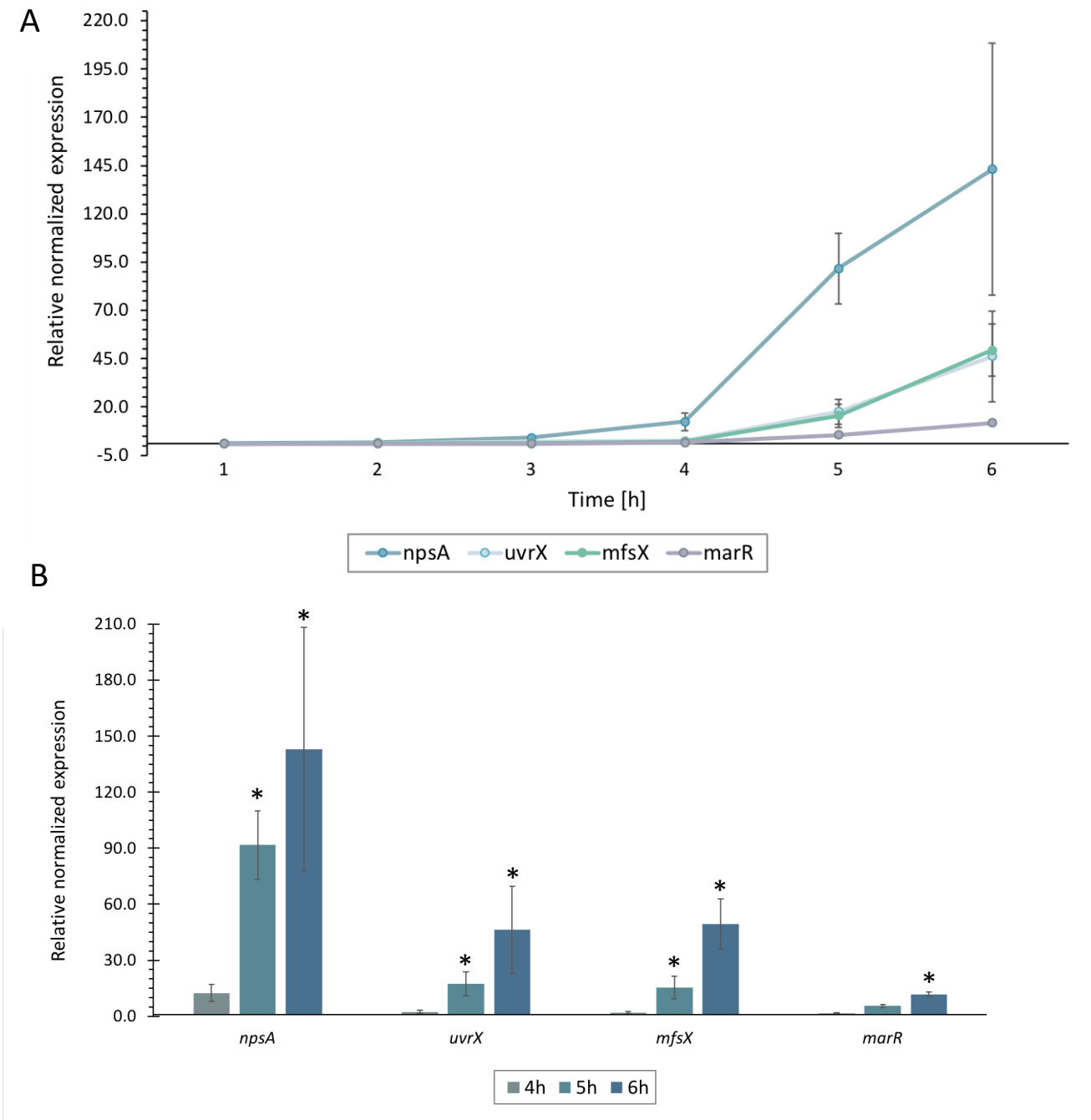

Figure 34. In vitro *npsA, uvrX, mfsX* and *marR* expression increase with time. Relative expression of TM immunity genes and toxin gene as well as marR during the continuous growth of *K. oxytoca* AHC-6 was measured via qRT-PCR. The relative expression levels of target genes relative to the control 0.5 h samples at corresponding time points were calculated using the Pfaffl-Method and normalized to the expression of the reference gene *16S*. Bars represent the mean ± SD (n = 3). (B) Significance of results was determined with Kruskal-Wallis followed by Dunn's multiple comparison (*$P \leq 0.05$)

Taken together, we have established a qRT-PCR analysis to examine gene expression in *K.oxytoca*. Further, this analysis was the first step towards enhancing the knowledge about the regulation of the *K. oxytoca* TM immunity genes.

5 Discussion

5.1 *E. coli ΔuvrA* is hypersensitive to TM

The first part of this study investigated the antimicrobial activities of *K. oxytoca* tilimycin against *E. coli* Δ*uvrA*. It was shown by Unterhauser et al. that tilimycin is a DNA-damaging agent causing strand breakage in mammalian cells and possessing antimicrobial activities against anaerobic bacteria of the human gut. We hypothesized that the *E. coli* Δ*uvrA* mutant strain should be more susceptible to TM compared to *E. coli* WT because of the absence of UvrA, which initiates a key DNA damage repair mechanism.

The susceptibility of *E. coli* WT and *E. coli* Δ*uvrA* to TM was compared using a cell viability assay. The strains were treated either with 85 µM tilimycin or 0.58% Ethanol as a control for 2 h in broth media with arabinose. To guarantee the same conditions for all strains the same amounts of cells were used for TM treatment (OD_{600} 0.1). Further, strains were carrying either a complementation vector or the empty vector pBAD33. The percentage of cell viability was calculated relative to the control by determining the CFU/ml of the plated dilutions on agar plates. As expected, *E. coli* Δ*uvrA* was hypersensitive to TM compared to *E. coli* WT and showed a 6-fold decrease in cell viability. Further, expression of *uvrA* in trans was able to partially restore the TM resistance of *E. coli* Δ*uvrA* (Figure 6). This might be due to a different promotor of the vector compared to the native and different mechanisms of induction of gene expression.

In general, these results agree with previous research about TM. It was shown that TM has genotoxic effects on host cells in vitro and in vivo including DNA single-strand and double-strand breaks. Further it was shown in mutant haploid human cells that survival following TM exposure requires activation of the DNA damage repair mechanism TCR, a subpathway of NER [95]. TCR targets DNA alterations that inhibit the translocation of the RNA polymerase (RNAP) through expressed genes and is well characterized in bacteria. TCR is activated upon transcription blockage as soon as the RNAP recognizes a lesion during gene transcription. After the transcription repair coupling factor (TCRF or Mfd) binds to the arrested RNAP, which releases RNA, it recruits UvrA leading to the initiation of the GGR. Initiation of repair is evidently dependent on UvrA and UvrB after the release of the RNAP [104,131].

Therefore, the results presented here support the conclusion that TM has antimicrobial and DNA-damaging effects on bacteria of the human gut like *E. coli*. However, since cell viability includes bacterial growth and survival, the method used in this study cannot distinguish between bactericidal and bacteriostatic effects of TM. One possible way to investigate the effects of TM on growth and survival would be to pursue growth during the established cell viability assay.

5.2 Expression of *uvrX* in *E. coli* increases TM resistance

Previous gene homology comparison revealed identities between 40 and 52% between *K. oxytoca uvrX* and the related genes *S. peucetius drrC* and *E. coli* K12 *uvrA*. Here we aimed to characterize the function of the *K. oxytoca* AHC-6 *uvrX* gene using the TM hypersensitive *E. coli* Δ*uvrA* strain. For this purpose, we constructed a *uvrX* complementation vector and analyzed the effect of heterologous *uvrX* expression in *E. coli* Δ*uvrA* on TM resistance.

The results revealed that *uvrX* expression in the *E. coli* Δ*uvrA* mutant and WT increased significantly the TM resistance (Figure 7). This suggests that *K. oxytoca* AHC-6 *uvrX* is a TM immunity gene. Since UvrX was able to protect *E. coli* Δ*uvrA* mutant from the lethality of TM, it is likely that UvrX facilitates the repair of DNA damage caused by TM. In addition, we proposed that UvrX repairs TM caused DNA damage specifically because UvrX confers even higher TM resistance to *E. coli* compared to *uvrA* itself. The UvrX mediated increase of TM resistance in the WT strain supports this hypothesis. Because of the similarity between *uvrX* and *drrC* genes we speculate that UvrX inhibits the binding of TM to genomic DNA.

Thus far the mechanism of UvrX-conferred TM resistance remains unclear. However, *K. oxytoca* AHC-6 *uvrX* clearly has a TM protective effect on *E. coli*.

5.3 *K. oxytoca* AHC-6 UvrX is involved in nucleotide excision repair independent of UvrB

The viability assay results using *E. coli ΔuvrA* indicate that UvrX confers TM resistance by facilitating the repair of DNA damage. Since UvrX shows homology to the related protein DrrC and UvrA we asked whether UvrX accomplishes TM resistance by acting like *S. peucetius* DrrC or *E. coli* UvrA. With protein fold prediction of UvrX via PHYRE2, we could confirm that UvrX has conserved structures common in UVR proteins within the ABC protein family. A more detailed analysis of the sequence and protein structure identified the UvrA homolog UvrX as Class II type

of UvrA proteins, which lacks the UvrB binding domain. Taking these findings together, we hypothesized that UvrX might be involved in NER independently of UvrB and thus possibly recognizing TM-bound DNA complexes in a similar way as DrrC.

5.3.1 UvrX is a member of the ATP-binding cassette protein family

In-silico analysis of the UvrX protein structure showed the presence of two NBDs each comprising ATP-binding and ABC-signature subdomains (Figure 21). These structures are conserved in proteins that belong to the ABC protein family involved in transport, translation elongation, and DNA repair [122]. Overlap of the predicted protein structure of UvrX and dnUvrA2 revealed high similarity, which permits the use of dnUvrA2 as a template for homology modeling. Validation of the 3D model via PROCHECK web portal indicates that 91.3% of residues are present in the favored regions and 0.3% in the outlier region (Figure 35) [114]. In general, the Ramachandran plot visualize energetically allowed regions for backbone angles against amino acid residues in protein structures [132]. According to PROCHECK a good quality model would be expected to have over 90% in the favoured regions. This results imply that the predicted UvrX protein structure is reliable because the outliers derive from the quality of the template dnUvrA2.

		No. of residues	%-tage
Most favoured regions	[A,B,L]	620	91.3%
Additional allowed regions	[a,b,l,p]	53	7.8%
Generously allowed regions	[~a,~b,~l,~p]	4	0.6%
Disallowed regions	[XX]	2	0.3%*
Non-glycine and non-proline residues		679	100.0%
End-residues (excl. Gly and Pro)		3	
Glycine residues		79	
Proline residues		52	
Total number of residues		813	

Figure 35. Ramachandran plot statistics of the predicted UvrX protein structure

Identical to dnUvrA2, UvrX comprises an insertion domain (ID) within the N-terminal NBD (Figure 21). Previous research on dnUvrA2 suggests that the ID is directly involved in DNA binding. Further, it was shown that UvrA binds specifically to sites of DNA damage and that its efficient recognition is dependent on the presence of these domains [123]. These observations suggest that UvrX is a DNA-binding protein that is involved in DNA-damage repair.

Further, sequence analysis of UvrX identified several motifs including Walker A, Walker B, and ABC-signature motif, Q-loop, D-loop, and H-loop. The Walker A motif and the Walker B motif are

highly conserved sequence motifs in all ABC systems and indicate the presence of nucleotide-binding sites. The signature motif is unique to ABC proteins and participates in ATP binding and hydrolysis [121,122]. The additional Q-, D- and H-loop motifs contain only one highly conserved domain and have different functions during ATP-hydrolysis and dimerization [121,133]. These conserved motifs were discovered via the NCBI CDD and could be located within the UvrX protein sequence, which verified the outcome of the CDD search. ABC proteins are remarkably conserved in the primary protein sequence and in their organization [122]. Therefore, we conclude that UvrX belongs to the UvrA protein family within the ABC protein family [122,134].

5.3.2 Functional characterization of UvrX

Protein structure and sequence analysis identified UvrX as an ABC protein that shares high identity with dnUvrA2. Therefore, we hypothesized that UvrX acts similarly to dnUvrA2. In bacteria, UvrA proteins recognize damaged DNA and initiate the multistep DNA damage repair mechanism NER and play a role during the already mentioned TCR.

UvrA homologs are common in different bacterial species. Studies of these UvrA homologs identified that the UvrA family can be grouped into five distinctive classes (Figure 36). The difference between the various categories is a deletion of specific domains or gene duplication as well as both. Class II UvrA proteins have a deletion of about 150 amino acids, including the C1 motif of the zinc-finger (Cys-XX-Cys). All UvrA proteins contain the C2 motif compared to the C1 motif, which can only be found in a part of proteins [135]. Protein structure prediction and analysis of UvrX revealed that UvrX also lacks this 150-residue region, including the C1 motif present in drUvrA1 and bstUvrA1. These characteristics place UvrX in the class II of UvrA proteins.

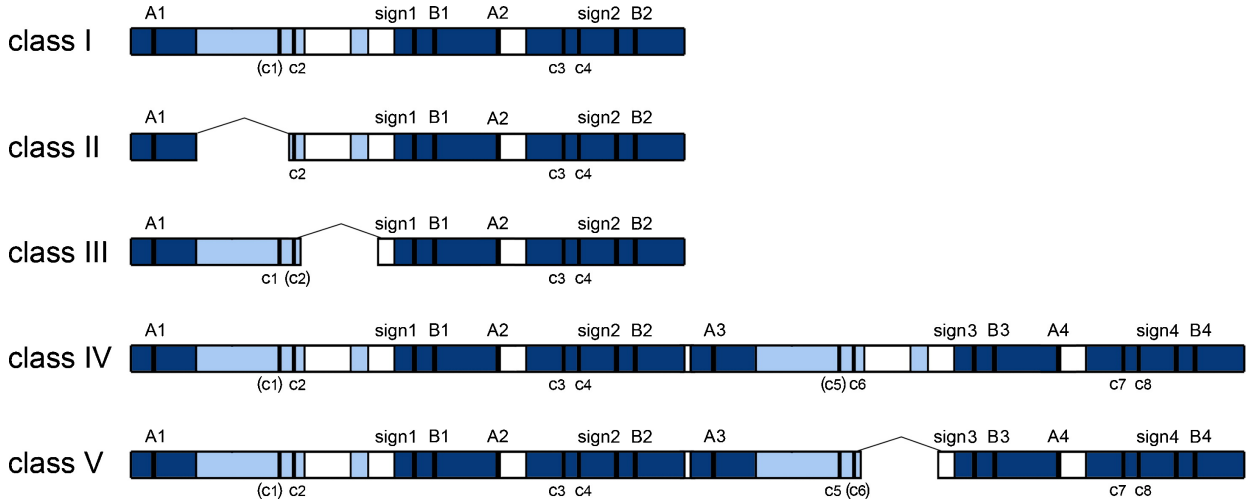

Figure 36. Different classes of UvrA homologs found in bacteria. Dark blue area's represent domains that are 65–75% conserved among all UvrA proteins. Light blue regions are 30–40% conserved and white regions are 10–15% conserved. The Walker A motifs (A1–A4), the Walker B motifs (B1–B4) and the ABC signature motifs (signs 1–4) are indicated. The CysXXCys sequences that have been implicated in Zn coordination are indicated with c1–c8. When placed between brackets the sequence is not always present in the different UvrA proteins belonging to that particular class. Class I proteins are full-length UvrA proteins that are present in most bacterial species, including *E. coli*. Classes II and III proteins contain large deletions, each of a different region. Class IV proteins are duplications of the full-length UvrA protein and Class V proteins are duplications with a deletion in the C-terminal half. (Figure from [10])

Class II UvrA proteins are mostly found in *Actinobacteria* as well as *Firmicutes* and *Proteobacteria* in conjunction with either Class I or Class IV UvrA homologs. Several studies on different class II UvrA proteins suggest that these homologs are rather involved in antibiotic resistance than in DNA repair [10]. For example, *S. peucetius drrC* encodes a Class II UvrA protein, that mediates self-resistance by removing the intercalated antibiotic from the DNA [49]. Interestingly, it has been shown that the 150-residue is essential for stable interaction of UvrA with UvrB and consequently for nucleotide excision repair [136]. Since UvrX lacks this important region, UvrX might mediate TM resistance by DNA repair independent of the NER similar to DrrC. Taken together, these finding suggests a model where UvrX scans the DNA for bound TM and facilitates self-resistance by removing encountered TM from DNA. Thus, the DNA is free of TM which guarantees DNA replication and transcription to continue unhindered.

5.4 *K. oxytoca* AHC-6 genes *mfsX* and *uvrX* are tilimycin immunity genes

To examine the role of *mfsX* and *uvrX* in *K. oxytoca* self-resistance we constructed an *mfsX uvrX* deletion strain of *K. oxytoca* AHC-6. Disruption of the genes was not lethal to either the toxin producing *K. oxytoca* AHC-6 *aphA* or toxin deficient Mut89 cells. However, the *K. oxytoca* AHC-6 Mut89 *mfsX uvrX* strain was considerably more sensitive to TM added externally in the culture medium compared to the parental strain. Moreover, the expression of both genes in trans was able to restore the TM resistance of the hypersensitive mutant strain. This shows that *mfsX*, *uvrX*, or both are involved in resistance by which *K. oxytoca* survives the toxic effects of TM.

Expression of *mfsX* in *K. oxytoca* AHC-6 Mut89 Δ*mfsX*, *uvrX* led to a significant increase in survival after TM treatment. Interestingly, *uvrX* expression conferred even 2-fold higher TM resistance to the Δ*mfsX*, *uvrX* mutant strain compared to *mfsX* expression. Besides, OD_{600} values showed that TM has no effect on the growth of *K. oxytoca* but a late-onset bactericidal activity. These results imply that *uvrX* has a pivotal role in TM resistance. The suggested role of UvrX to remove TM from genomic DNA may be crucial for self-resistance. However, it appears that *uvrX* and *mfsX* are required for conferring full complement of TM resistance in *K. oxytoca* AHC-6. In addition, to minimize the amount of DNA-bound TM, the organisms need a way to export the drug to avoid an accumulation of TM in the cell. *K. oxytoca mfsX* shares a high identity with *S. peucetius drrAB*, which encodes a multidrug transporter for the export of DNR [73]. Therefore, we hypothesis that *mfsX* mediates the export of TM. The lower TM resistance mediated by *mfsX* supports this hypothesis because *K. oxytoca* possesses several efflux transporters that may also function to export TM. However, further analysis would be needed to determine exactly how *mfsX* mediates TM resistance.

Contrary to expectations, expression of the *mfsX*, *uvrX* operon led to a lower TM resistance than *uvrX* alone. This reduced survival can be explained in part by the differences in the RBS. The RBS of *mfsX* and *uvrX* used in the pBAD33 vector was different compared to the chromosomal RBS, which might lead to an altered translation efficiency.

5.5 Establishing a qRT-PCR experiment

One purpose of this study was to establish a method for the determination of transcript levels in *K. oxytoca* to monitor the expression of the TM biosynthesis and TM immunity genes. Further, we attempted to investigate a correlation between biosynthesis and resistance regulation.

5.5.1 Validation of RNA integrity

In general, the expression of self-immunity genes in antibiotic producing bacteria is tightly connected to antibiotic biosynthesis gene expression. In this study, a qRT-PCR method was established to monitor the in vitro immunity gene and TM synthetase gene expression in *K. oxytoca* AHC-6.

The RNA integrity was assessed via denaturing agarose gel electrophoresis. Prior to the gel electrophoresis, we measured the concentration of the isolated RNA via NanoDrop. Moreover, this technique allows for assessing of the purity of DNA and RNA. The tested RNA samples revealed a ratio of absorbance OD 260/280 nm and OD 260/230 nm higher than or near 2 except the RNA isolated from the ONC (OD 260/230 of 1.15) (Table 1). Ratios significantly lower indicate the presence of contaminants [137]. Therefore, all samples aside from the ONC displayed a high RNA purity. However, we tested the RNA integrity of all samples by loading the same amount of RNA for every sample on a denaturing agarose gel.

On the denaturing agarose gel, RNA isolated from the ONC showed no sharp bands which indicates degradation. The other samples revealed sharp, clear 23S, 16S, and 5S rRNA bands. Unexpectedly, an additional rRNA fragment located between 23S and 16S was visible for all samples. In general, Gram-negative bacteria show only three fragments. However, some display four instead of three rRNA fragments due to a possible cleavage of the 23S rRNA fragment causing two molecules [138]. Furthermore, DNase digested RNA samples showed sharp rRNA fragments on the denaturing agarose gel. This result revealed that DNase treatment does not affect RNA quality.

5.5.2 *rpoB* as choice for control PCR amplification

First strand cDNA synthesis was assessed via control PCR amplification using *rpoB* as the target gene. On the agarose gel, the controls (RT-, NTC, NC) displayed no band. This result verifies the absence of genomic DNA contamination or reagent contamination of the RNA sample. As

expected, the RT-PCR products revealed a distinct 1120 bp product. The possible amplification of a large fragment suggests no RNA degradation. The signal intensity increases after 0.5 hours compared to time point 0. The intensity is reduced after 4 hours and is further decreasing causing a weak band after 6 hours. The observed variances in intensities could be attributed to diverse expression levels of *rpoB*. Although the *rpoB* gene was stated as a housekeeping gene in literature it reveals no stable expression during this study [129]. A stable expression of the target gene used for the control PCR amplification is required to assess the cDNA synthesis reaction for each sample. Consequently, we initially selected *rpoB* as the most suitable target gene. Despite this, we can still state that the reverse transcription reaction succeeded without any contaminations.

5.5.3 Reference gene validation

One of the most crucial steps in establishing qRT-PCR is the validation of the reference genes used for data normalization. In the best case, the reference gene is stably expressed despite differences in physiological states and experimental conditions. For that reason, any potential reference gene must be validated prior to its application in qRT-PCR [127].

Unfortunately, there is no validated reference gene for *K. oxytoca* described in the literature. However, we found several genes that have been stated as house keeping genes and validated reference genes for the related species *K. pneumoniae* [128,129]. In this study, we evaluated six candidate reference genes (*gapA*, *16S* rRNA, *mdh*, *rpoB*, *rho*, *proC)* for *K. oxytoca* AHC-6. The candidate reference gene *16S* represented the most stable expression in all conditions compared to the other candidates. Monitoring *16S* expression over time revealed differences in Cq values of *16S* of 0.71 cycles. These differences are higher than the recommended expression variations for reference genes. However, the expression of *16S* exhibited stable expression during further qRT-PCR experiments with a maximum difference between Cq values of 0.58. Generally, ribosomal RNA genes including *16S* are not recommended due to their high abundance of transcripts. This high abundance requires dilution of the cDNA samples before qRT-PCR reactions, thus increasing the possibility of dilution errors [139]. Given that our findings are based on a limited number of candidate reference genes, the results from this analysis determined *16S* as the most suitable reference gene for the aim of this study.

In general, two reference genes for data normalization are recommended to guarantee reliable and quality data. The MIQE guidelines allow normalization against a single reference gene if the gene exhibits stable expression under the experimental tested conditions [140]. Since the chosen reference gene *16S* revealed just sufficient stable expression, we recommend that follow up studies choose at least two internal controls and continue validation of more candidate reference genes. Moreover, several statistical algorithms as BestKeeper, NormFinder and RefFinder, are recommended to test the expression stability of the candidate genes [127]. The use of this commonly used software may be beneficial and time saving for the validation of candidate reference genes.

5.6 Is the expression of TM immunity genes coordinately regulated with the tilimycin gene expression?

In this study, we established a qRT-PCR analysis to investigate a time-dependent correlation between tilimycin immunity gene and TM gene expression. A simultaneous increase of the immunity genes *uvrX* and *mfsX* and the toxin gene *npsA* propose that these genes are coordinately regulated.

The expression levels of TM resistance genes and a toxin biosynthesis gene were determined via qRT-PCR. The mRNA levels of these genes increase over time, beginning after 4 h of *K. oxytoca* AHC-6 growth in vitro (Figure 22A). Despite the considerable standard deviation of the gene transcript levels at later timepoints, the results confirm a significant upregulation of gene expression after 6 h when compared to 1 h (Figure 22B). Generally, the qRT-PCR analysis revealed an unexpected considerable increase of *npsA* gene expression with an upregulation in transcript levels up to 143-fold.

The npsA upregulation was much higher compared to that of the other genes. Further, a 7.4-fold increase in expression of npsA was seen after 4 h as compared to 5 h. The biosynthesis gene expression correlates well with the previous monitoring of the time-dependent formation of TM that revealed an increase of TM in *K. oxytoca* after 8-10 h [119].

The TM immunity genes *mfsX* and *uvrX* revealed almost equal expression levels. Their transcript levels significantly increased at the entry of the stationary phase (5 & 6 h) compared to the 1 h transcript levels. The observed identical expression levels of the immunity genes correlate with

the organization of the genes in one operon. Moreover, their transcript levels increase in parallel with the expression of the TM biosynthetic gene *npsA*.

The expression of resistance genes in most antibiotic-producing bacteria is closely related to that of antibiotic biosynthetic genes. Further, resistance requires the expression of immunity genes in a timely manner: either prior to or along with antibiotic biosynthesis [126]. In *S. peucetius*, the transcriptional regulator DnrI binds to the promotor elements of the resistance genes *drrAB* and *drrC*, but their expression is induced by intracellular DNR [141]. The findings of this study suggest an equivalent regulation mechanism for TM resistance in *K. oxytoca*. We hypothesize that the expression of the immunity genes *mfsX* and *uvrX* is coordinately regulated with the TM biosynthesis gene expression. However, a more detailed analysis of the *mfsX*, *uvrX* expression is required to fully understand the molecular mechanisms underlying the regulation of immunity gene expression in *K. oxytoca*.

Usually, antibiotic biosynthetic gene clusters contain regulatory genes. The TM biosynthetic gene cluster of *K. oxytoca* AHC-6 contains the *marR* gene that encodes the MarR family transcriptional regulator [86]. Proteins of the MarR family contain a DNA-binding domain including a helix-turn-helix motif, which allows the derepression or activation of their target gene transcription. The majority of their target genes are critical to overcoming the effects of host-generated and externally produced antimicrobial compounds [142]. Therefore, we aim to characterize the role of *marR* regarding the regulation of TM immunity gene expression in *K. oxytoca*. The qRT-PCR analysis revealed a significant 11-fold increase in *marR* expression after 6 h. Nevertheless, *marR* is poorly expressed compared to the expression of the other observed genes. Unfortunately, our investigations so far have been limited to the early timepoints of TM production in *K. oxytoca* AHC-6, hence we are not able to form any conclusions at this time.

This study is the first step towards enhancing our understanding of the regulation of immunity gene expression in *K. oxytoca*. However, further investigations of the expression profile of the immunity genes at later time points in the *K. oxytoca* AHC-6 WT and *npsB* mutant strain will need to be performed to characterize the gene regulation.

6 References

1. Aminov RI (2010) A Brief History of the Antibiotic Era: Lessons Learned and Challenges for the Future. *Front Microbiol* 1.

2. Morehead MS, Scarbrough C (2018) Emergence of Global Antibiotic Resistance. *Prim Care Clin Off Pract* 45: 467–484.

3. World Health Organization (Ed.) (2014) Antimicrobial resistance: global report on surveillance, Geneva, Switzerland, World Health Organization.

4. Munita JM, Arias CA (2016) Mechanisms of Antibiotic Resistance. *Microbiol Spectr* 4.

5. D'Costa VM, King CE, Kalan L, et al. (2011) Antibiotic resistance is ancient. *Nature* 477: 457–461.

6. Sabtu N, Enoch DA, Brown NM (2015) Antibiotic resistance: what, why, where, when and how? *Br Med Bull* ldv041.

7. Surette MD, Wright GD (2017) Lessons from the Environmental Antibiotic Resistome. *Annu Rev Microbiol* 71: 309–329.

8. Benveniste R, Davies J (1973) Aminoglycoside Antibiotic-Inactivating Enzymes in Actinomycetes Similar to Those Present in Clinical Isolates of Antibiotic-Resistant Bacteria. *Proc Natl Acad Sci* 70: 2276–2280.

9. Hopwood DA (2007) How do antibiotic-producing bacteria ensure their self-resistance before antibiotic biosynthesis incapacitates them? *Mol Microbiol* 63: 937–940.

10. C Reygaert W, Department of Biomedical Sciences, Oakland University William Beaumont School of Medicine, Rochester, MI, USA (2018) An overview of the antimicrobial resistance mechanisms of bacteria. *AIMS Microbiol* 4: 482–501.

11. Wilson DN (2014) Ribosome-targeting antibiotics and mechanisms of bacterial resistance. *Nat Rev Microbiol* 12: 35–48.

12. Wright G (2005) Bacterial resistance to antibiotics: Enzymatic degradation and modification. *Adv Drug Deliv Rev* 57: 1451–1470.

13. Murray IA, Gil JA, Hopwood DA, et al. (1989) Nucleotide sequence of the chloramphenicol acetyltransferase gene of Streptomyces acrimycini. *Gene* 85: 283–291.

14. Schwarz S, Kehrenberg C, Doublet B, et al. (2004) Molecular basis of bacterial resistance to chloramphenicol and florfenicol. *FEMS Microbiol Rev* 28: 519–542.

15. Abraham EP, Chain E (1988) An Enzyme from Bacteria Able to Destroy Penicillin. *Rev Infect*

Dis 10: 677–678.

16. Livermore DM (2008) Defining an extended-spectrum β-lactamase. *Clin Microbiol Infect* 14: 3–10.

17. Nordmann P, Poirel L, Walsh TR, et al. (2011) The emerging NDM carbapenemases. *Trends Microbiol* 19: 588–595.

18. Rossolini GM, D'Andrea MM, Mugnaioli C (2008) The spread of CTX-M-type extended-spectrum b-lactamases. *Clin Microbiol Infect* 14 (Suppl. 1): 33–41.

19. Bonnet R (2004) Growing Group of Extended-Spectrum β-Lactamases: the CTX-M Enzymes. *Antimicrob Agents Chemother* 48: 1–14.

20. Ogawara H (2016) Self-resistance in Streptomyces, with Special Reference to β-Lactam Antibiotics. *Molecules* 21: 1–3.

21. Allen HK, Moe LA, Rodbumrer J, et al. Functional metagenomics reveals diverse b-lactamases in a remote Alaskan soil. *ISME J* 9.

22. Ogawara H, Horikawa S (1980) Penicillin-binding proteins of Streptomyces cacaoi, Streptomyces olivaceus, and Streptomyces clavuligerus. *Antimicrob Agents Chemother* 17: 1–7.

23. Pagès J-M, James CE, Winterhalter M (2008) The porin and the permeating antibiotic: a selective diffusion barrier in Gram-negative bacteria. *Nat Rev Microbiol* 6: 893–903.

24. Kojima S, Nikaido H (2013) Permeation rates of penicillins indicate that Escherichia coli porins function principally as nonspecific channels. *Proc Natl Acad Sci* 110: E2629–E2634.

25. Nikaido H (2003) Molecular basis of bacterial outer membrane permeability revisited. *Microbiol Mol Biol Rev MMBR* 67: 593–656.

26. Hancock REW (2003) On the mechanism of solute uptake in Pseudomonas. *Front Biosci* 8: s472-483.

27. Tran Q-T, Williams S, Farid R, et al. (2013) The translocation kinetics of antibiotics through porin OmpC: Insights from structure-based solvation mapping using WaterMap. *Proteins Struct Funct Bioinforma* 81: 291–299.

28. Doménech-Sánchez A, Martínez-Martínez L, Hernández-Allés S, et al. (2003) Role of Klebsiella pneumoniae OmpK35 porin in antimicrobial resistance. *Antimicrob Agents Chemother* 47: 3332–3335.

29. Hasdemir UO, Chevalier J, Nordmann P, et al. (2004) Detection and Prevalence of Active Drug Efflux Mechanism in Various Multidrug-Resistant Klebsiella pneumoniae Strains from Turkey. *J Clin Microbiol* 42: 2701–2706.

30. Costerton JW, Stewart PS, Greenberg EP (1999) Bacterial biofilms: a common cause of

persistent infections. *Science* 284: 1318–1322.

31. Anderl JN, Franklin MJ, Stewart PS (2000) Role of antibiotic penetration limitation in Klebsiella pneumoniae biofilm resistance to ampicillin and ciprofloxacin. *Antimicrob Agents Chemother* 44: 1818–1824.

32. Walters MC, Roe F, Bugnicourt A, et al. (2003) Contributions of antibiotic penetration, oxygen limitation, and low metabolic activity to tolerance of Pseudomonas aeruginosa biofilms to ciprofloxacin and tobramycin. *Antimicrob Agents Chemother* 47: 317–323.

33. Brooun A, Liu S, Lewis K (2000) A dose-response study of antibiotic resistance in Pseudomonas aeruginosa biofilms. *Antimicrob Agents Chemother* 44: 640–646.

34. Gilbert P, Allison DG, McBain AJ (2002) Biofilms in vitro and in vivo: do singular mechanisms imply cross-resistance? *J Appl Microbiol* 92 Suppl: 98S-110S.

35. Zhao X, Yu Z, Ding T (2020) Quorum-Sensing Regulation of Antimicrobial Resistance in Bacteria. *Microorganisms* 8: 425.

36. Lewis K (2007) Persister cells, dormancy and infectious disease. *Nat Rev Microbiol* 5: 48–56.

37. Campbell EA, Korzheva N, Mustaev A, et al. (2001) Structural mechanism for rifampicin inhibition of bacterial rna polymerase. *Cell* 104: 901–912.

38. Floss HG, Yu T-W (2005) Rifamycin-mode of action, resistance, and biosynthesis. *Chem Rev* 105: 621–632.

39. Goldstein BP (2014) Resistance to rifampicin: a review. *J Antibiot (Tokyo)* 67: 625–630.

40. Weisblum B (1995) Erythromycin resistance by ribosome modification. *Antimicrob Agents Chemother* 39: 577–585.

41. Roberts MC, Sutcliffe J, Courvalin P, et al. (1999) Nomenclature for macrolide and macrolide-lincosamide-streptogramin B resistance determinants. *Antimicrob Agents Chemother* 43: 2823–2830.

42. Matsuoka M, Sasaki T (2004) Inactivation of Macrolides by Producers and Pathogens. *Curr Drug Target -Infect Disord* 4: 217–240.

43. Hartman BJ, Tomasz A (1984) Low-affinity penicillin-binding protein associated with beta-lactam resistance in Staphylococcus aureus. *J Bacteriol* 158: 513–516.

44. Utsui Y, Yokota T (1985) Role of an altered penicillin-binding protein in methicillin- and cephem-resistant Staphylococcus aureus. *Antimicrob Agents Chemother* 28: 397–403.

45. Ubukata K, Yamashita N, Konno M (1985) Occurrence of a beta-lactam-inducible penicillin-binding protein in methicillin-resistant staphylococci. *Antimicrob Agents Chemother* 27: 851–857.

46. Brodersen DE, Clemons WM, Carter AP, et al. (2000) The structural basis for the action of

the antibiotics tetracycline, pactamycin, and hygromycin B on the 30S ribosomal subunit. *Cell* 103: 1143–1154.

47. Connell SR, Tracz DM, Nierhaus KH, et al. (2003) Ribosomal protection proteins and their mechanism of tetracycline resistance. *Antimicrob Agents Chemother* 47: 3675–3681.

48. Li W, Atkinson GC, Thakor NS, et al. (2013) Mechanism of tetracycline resistance by ribosomal protection protein Tet(O). *Nat Commun* 4: 1477.

49. Prija F, Prasad R (2017) DrrC protein of Streptomyces peucetius removes daunorubicin from intercalated dnrI promoter. *Microbiol Res* 202: 30–35.

50. Villagra NA, Fuentes JA, Jofre MR, et al. (2012) The carbon source influences the efflux pump-mediated antimicrobial resistance in clinically important Gram-negative bacteria. *J Antimicrob Chemother* 67: 921–927.

51. Lee A, Mao W, Warren MS, et al. (2000) Interplay between Efflux Pumps May Provide Either Additive or Multiplicative Effects on Drug Resistance. *J Bacteriol* 182: 3142–3150.

52. Tal N, Schuldiner S (2009) A coordinated network of transporters with overlapping specificities provides a robust survival strategy. *Proc Natl Acad Sci* 106: 9051–9056.

53. Masi M, Réfregiers M, Pos KM, et al. (2017) Mechanisms of envelope permeability and antibiotic influx and efflux in Gram-negative bacteria. *Nat Microbiol* 2: 17001.

54. Du D, van Veen HW, Murakami S, et al. (2015) Structure, mechanism and cooperation of bacterial multidrug transporters. *Curr Opin Struct Biol* 33: 76–91.

55. Neuberger A, Du D, Luisi BF (2018) Structure and mechanism of bacterial tripartite efflux pumps. *Res Microbiol* 169: 401–413.

56. Zgurskaya HI, Nikaido H (2000) Multidrug resistance mechanisms: drug efflux across two membranes. *Mol Microbiol* 37: 219–225.

57. Dawson RJP, Locher KP (2006) Structure of a bacterial multidrug ABC transporter. *Nature* 443: 180–185.

58. Biemans-Oldehinkel E, Doeven MK, Poolman B (2006) ABC transporter architecture and regulatory roles of accessory domains. *FEBS Lett* 580: 1023–1035.

59. ter Beek J, Guskov A, Slotboom DJ (2014) Structural diversity of ABC transporters. *J Gen Physiol* 143: 419–435.

60. Locher KP (2016) Mechanistic diversity in ATP-binding cassette (ABC) transporters. *Nat Struct Mol Biol* 23: 487–493.

61. Cundliffe E (1989) How Antibiotic-Producing Organisms Avoid Suicide. *Annu Rev Microbiol* 43: 207–233.

62. Arcamone F, Cassinelli G, Fantini G, et al. (1969) Adriamycin, 14-hydroxydaimomycin, a new antitumor antibiotic fromS. Peucetius var.caesius. *Biotechnol Bioeng* 11: 1101–1110.

63. Aubel-Sadron G, Londos-Gagliardi D (1984) Daunorubicin and doxorubicin, anthracycline antibiotics, a physicochemical and biological review. *Biochimie* 66: 333–352.

64. Quigley GJ, Wang AH, Ughetto G, et al. (1980) Molecular structure of an anticancer drug-DNA complex: daunomycin plus d(CpGpTpApCpG). *Proc Natl Acad Sci* 77: 7204–7208.

65. Madduri K, Hutchinson CR (1995) Functional characterization and transcriptional analysis of the dnrR1 locus, which controls daunorubicin biosynthesis in Streptomyces peucetius. *J Bacteriol* 177: 1208–1215.

66. Guilfoile PG, Hutchinson CR (1991) A bacterial analog of the mdr gene of mammalian tumor cells is present in Streptomyces peucetius, the producer of daunorubicin and doxorubicin. *Proc Natl Acad Sci* 88: 8553–8557.

67. Lomovskaya N, Hong SK, Kim SU, et al. (1996) The Streptomyces peucetius drrC gene encodes a UvrA-like protein involved in daunorubicin resistance and production. *J Bacteriol* 178: 3238–3245.

68. Karuppasamy K, Srinivasan P, Ashokkumar B, et al. (2015) Partial loss of self-resistance to daunorubicin in drrD mutant of Streptomyces peucetius. *Biochem Eng J* 102: 98–107.

69. Kaur P (1997) Expression and characterization of DrrA and DrrB proteins of Streptomyces peucetius in Escherichia coli: DrrA is an ATP binding protein. *J Bacteriol* 179: 569–575.

70. Rao DK, Kaur P (2008) The Q-Loop of DrrA Is Involved in Producing the Closed Conformation of the Nucleotide Binding Domains and in Transduction of Conformational Changes between DrrA and DrrB †. *Biochemistry* 47: 3038–3050.

71. Kaur P, Russell J (1998) Biochemical Coupling between the DrrA and DrrB Proteins of the Doxorubicin Efflux Pump of *Streptomyces peucetius*. *J Biol Chem* 273: 17933–17939.

72. Gandlur SM, Wei L, Levine J, et al. (2004) Membrane Topology of the DrrB Protein of the Doxorubicin Transporter of *Streptomyces peucetius*. *J Biol Chem* 279: 27799–27806.

73. Li W, Sharma M, Kaur P (2014) The DrrAB Efflux System of *Streptomyces peucetius* Is a Multidrug Transporter of Broad Substrate Specificity. *J Biol Chem* 289: 12633–12646.

74. Rahman SJ, Kaur P (2018) Conformational changes in a multidrug resistance ABC transporter DrrAB: Fluorescence-based approaches to study substrate binding. *Arch Biochem Biophys* 658: 31–45.

75. Kacinski BM, Rupp WD (1984) Interactions of the UVRABC endonuclease in vivo and in vitro with DNA damage produced by antineoplastic anthracyclines. *Cancer Res* 44: 3489–3492.

76. Hogenauer C, Hammer HF, Krejs GJ, et al. (1998) Mechanisms and Management of Antibiotic-Associated Diarrhea. *Clin Infect Dis* 27: 702–710.

77. McFarland LV (1998) Epidemiology, Risk Factors and Treatments for Antibiotic-Associated Diarrhea. *Dig Dis* 16: 292–307.

78. Leekha S, Aronhalt KC, Sloan LM, et al. (2013) Asymptomatic Clostridium difficile colonization in a tertiary care hospital: Admission prevalence and risk factors. *Am J Infect Control* 41: 390–393.

79. Smits WK, Lyras D, Lacy DB, et al. (2016) Clostridium difficile infection. *Nat Rev Dis Primer* 2: 16020.

80. Larcombe S, Hutton ML, Lyras D (2016) Involvement of Bacteria Other Than Clostridium difficile in Antibiotic-Associated Diarrhoea. *Trends Microbiol* 24: 463–476.

81. Högenauer C, Langner C, Beubler E, et al. (2006) Klebsiella oxytoca as a causative organism of antibiotic-associated hemorrhagic colitis. *N Engl J Med* 355: 2418–2426.

82. Beaugerie L, Metz M, Barbut F, et al. (2003) Klebsiella oxytoca as an agent of antibiotic-associated hemorrhagic colitis. *Clin Gastroenterol Hepatol Off Clin Pract J Am Gastroenterol Assoc* 1: 370–376.

83. Pérez-Vazquez M, Oteo-Iglesias J, Sola-Campoy PJ, et al. (2019) Characterization of Carbapenemase-Producing *Klebsiella oxytoca* in Spain, 2016–2017. *Antimicrob Agents Chemother* 63: e02529-18, /aac/63/6/AAC.02529-18.atom.

84. Zollner-Schwetz I, Högenauer C, Joainig M, et al. (2008) Role of Klebsiella oxytoca in antibiotic-associated diarrhea. *Clin Infect Dis Off Publ Infect Dis Soc Am* 47: e74-78.

85. Joainig MM, Gorkiewicz G, Leitner E, et al. (2010) Cytotoxic Effects of *Klebsiella oxytoca* Strains Isolated from Patients with Antibiotic-Associated Hemorrhagic Colitis or Other Diseases Caused by Infections and from Healthy Subjects. *J Clin Microbiol* 48: 817–824.

86. Schneditz G, Rentner J, Roier S, et al. (2014) Enterotoxicity of a nonribosomal peptide causes antibiotic-associated colitis. *Proc Natl Acad Sci* 111: 13181–13186.

87. Shioiri T, Aoyama T, Yamagami N, et al. (1995) Structure-cytotoxicity relationship of tilivalline derivatives. *Anticancer Drug Des* 10: 167–176.

88. Mohr N, Budzikiewicz H (1982) Tilivalline, a new pyrrolo[2, 1-c][1,4] benzodiazepine metabolite from klebsiella. *Tetrahedron* 38: 147–152.

89. McErlean M, Overbay J, Van Lanen S (2019) Refining and expanding nonribosomal peptide synthetase function and mechanism. *J Ind Microbiol Biotechnol* 46: 493–513.

90. Caboche S, Pupin M, Leclère V, et al. (2008) NORINE: a database of nonribosomal peptides.

Nucleic Acids Res 36: D326-331.

91. Karaolis DKR (2001) Pathogenicity Islands, *Encyclopedia of Genetics*, Elsevier, 1422–1424.

92. Schneditz G (2015) The colitogenic metabolite of K. oxytoca disrupts microtubule dynamics.

93. Dornisch E, Pletz J, Glabonjat RA, et al. (2017) Biosynthesis of the Enterotoxic Pyrrolobenzodiazepine Natural Product Tilivalline. *Angew Chem Int Ed* 56: 14753–14757.

94. Unterhauser K (2019) Klebsiella oxytoca enterotoxins tilimycin and tilivalline have distinct host DNA damaging and microtubule stabilizing activities.

95. Unterhauser K, Pöltl L, Schneditz G, et al. (2019) *Klebsiella oxytoca* enterotoxins tilimycin and tilivalline have distinct host DNA-damaging and microtubule-stabilizing activities. *Proc Natl Acad Sci* 116: 3774–3783.

96. Hartley JA (2011) The development of pyrrolobenzodiazepines as antitumour agents. *Expert Opin Investig Drugs* 20: 733–744.

97. Brucoli F, Guzman JD, Basher MA, et al. (2016) DNA sequence-selective C8-linked pyrrolobenzodiazepine–heterocyclic polyamide conjugates show anti-tubercular-specific activities. *J Antibiot (Tokyo)* 69: 843–849.

98. Rahman KM, Vassoler H, James CH, et al. (2010) DNA Sequence Preference and Adduct Orientation of Pyrrolo[2,1-c][1,4]benzodiazepine Antitumor Agents. *ACS Med Chem Lett* 1: 427–432.

99. Basher MA, Rahman KM, Jackson PJM, et al. (2017) Sequence-selective binding of C8-conjugated pyrrolobenzodiazepines (PBDs) to DNA. *Biophys Chem* 230: 53–61.

100. Mantaj J, Jackson PJM, Rahman KM, et al. (2017) From Anthramycin to Pyrrolobenzodiazepine (PBD)-Containing Antibody-Drug Conjugates (ADCs). *Angew Chem Int Ed Engl* 56: 462–488.

101. Hadjivassileva T, Thurston DE, Taylor PW (2005) Pyrrolobenzodiazepine dimers: novel sequence-selective, DNA-interactive, cross-linking agents with activity against Gram-positive bacteria. *J Antimicrob Chemother* 56: 513–518.

102. Alexander EM, Kreitler DF, Guidolin V, et al. (2020) Biosynthesis, Mechanism of Action, and Inhibition of the Enterotoxin Tilimycin Produced by the Opportunistic Pathogen Klebsiella oxytoca. *ACS Infect Dis* acsinfecdis.0c00326.

103. Smith J, Mun Tho L, Xu N, et al. (2010) The ATM–Chk2 and ATR–Chk1 Pathways in DNA Damage Signaling and Cancer, *Advances in Cancer Research*, Elsevier, 73–112.

104. Hanawalt PC, Spivak G (2008) Transcription-coupled DNA repair: two decades of progress and surprises. *Nat Rev Mol Cell Biol* 9: 958–970.

105. Jaspers NGJ, Raams A, Kelner MJ, et al. (2002) Anti-tumour compounds illudin S and Irofulven induce DNA lesions ignored by global repair and exclusively processed by transcription- and replication-coupled repair pathways. *DNA Repair* 1: 1027–1038.

106. Cockerill FR, Clinical and Laboratory Standards Institute (Eds.) (2012) Performance standards for antimicrobial disk susceptibility tests; approved standard, Wayne, PA, Committee for Clinical Laboratory Standards.

107. Woodcock DM, Crowther PJ, Doherty J, et al. (1989) Quantitative evaluation of *Escherichia coli* host strains for tolerance to cytosine methylation in plasmid and phage recombinants. *Nucleic Acids Res* 17: 3469–3478.

108. Baba T, Ara T, Hasegawa M, et al. (2006) Construction of *Escherichia coli* K-12 in-frame, single-gene knockout mutants: the Keio collection. *Mol Syst Biol* 2.

109. NCBI Accession Number: HG425356.

110. Marlene Hiesinger (2019) Characterization of immunity genes in Klebsiella oxytoca AHC-6. *Proj Lab* Institute of Molecular Biosciences, University of Graz.

111. Guzman LM, Belin D, Carson MJ, et al. (1995) Tight regulation, modulation, and high-level expression by vectors containing the arabinose PBAD promoter. *J Bacteriol* 177: 4121–4130.

112. Kelley LA, Mezulis S, Yates CM, et al. (2015) The Phyre2 web portal for protein modeling, prediction and analysis. *Nat Protoc* 10: 845–858.

113. Bhattacharya D, Nowotny J, Cao R, et al. (2016) 3Drefine: an interactive web server for efficient protein structure refinement. *Nucleic Acids Res* 44: W406–W409.

114. Laskowski RomanA, Rullmann JAntoonC, MacArthur MalcolmW, et al. (1996) AQUA and PROCHECK-NMR: Programs for checking the quality of protein structures solved by NMR. *J Biomol NMR* 8.

115. Schrödinger The PyMOL Molecular Graphics System, LLC.

116. Marchler-Bauer A, Bo Y, Han L, et al. (2017) CDD/SPARCLE: functional classification of proteins via subfamily domain architectures. *Nucleic Acids Res* 45: D200–D203.

117. NCBI Resource Coordinators, Agarwala R, Barrett T, et al. (2018) Database resources of the National Center for Biotechnology Information. *Nucleic Acids Res* 46: D8–D13.

118. Madeira F, Park Y mi, Lee J, et al. (2019) The EMBL-EBI search and sequence analysis tools APIs in 2019. *Nucleic Acids Res* 47: W636–W641.

119. Dornisch E (2017) Biosynthesis of the K. oxytoca enterotoxin tilivalline and discovery of its toxic precursor tilimycin.

120. Marchler-Bauer A, Derbyshire MK, Gonzales NR, et al. (2015) CDD: NCBI's conserved

domain database. *Nucleic Acids Res* 43: D222–D226.

121. Davidson AL, Chen J (2004) ATP-Binding Cassette Transporters in Bacteria. *Annu Rev Biochem* 73: 241–268.

122. Davidson AL, Dassa E, Orelle C, et al. (2008) Structure, function, and evolution of bacterial ATP-binding cassette systems. *Microbiol Mol Biol Rev MMBR* 72: 317–364, table of contents.

123. Timmins J, Gordon E, Caria S, et al. (2009) Structural and Mutational Analyses of Deinococcus radiodurans UvrA2 Provide Insight into DNA Binding and Damage Recognition by UvrAs. *Structure* 17: 547–558.

124. Poirot O, O'Toole E, Notredame C Tcoffee@igs: a web server for computing, evaluating and combining multiple sequence alignments. 4.

125. Notredame C, Higgins DG, Heringa J (2000) T-coffee: a novel method for fast and accurate multiple sequence alignment 1 1Edited by J. Thornton. *J Mol Biol* 302: 205–217.

126. Mak S, Xu Y, Nodwell JR (2014) The expression of antibiotic resistance genes in antibiotic-producing bacteria: Antibiotic resistance in antibiotic-producing bacteria. *Mol Microbiol* 93: 391–402.

127. Taylor SC, Nadeau K, Abbasi M, et al. (2019) The Ultimate qPCR Experiment: Producing Publication Quality, Reproducible Data the First Time. *Trends Biotechnol* 37: 761–774.

128. Gomes AÉI, Stuchi LP, Siqueira NMG, et al. (2018) Selection and validation of reference genes for gene expression studies in Klebsiella pneumoniae using Reverse Transcription Quantitative real-time PCR. *Sci Rep* 8: 9001.

129. Herzog KAT, Schneditz G, Leitner E, et al. (2014) Genotypes of Klebsiella oxytoca Isolates from Patients with Nosocomial Pneumonia Are Distinct from Those of Isolates from Patients with Antibiotic-Associated Hemorrhagic Colitis. *J Clin Microbiol* 52: 1607–1616.

130. Thellin O, Zorzi W, Lakaye B, et al. (1999) Housekeeping genes as internal standards: use and limits. *J Biotechnol* 75: 291–295.

131. Spivak G (2016) Transcription-coupled repair: an update. *Arch Toxicol* 90: 2583–2594.

132. Richardson JS (1981) The anatomy and taxonomy of protein structure. *Adv Protein Chem* 34: 167–339.

133. Liu X (2019) ABC Family Transporters, In: Liu X, Pan G (Eds.), *Drug Transporters in Drug Disposition, Effects and Toxicity*, Singapore, Springer Singapore, 13–100.

134. Case BC, Hartley S, Osuga M, et al. (2019) The ATPase mechanism of UvrA2 reveals the distinct roles of proximal and distal ATPase sites in nucleotide excision repair. *Nucleic Acids Res* 47: 4136–4152.

135. Goosen N, Moolenaar GF (2008) Repair of UV damage in bacteria. *DNA Repair* 7: 353–379.

136. Pakotiprapha D, Inuzuka Y, Bowman BR, et al. (2008) Crystal Structure of Bacillus stearothermophilus UvrA Provides Insight into ATP-Modulated Dimerization, UvrB Interaction, and DNA Binding. *Mol Cell* 29: 122–133.

137. © 2010 Thermo Fisher Scientific Inc. NanoDrop 1000 Spectrophotometer V3.8 User's manual.

138. Phongsisay V, Perera VN, Fry BN (2007) Evaluation of eight RNA isolation methods for transcriptional analysis in Campylobacter jejuni. *J Microbiol Methods* 68: 427–429.

139. Desroche N, Beltramo C, Guzzo J (2005) Determination of an internal control to apply reverse transcription quantitative PCR to study stress response in the lactic acid bacterium Oenococcus oeni. *J Microbiol Methods* 60: 325–333.

140. Bustin SA, Benes V, Garson JA, et al. (2009) The MIQE Guidelines: Minimum Information for Publication of Quantitative Real-Time PCR Experiments. *Clin Chem* 55: 611–622.

141. Prija F, Srinivasan P, Das S, et al. (2017) DnrI of *Streptomyces peucetius* binds to the resistance genes, *drrAB* and *drrC* but is activated by daunorubicin. *J Basic Microbiol* 57: 862–872.

142. Beggs GA, Brennan RG, Arshad M (2020) MarR family proteins are important regulators of clinically relevant antibiotic resistance. *Protein Sci* 29: 647–653.

7 Appendix

```
UvrX7G            1 MKTHDAIKIIGARQNNLQDIDVEVPKNKITVFTGVSGSGKSSLVFGTIAAESQRQLNDTF
UvrX8G            1 MKTHDAIKIIGARQNNLQDIDVEVPKNKITVFTGVSGSGKSSLVFGTIAAESQRQLNDTF
WP_064398705      1 MKTHDAIKIIGARQNNLQDIDVEVPKNKITVFTGVSGSGKSSLVFGTIAAESQRQLNDTF
WP_200784965.1    1 MKTHDAIKIIGARQNNLQDIDVEVPKNKITVFTGVSGSGKSSLVFGTIAAESQRQLNDTF
WP_142477393.1    1 MKTHDAIKIIGARQNNLQDIDVEVPKNKITVFTGVSGSGKSSLVFGTIAAESQRQLNDTF
WP_064356495.1    1 MKTHDAIKIIGARQNNLQDIDVEVPKNKITVFTGVSGSGKSSLVFGTIAAESQRQLNDTF

UvrX7G           61 PPFIRHRLPHYGNPEVDEIENLSVAIIIDQKRIGGNARSTVGTASDIYTLLRLLFSRVGE
UvrX8G           61 PPFIRHRLPHYGNPEVDEIENLSVAIIIDQKRIGGNARSTVGTASDIYTLLRLLFSRVGE
WP_064398705     61 PPFIRHRLPHYGNPEVDEIENLSVAIIIDQKRIGGNARSTVGTASDIYTLLRLLFSRVGE
WP_200784965.1   61 PPFIRHRLPHYGNPEVDEIENLSVAIIIDQKRIGGNARSTVGTASDIYTLLRLLFSRVGE
WP_142477393.1   61 PPFIRHRLPHYGNPEVDEIENLSVAIIIDQKRIGGNARSTVGTASDIYTLLRLLFSRVGE
WP_064356495.1   61 PPFIRHRLPHYGNPEVDEIENLSVAIIIDQKRIGGNARSTVGTASDIYTLLRLLFSRVGE

UvrX7G          121 PFVGYSNVFSFNHPAGMCATCDGLGIASTIDINHLIDSNLSLNEGAIRYPSFAPGSWRWK
UvrX8G          121 PFVGYSNVFSFNHPAGMCATCDGLGIASTIDINHLIDSNLSLNEGAIRYPSFAPGSWRWK
WP_064398705    121 PFVGYSNVFSFNHPAGMCATCDGLGIASTIDINHLIDSNLSLNEGAIRYPSFAPGSWRWK
WP_200784965.1  121 PFVGYSNVFSFNHPAGMCATCDGLGIASTIDINHLIDSNLSLNEGAIRYPSFAPGSWRWK
WP_142477393.1  121 PFVGYSNVFSFNHPAGMCATCDGLGIASTIDINHLIDSNLSLNEGAIRYPSFAPGSWRWK
WP_064356495.1  121 PFVGYSNVFSFNHPAGMCATCDGLGIASTIDINHLIDSNLSLNEGAIRYPSFAPGSWRWK

UvrX7G          181 RYVYSGLFDADKKIADYSKEERELLLYADNLTPEAPLAGWPKSAKFEGVITRFTRSYLKQ
UvrX8G          181 RYVYSGLFDADKKIADYSKEERELLLYADNLTPEAPLAGWPKSAKFEGVITRFTRSYLKQ
WP_064398705    181 RYVYSGLFDADKKIADYSKEERELLLYADNLTPEAPLAGWPKSAKFEGVITRFTRSYLKQ
WP_200784965.1  181 RYVYSGLFDADKKIADYSKEERELLLYADNLTPEAPLAGWPKSAKFEGVITRFTRIYLKQ
WP_142477393.1  181 RYVYSGLFDADKKIADYSKEERELLLYADNLTPEAPLAGWPKSAKFEGVITRFTRSYLKQ
WP_064356495.1  181 RYVYSGLFDADKKIADYSKEERELLLYADNLTPEAPLAGWPKSAKFEGVITRFTRSYLKQ

UvrX7G          241 ETKDTKTEEFQRVVSLQVCPSCQGMRLNEEILSCRIRGKNIGECATLPVTELKLFVEKLD
UvrX8G          241 ETKDTKTEEFQRVVSLQVCPSCQGMRLNEEILSCRIRGKNIGECATLPVTELKLFVEKLD
WP_064398705    241 ETKDTKTEEFQRVVSLQVCPSCQGMRLNEEILSCRIRGKNIGECATLPVTELKLFVEKLD
WP_200784965.1  241 ETKDTKTEEFQRVVSLQVCPSCQGMRLNEEILSCRIRGKNIGECATLPVTELKLFVEKLD
WP_142477393.1  241 ETKDTKTEEFQRVVSLQVCPSCQGMRLNEEILSCRIRGKNIGECATLPVTELKLFVEKLD
WP_064356495.1  241 ETKDTKTEEFQRVVSLQVCPSCQGMRLNEEILSCRIRGKNIGECATLPVTELKLFVEKLD

UvrX7G          301 YPEVRPLIEALLERLDAMCAVGLGYLDLNRTTPSLSGGESQRLKMVRHLGSSLTGIVYII
UvrX8G          301 YPEVRPLIEALLERLDAMCAVGLGYLDLNRTTPSLSGGESQRLKMVRHLGSSLTGIVYII
WP_064398705    301 YPEVRPLIEALLERLDAMCAVGLGYLDLNRTTPSLSGGESQRLKMVRHLGSSLTGIVYII
WP_200784965.1  301 YPEVRPLIEALLERLDAMCAVGLGYLDLNRTTPSLSGGESQRLKMVRHLGSSLTGIVYII
WP_142477393.1  301 YPEVRPLIEALLERLDAMCAVGLGYLDLNRTTPSLSGGESQRLKMVRHLGSSLTGIVYII
WP_064356495.1  301 YPEVRPLIEALLERLDAMCAVGLGYLDLNRTTPSLSGGESQRLKMVRHLGSSLTGIVYII

UvrX7G          361 DEPSTGLHPADIVKLNVLIGKLRDKGNTILMVEHDPDMIAIAEHVIDLGPGAGKQGGNIV
UvrX8G          361 DEPSTGLHPADIVKLNVLIGKLRDKGNTILMVEHDPDMIAIAEHVIDLGPGAGKQGGNIV
WP_064398705    361 DEPSTGLHPADIVKLNVLIGKLRDKGNTILMVEHDPDMIAIAEHVIDLGPGAGKQGGNIV
WP_200784965.1  361 DEPSTGLHPADIVKLNVLIGKLRDKGNTILMVEHDPDMIAIAEHVIDLGPGAGKQGGNIV
WP_142477393.1  361 DEPSTGLHPADIVKLNVLIGKLRDKGNTILMVEHDPDMIAIAEHIIDLGPGAGKQGGNIV
WP_064356495.1  361 DEPSTGLHPADIVKLNVLIGKLRDKGNTILMVEHDPDMIAIAEHVIDLGPGAGKQGGNIV

UvrX7G          421 FEGDLSALKQSQTLTGRYFSSRAEINKKPRCAKGYISVRNATLHNLHNLSVDVPLSVMVA
UvrX8G          421 FEGDLSALKQSQTLTGRYFSSRAEINKKPRCAKGYISVRNATLHNLHNLSVDVPLSVMVA
WP_064398705    421 FEGDLSALKQSQTLTGRYFSSRAEINKKPRCAKGYISVRNATLHNLHNLSVDVPLSVMVA
WP_200784965.1  421 FEGDLSALKQSQTLTGRYFSSRAEINKKPRCAKGYISVRNATLHNLHNLSVDVPLSVMVA
WP_142477393.1  421 FEGDLSALKQSQTLTGRYFSSRAEINKKPRCAKGYISVRNATLHNLHNLSVDVPLSVMVA
WP_064356495.1  421 FEGDLSALKQSQTLTGRYFSSRAEINKKPRCAKGYISVRNATLHNLHNLSVDVPLSVMVA

UvrX7G          481 VTGVAGSGKSSFVMGALAPQCPEAIVIDQKPIHTSIRSHIASWCGAFDTIRSLFAEKNHV
UvrX8G          481 VTGVAGSGKSSFVMGALAPQCPEAIVIDQKPIHTSIRSHIASWCGAFDTIRSLFAEKNHV
WP_064398705    481 VTGVAGSGKSSFVMGALAPQCPEAIVIDQKPIHTSIRSHIASWCGAFDTIRSLFAEKNHV
WP_200784965.1  481 VTGVAGSGKSSFVMGALAPQCPEAIVIDQKPIHTSIRSHIASWCGAFDTIRSLFAEKNHV
WP_142477393.1  481 VTGVAGSGKSSFVMGALAPQCPEAIVIDQKPIHTSIRSHIASWCGAFDTIRSLFAEKNQV
WP_064356495.1  481 VTGVAGSGKSSFVMGALAPQCPEAIVIDQKPIHTSIRSHIASWCGAFDTIRSLFAEKNQV
```

Figure A1. Sequence alignment of UvrX7G, UvrX8G and four *K. oxytoca* protein sequences.

```
uvrX    1 ATGAAAACCCATGACGCTATAAAAATCATTGGTGCAAGGCAAAATAATTTGCAAGATATT
uvrX   61 GATGTAGAGGTCCCTAAAAATAAAATAACAGTTTTTACCGGTGTTTCCGGATCGGGTAAA
uvrX  121 AGCTCTTTAGTATTCGGAACTATAGCGGCGGAATCTCAGCGACAGTTAAATGACACGTTT
uvrX  181 CCACCTTTTATTCGCCATCGCTTACCACATTATGGTAATCCTGAAGTCGATGAAATTGAA
uvrX  241 AACCTGTCGGTGGCCATTATTATTGACCAAAAACGTATTGGTGGCAACGCACGTTCGACG
uvrX  301 GTGGGCACCGCATCAGATATTTATACCCTACTACGGCTACTCTTTTCTCGTGTCGGCGAA
uvrX  361 CCTTTCGTAGGTTATTCGAATGTTTTTTCATTCAATCATCCTGCGGGGATGTGTGCGACA
uvrX  421 TGCGACGGGTTGGGCATTGCCAGTACTATTGATATCAACCATCTGATTGATTCAAATCTG
uvrX  481 TCGTTAAATGAAGGAGCTATTCGTTATCCTTCTTTTGCGCCAGGCTCATGGCGCTGGAAA
uvrX  541 CGTTATGTTTATTCAGGACTTTTTGATGCCGATAAAAAAATCGCGGATTATTCAAAAGAG
uvrX  601 GAGCGAGAATTATTACTTTATGCGGATAATCTCACTCCTGAAGCGCCGTTAGCCGGTTGG
uvrX  661 CCTAAGAGTGCAAAGTTTGAAGGCGTCATTACGCGCTTTACGCGAAGTTATTTAAAACAA
uvrX  721 GAAACTAAAGATACTAAAACTGAGGAATTTCAGCGAGTCGTTAGTTTGCAGGTTTGCCCT
uvrX  781 TCTTGTCAGGGTATGAGGCTTAACGAGGAAATACTTTCCTGCCGGATTAGAGGGAAAAAT
uvrX  841 ATTGGCGAATGCGCAACGCTGCCTGTCACAGAGTTAAAGCTGTTTGTAGAAAAGCTCGAT
uvrX  901 TACCCTGAAGTCAGGCCGCTGATCGAAGCATTGCTGGAAAGGTTGGATGCCATGTGTGCA
uvrX  961 GTAGGCTTGGGATATCTGGATTTGAACCGTACGACCCCTAGCTTATCGGGCGGTGAGTCC
uvrX 1021 CAGCGGTTGAAAATGGTCCGACATCTGGGAAGTAGTCTGACCGGGATCGTTTATATAATT
uvrX 1081 GATGAACCCAGTACCGGCCTGCATCCAGCAGATATAGTGAAATTGAATGTTTTAATTGGA
uvrX 1141 AAACTACGCGACAAAGGCAATACCATTCTGATGGTGGAGCACGACCCGGACATGATAGCG
uvrX 1201 ATAGCCGAGCATGTTATTGATTTAGGGCCAGGAGCGGGTAAGCAAGGCGGGAATATTGTC
uvrX 1261 TTTGAGGGCGACCTGTCGGCACTTAAGCAATCCCAAACCTTGACGGGTCGATATTTCTCT
uvrX 1321 TCACGGGCAGAGATAAATAAGAAACCGAGATGTGCCAAGGGTTATATATCGGTAAGAAAC
uvrX 1381 GCCACATTGCATAACCTGCATAACTTATCGGTAGACGTGCCTTTAAGCGTTATGGTCGCT
uvrX 1441 GTGACGGGAGTCGCTGGATCGGGCAAAAGTTCATTCGTTATGGGGGCCCTGGCGCCACAA
uvrX 1501 TGTCCGGAGGCGATCGTTATCGATCAAAAACCGATACATACCTCAATTCGATCGCATATT
uvrX 1561 GCTTCCTGGTGCGGTGCATTTGATACGATCCGTTCGCTGTTTGCCGAAAAAAACCATGTG
uvrX 1621 TCAGCGTCGTGGTTTAGCGCTAATGCCAAAGGGGCTTGTCCGGAATGTAATGGGCTAGGG
uvrX 1681 GTAATACAAACCGATCTGGCATTTATGGATACGGTTACGTTGCCATGTGAGGCCTGCCAG
uvrX 1741 GGGCAGCGCTATAACCCACAAGCGCTGAAATATCGTTATCAGGGAAAAAGTATTGCTGAG
uvrX 1801 GTATTATCCCTGTCGATTAATGATGCCTGCGAATTTTTCCTTAATGAGCCACAGCTCAGG
uvrX 1861 CCAATTTTTCGTAGCCTGGTCGAAGTCGGGTTGGGATATTTACGCTTGGGTGAATCGTTA
uvrX 1921 AATCATCTTTCAGGCGGTGAATGCCAGCGGCTGAAGTTAGCGTCACAATTAAATCATGAT
uvrX 1981 AGTGACATGTATATTTTCGATGAGCCAACCACGGGTCTTCATCCCAGTGATGTAGCCTCG
uvrX 2041 CTGTTGAAACTATTTAACCGACTGGTAGCGCGCGGAAACACCGTCATTATTATTGAACAT
uvrX 2101 AATATGGAGTTGATCGCTCAGGCTGACTGGATTATTGATATTGGACCTTATGCCGGGAAA
uvrX 2161 GAAGGGGGGGGATTATTGTTTAGCGGTACACCCGAATCGATGCTGGCCTGTCGCCATTCA
uvrX 2221 TTAACCGCAGAGTGGTTGCGCAAACATTGCCGGATGGAGTGA
```

Figure A2. Sequence of *uvrX* (*uvrX8G*) from *K. oxytoca* AHC-6.

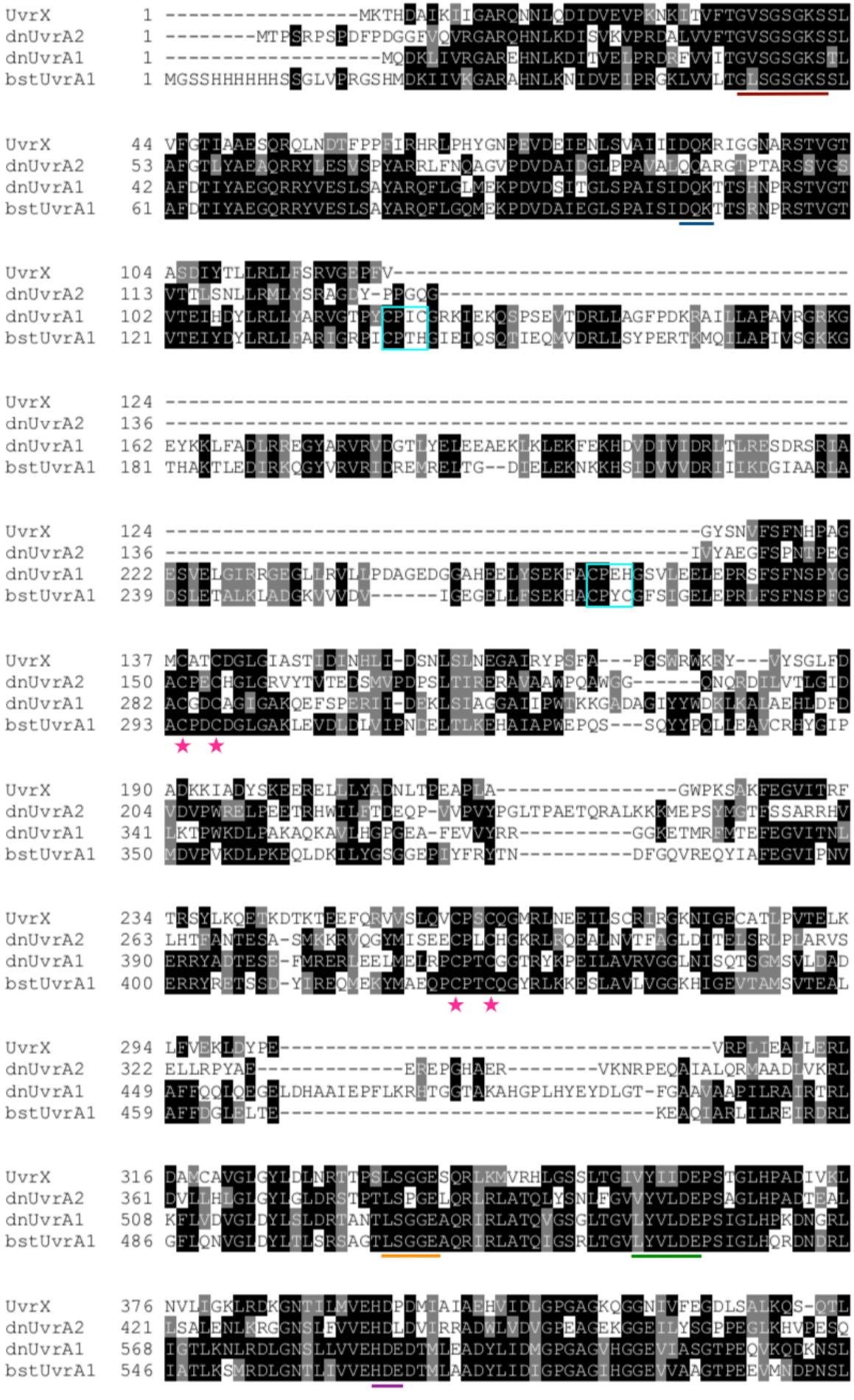
UvrX
dnUvrA2
dnUvrA1
bstUvrA1

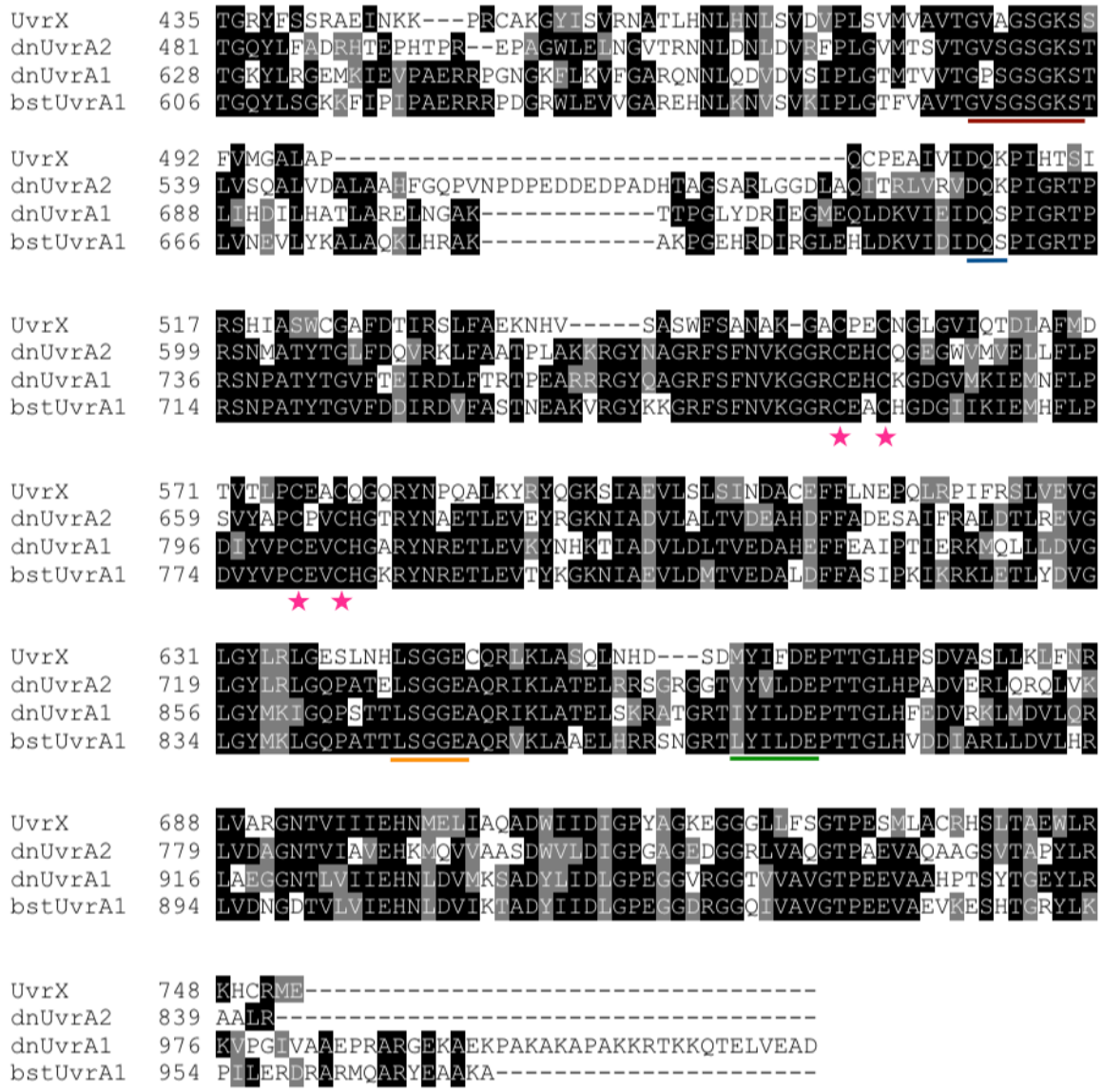

Figure A3. Sequence alignment of *K. oxytoca* AHC-6, *D. radiodurans* UvrA1 and UvrA2 and *B. stearothermophilus* UvrA1. Conserved regions are highlighted in black and conserved ABC motifs were underlined: Walker A (red), Walker B (green), Q-loop (blue), ABC-signature motif (orange), H-loop (purple). Zinc-coordinating residues (Cys-XX-Cys motif) are indicated with stars and additional motifs are boxed in turquoise.

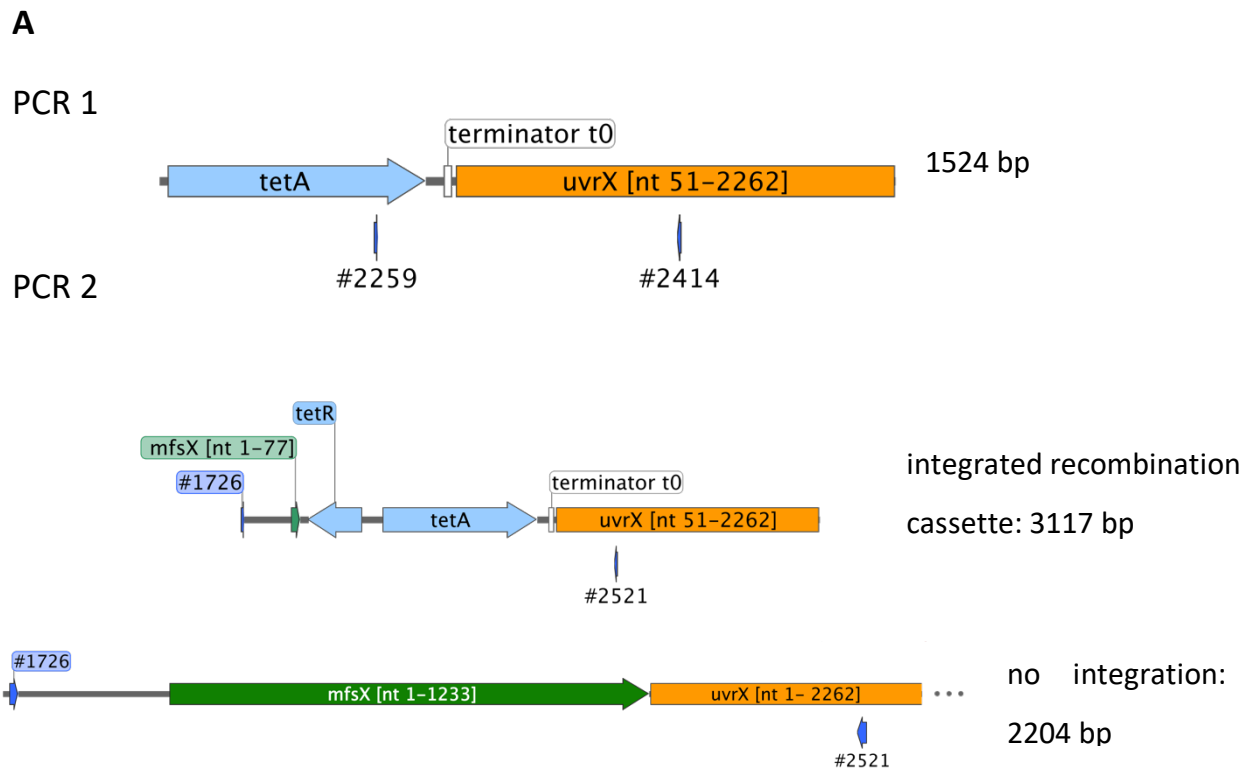

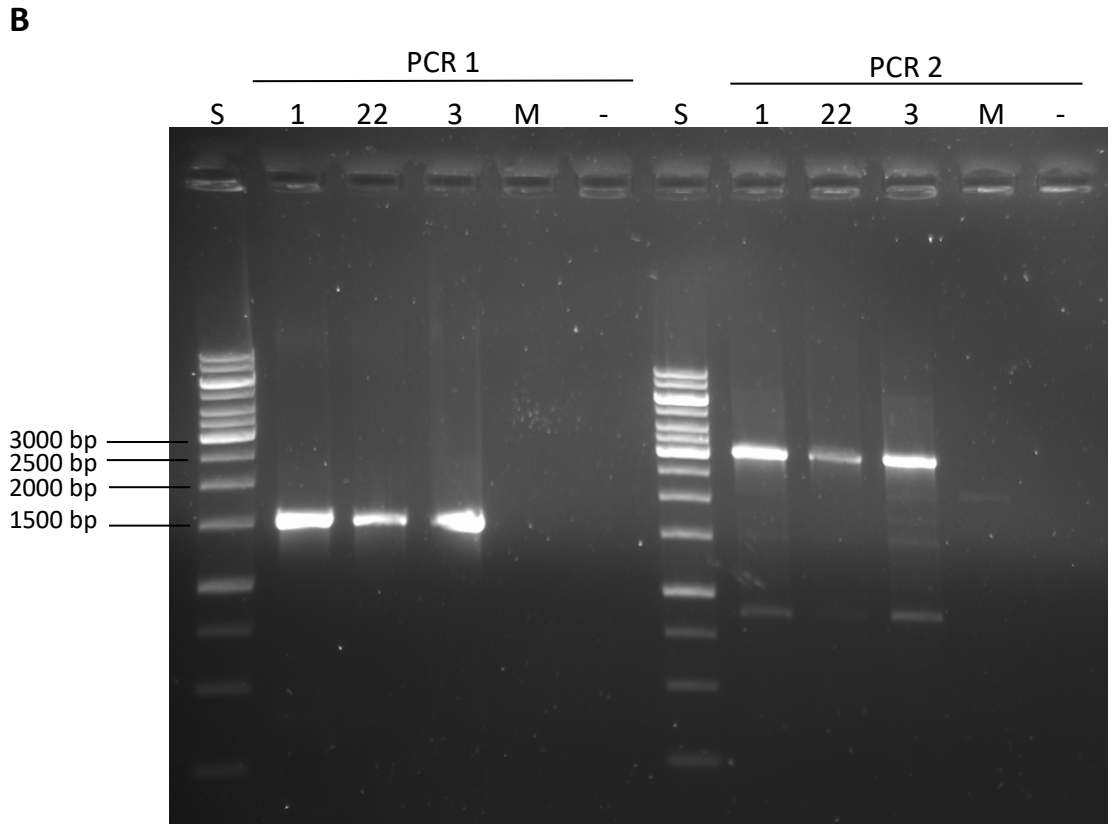

Figure A4. Primer setting and colony PCR of the recombinants. (A) Part of the *K. oxytoca* AHC-6 Mut89 and Mut89 *ΔmfsX, uvrX* sequence with the primer binding sites used to verify the integration of the recombination cassette via colony PCR (B) *K. oxytoca* AHC-6 Mut89 [pKOBEG] cells were transformed with the recombination cassette. After incubation on CASO plates with Tet the gDNA of the recombinants was isolated and the presence of the recombination cassette and the correct integration in the genome was tested via PCR. PCR products of the recombined *K. oxytoca* AHC-6 Mut89 clones. S...1kb DNA ladder; 1, 22, 3...*K. oxytoca* AHC-6 Mut89 recombinants (1 & 3: 100 ng; 22: 300 ng); M...*K. oxytoca* AHC-6 Mut89; -...negative control

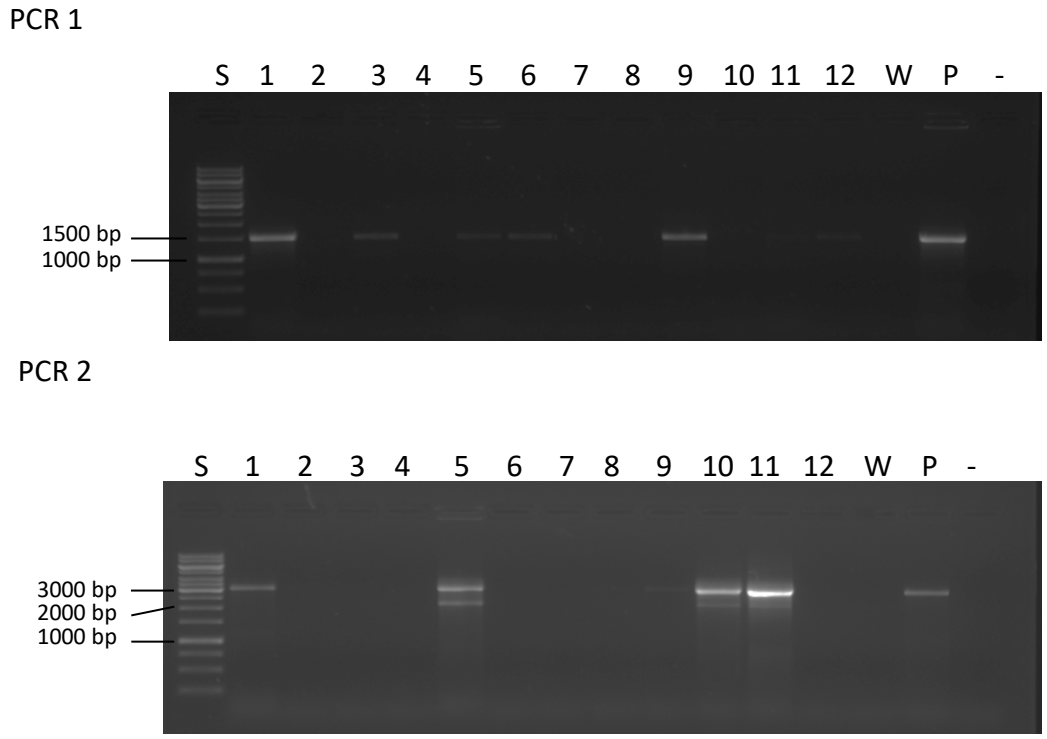

Figure A5. Colony PCR of the recombinants. The strain *K. oxytoca* AHC-6 *aphA* [pKOBEG] was transformed with the recombination cassette. After incubation on CASO or M63 plates with Tet the presence of the recombination cassette and the correct integration in the genome was tested via colony PCR (Primer setting see Figure A4). Colony PCR products of the recombined *K. oxytoca* AHC-6 *aphA* clones. S...1kb DNA ladder; 1-12...*K. oxytoca* AHC-6 *aphA* recombinants; W...*K. oxytoca* AHC-6 *aphA*; P...*K. oxytoca* AHC-6 Mut89 Δ*mfsX, uvrX*; -...negative control

1,2,4,5: CASO and 600 ng; 6-8: CASO and 300 ng; 3: M63 and 300 ng; 9-11: M63 and 600 ng; 12: 100ng

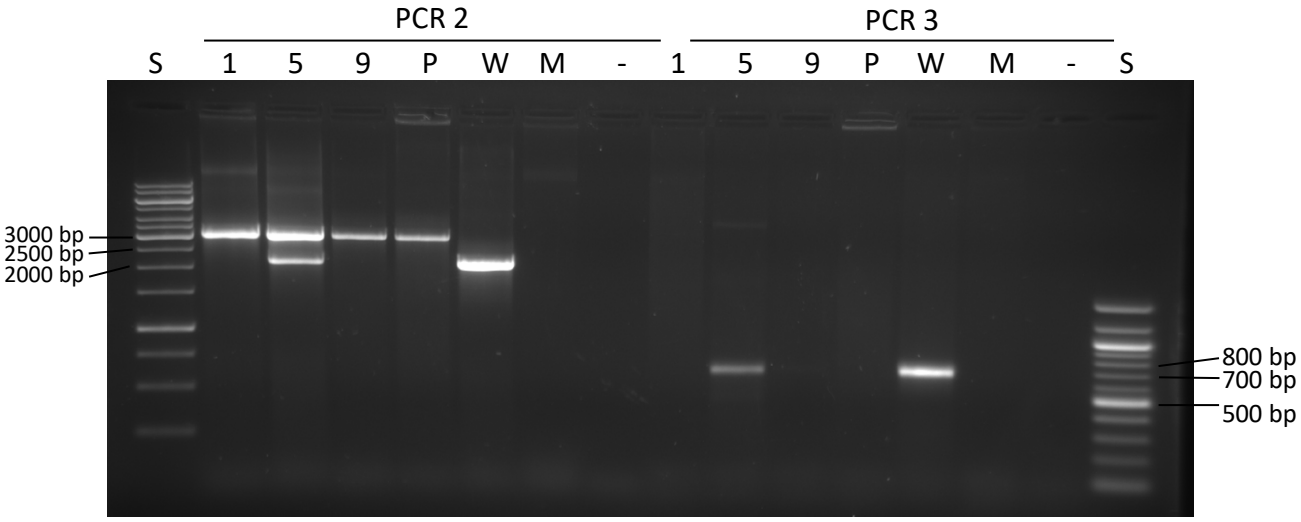

Figure A6. PCR products of the recombinants. The gDNA from three positive recombinants (Figure A5) was isolated and the presence of the recombination cassette (PCR 2 see Figure A4) and the absence of the deleted part of *mfsX* (primers binding in *mfsX*; 663 bp PCR product with the native sequence). PCR products of the recombined *K. oxytoca* AHC-6 *aphA* clones. S...1kb DNA ladder; 1-5...*K. oxytoca* AHC-6 *aphA* recombinants; P... *K. oxytoca* AHC-6 Mut89 Δ*mfsX, uvrX;* W... *K. oxytoca* AHC-6 *aphA*; M... *K. oxytoca* AHC-6 Mut89; -...negative control

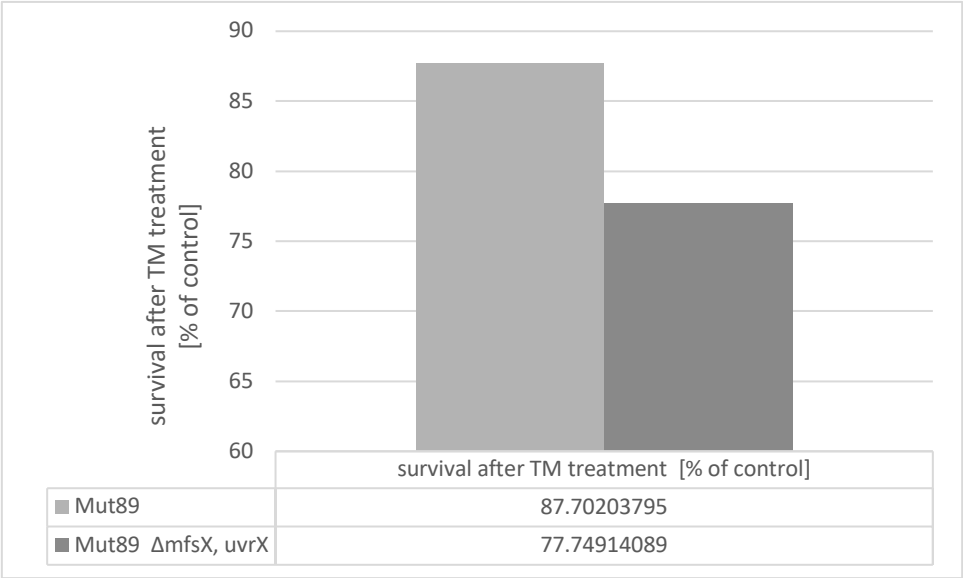

Figure A7. *K. oxytoca* Δ*mfsX, uvrX* is more sensitive to TM compared to the Mut89 parent strain. Viability of *K. oxytoca* strains after 2h of TM treatment with 85 µM TM. The colony forming units were normalized to the solvent control (EtOH) (n = 1).

Table A1. Transcript levels of candidate reference genes at different time points assessed in *K. oxytoca* AHC-6. The mean Cq values of the technical replicated and the range between the Cq values is shown.

Gene	Time point [h]	Mean Cq	Δ Cq (0.5 - 2 h)
16S	0	19.48	0.4
	0.5	17.76	
	1	18.05	
	2	18.16	
gapA	0	22.44	3.05
	0.5	19.27	
	1	17.76	
	2	16.22	
mdh	0	27.78	0.73
	0.5	24.82	
	1	24.57	
	2	24.09	
rpoB	0	18.99	2.36
	0.5	17.94	
	1	19.37	
	2	20.30	
proC	0	29.49	0.82
	0.5	24.07	
	1	24.27	
	2	23.45	
rho	0	22.02	4.46
	0.5	24.59	
	1	20.13	
	2	20.53	

Table A2. In vitro relative normalized expression of *npsA*, *uvrX*, *mfsX* and *marR* during *K. oxytoca* AHC-6 growth. The relative expression levels of target genes relative to the control 0.5 h samples at corresponding time points were calculated using the Pfaffl-Method and normalized to the expression of the reference gene *16S*.

		Relative normalized expression			
Gene	Time point [h]	1	2	3	Mean ± SD
npsA	1	1.00	1.27	1.16	1.1 ± 0.1
	2	1.27	1.71	1.61	1.5 ± 0.2
	3	4.31	4.05	3.91	4.1 ± 0.2
	4	12.27	18.18	6.92	12.5 ± 4.6
	5	89.11	115.34	70.56	91.7 ± 18.4
	6	82.43	233.40	113.50	143.1 ± 65.1
uvrX	1	0.94	0.94	0.88	0.9 ± 0.03
	2	1.51	1.26	1.01	1.3 ± 0.2
	3	2.15	1.67	2.07	2.0 ± 0.2
	4	2.67	3.23	1.28	2.4 ± 0.8
	5	19.48	24.19	8.85	17.5 ± 6.4
	6	37.46	78.30	23.02	46.3 ± 23.4
mfsX	1	0.95	1.01	0.76	0.9 ± 0.1
	2	1.21	1.58	1.30	1.4 ± 0.20
	3	1.13	1.12	1.22	1.2 ± 0.04
	4	1.72	2.92	1.52	2.1 ± 0.6
	5	17.54	21.40	7.27	15.4 ± 6.0
	6	53.30	63.59	31.36	49.4 ± 13.4
marR	1	1.08	1.03	0.91	1.0 ± 0.1
	2	1.03	1.03	1.13	1.1 ± 0.05
	3	1.02	0.99	1.01	1.0 ± 0.01
	4	1.21	2.10	1.55	1.6 ± 0.4
	5	5.02	6.74	4.69	5.5 ± 0.9
	6	11.20	13.31	10.60	11.7 ± 1.2